TÉCNICO LISBOA

Investigation of neurovascular changes during migraine attacks using BOLD-fMRI

Sofia da Silva Cotrim

Thesis to obtain the Master of Science Degree in

Biomedical Engineering

Supervisor(s): Prof. Patrícia Margarida Piedade Figueiredo
Dr. Raquel Santos Gil-Gouveia

Examination Committee

Chairperson: Prof. João Miguel Raposo Sanches
Supervisor: Dr. Raquel Santos Gil-Gouveia
Member of the Committee: Dr. Pedro Miguel Araújo Campos Castro

January 2021

Dedicated to my parents.

Declaration

I declare that this document is an original work of my own autorship and that it fulfills all the requirements of the Code of Conduct and Good Practices of the Universidade de Lisboa.

Preface

The work presented in this thesis was performed at LaSEEB, a research lab of ISR-Lisboa at Instituto Superior Técnico, between February and December of 2020, under the supervision of Professor Patrícia Figueiredo and Doctor Raquel Gil-Gouveia from Hospital da Luz.

Acknowledgments

Firstly, I would like to thank my supervisors, Prof. Patrícia Figueiredo and Dr. Raquel Gil-Gouveia, for their consistent support and crucial guidance during the running of this project. Without their critical view and analytic thinking, this work would never been possible. Their warm smiles and contagious enthusiasm in each and every online meeting were a source of inspiration and motivation, very much needed in the pandemic during which this work was developed.

Further, I want to show gratitude to Joana Pinto for her support and patience, as well as her essential tips and expertise. It was a great honor to work with such an intelligent, caring and hardworking person.

I am also thankful to LaSEEB for receiving me and giving me the opportunity to develop this dissertation.

During the past 5 years, I was fortunate enough to meet incredible people who rapidly became friends. I want to acknowledge André Miranda, André Vieira, Carlota, Catarina, Folque, Leo, Mada, Manuel, Margarida Lopes, Margarida Pinho, Rafa, Rosa and Tostas. Without you, my journey at Técnico would have been immensely harder. I am forever grateful to you, for showing me that everything is easier and funnier when done with people we love. The same applies to the ones who were present before university and grew up with me along the years. To Bia, who I love with all my heart, Cátia, Compõete, Maria, Mariana, and Pereira, for always making me laugh until my belly hurts, and to my coaches, Isabel and Rute, for never stop believing in me.

Finally, but definitely not less important, I want to thank my family. Mom and dad, there is no way I can express my gratitude to you: for always putting me first, for the sacrifices you have done to provide me with the best education, the unconditional love and support, and for always letting me fly as high as I wanted. To my beautiful sister who, besides making sure I always had something to eat when I got home late at night, has always let me be the purest version of myself. Thank you for supporting, helping and caring for me.

Resumo

Motivação: A enxaqueca é uma patologia neurológica extremamente debilitante, associada a um elevado risco de doença cardiovascular. A avaliação da vasoreatividade cerebral (CVR), utilizada para a deteção de patologia cerebrovascular, tem mostrado alterações nos doentes com enxaqueca.

Objetivo: Estudo dos mecanismos neurovasculares da enxaqueca através da comparação da CVR durante ataques espontâneos comparativamente a períodos sem dor na enxaqueca.

Métodos: Foram estudadas pacientes com enxaqueca episódica durante os períodos ictal e interictal da doença, utilizando dados de ressonância magnética funcional (fMRI) obtidos durante tarefas motoras, visuais, e apneia. Foram criados os mapas de ativação cerebral e efetuado o cálculo da amplitude (CVR, mudança percentual de sinal) e o tempo de pico (TTP) da resposta à apneia. Posteriormente, procedeu-se à investigação de diferenças na ativação cerebral bem como na CVR e TTP entre os períodos ictal e interictal. Os valores individuais médios de CVR e TTP obtidos para as regiões de interesse foram correlacionados com características clínicas da enxaqueca.

Resultados: Tanto a CVR como o TTP revelaram estar elevados em regiões occipitais durante o ataque de enxaqueca comparativamente ao período interictal. Os valores de CVR e TTP não mostraram correlação com as características clínicas da enxaqueca.

Conclusões: Estes resultados são consistentes com relatos anteriores de CVR diminuída na circulação cerebral posterior no período interictal da enxaqueca comparativamente a controlos, e também com a presença de lesões isquémicas na mesma região. Simultaneamente, confirmam a maior vulnerabilidade do lobo occipital e da circulação cerebral posterior nos enfartes cerebrais na enxaqueca. Estes resultados contribuem com nova evidência para a reduzida literatura sobre o período ictal da enxaqueca, e este é o segundo estudo a avaliar a CVR de todo o cérebro utilizando fMRI.

Palavras-chave: enxaqueca episódica, ressonância magnética funcional, vasoreatividade cerebral, apneia, lobo occipital

Abstract

Motivation: Migraine is a disabling neurological condition, associated with an increased risk of cardiovascular disease. Cerebrovascular reactivity (CVR) measurements have the potential to detect cerebrovascular pathophysiology and have been shown to be altered in migraine.

Objective: To elucidate neurovascular mechanisms in migraine by investigating CVR changes during spontaneous attacks (ictal phase) compared to pain-free periods (interictal phase).

Methods: Patients with episodic migraine without aura were studied during ictal and interictal phases. BOLD-fMRI data were acquired during a breath-holding (BH) challenge, to map CVR, as well as during two brain activation tasks (visual and motor), to map cerebrovascular changes in response to brain activation. Whole-brain activation maps were obtained through a general linear model analysis, and the amplitude (CVR, percent signal change) and time-to-peak (TTP) of the BH BOLD response were computed in each voxel. Next, group-level analysis was performed to identify differences in CVR and TTP, as well as in brain activation in response to sensory stimuli between ictal and interictal phases. Additionally, correlation analysis was performed between the individual mean CVR and TTP values across regions-of-interest and migraine clinical features.

Results: Increased CVR and TTP were found in occipital regions during the attack compared with the pain-free period. No significant correlation was found between CVR and TTP values and migraine clinical features.

Conclusions: These results are consistent with previously reported reduced reactivity of the posterior cerebral circulation in the interictal phase of migraineurs relative to controls, and also with the presence of ischemic-like lesions in the posterior circulation of migraineurs. It also confirms the vulnerability of the occipital lobe and posterior cerebral circulation regarding cerebral infarcts in migraine. These findings contribute with new evidence to the limited literature regarding the ictal phase of migraine, and this is the second only study evaluating CVR across the whole-brain on a voxel-by-voxel basis using fMRI.

Keywords: episodic migraine, functional magnetic resonance imaging, cerebrovascular reactivity, breath-holding, occipital lobe

Contents

Declaration v
Preface vii
Acknowledgments ix
Resumo xi
Abstract xiii
List of Tables xix
List of Figures xxi
Acronyms xxv

1 Introduction **1**
1.1 Motivation 1
1.2 Thesis objectives 2
1.3 Publications arising from this thesis 3
1.4 Thesis Outline 3

2 Theoretical Background **5**
2.1 Migraine 5
2.1.1 Migraine pathophysiology 7
2.1.2 Migraine-associated vasculopathy 8
2.2 Cerebrovascular Reactivity (CVR) 9
2.2.1 Vasoactive stimuli 10
2.2.2 Neuroimaging techniques for CBF assessment 12
2.2.3 Breath-holding data acquisition parameters 13
2.3 Functional Magnetic Resonance Imaging 15
2.3.1 The BOLD contrast 15
2.3.2 fMRI data preprocessing 16
2.3.3 Subject-level fMRI data analysis 17
2.3.3.1 The General Linear Model approach 17
2.3.3.2 Breath-hold fMRI data modelling 21
2.3.3.3 Cerebrovascular Reactivity (CVR) and Time-To-Peak (TTP) maps 23
2.3.4 Group-level fMRI data analysis 23

2.3.4.1 Region-specific analysis . . . 24
2.3.4.1.1 Cerebral lobes . . . 24
2.3.4.1.2 Arterial flow territories . . . 25

3 State of the art **27**

4 Materials and Methods **31**
4.1 Participants and data . . . 31
4.1.1 Participants . . . 31
4.1.2 Study design . . . 32
4.1.3 Image acquisition . . . 32
4.2 BOLD-fMRI data processing and analysis . . . 34
4.2.1 Preprocessing and registration . . . 34
4.2.1.1 Preprocessing . . . 34
4.2.1.2 Registration and normalization . . . 36
4.2.2 Subject-level BOLD-fMRI data analysis . . . 37
4.2.2.1 Function-specific BOLD fMRI data analysis . . . 37
4.2.2.2 Breath-hold BOLD fMRI data analysis . . . 39
4.2.2.2.1 Cerebrovascular reactivity (CVR) and time-to-peak (TTP) maps computation . . . 40
4.2.3 Group-level BOLD-fMRI data analysis . . . 42
4.2.3.1 Voxel-wise analysis . . . 42
4.2.3.1.1 Whole-brain . . . 43
4.2.3.1.2 Region-specific . . . 43
4.2.3.1.2.1 Cerebral lobes . . . 43
4.2.3.1.2.2 Arterial flow territories . . . 44
4.2.3.2 Region-of-interest (ROI) analysis . . . 46
4.2.3.2.1 Correlation with clinical features . . . 46

5 Results and Discussion **49**
5.1 Subject-level BOLD-fMRI data analysis . . . 49
5.1.1 Function-specific BOLD fMRI data analysis . . . 49
5.1.2 Breath-hold BOLD fMRI data analysis . . . 51
5.1.2.1 Cerebrovascular reactivity (CVR) and time-to-peak (TTP) maps computation . . . 51
5.2 Group-level BOLD-fMRI data analysis . . . 52
5.2.1 Voxel-wise analysis . . . 52
5.2.1.1 Whole-brain . . . 52
5.2.1.2 Region-specific . . . 55
5.2.1.2.1 Cerebral lobes . . . 55

5.2.1.2.2 Arterial flow territories 56
5.2.2 Region-of-interest (ROI) analysis 61
5.2.2.1 Correlation with clinical features 62

6 Conclusions **65**
6.1 Limitations and future work 65

Bibliography **69**

List of Tables

2.1 Advantages and disadvantages of several vasoactive stimuli for hypercania induction (acetazolamide injection, CO_2 inhalation, and breath-holding). 12

2.2 Advantages and disadvantages of several neuroimaging techniques for CBF assessment: Transcranial Doppler Ultrasound (TCD), radiotracer imaging techniques (SPECT and PET), and functional Magnetic Resonance Imaging (fMRI). 13

3.1 Cerebrovascular reactivity studies in migraine, presented in chronological order (most recent first). 29

4.1 Demographics and clinical parameters, averaged across participants. 31

4.2 Clinical parameters characterising the ongoing attack in S1, averaged across participants. 32

4.3 Acquisition parameters referent to the three BOLD datasets (breath-holding challenge, motor task, and visual stimulation). 33

4.4 General migraine clinical parameters and migraine clinical parameters characterizing the ongoing attack in the day of S1, for each participant. 47

5.1 Characteristics of the two larger clusters showing significant ictal $>$ interictal brain activation differences in response to visual stimulation. 53

5.2 Pearson correlation analysis between mean CVR and TTP values within the regions-of-interest (ROIs) in each session and participants' general clinical parameter and clinical parameters characterizing the ongoing attack. The ρ corresponds to the Pearson correlation coefficient. 63

List of Figures

2.1 Graphical representation of the migraine cycle, with the ictal phase representing a whole attack and the interictal corresponding to the between-attack phase. Within a complete classic migraine attack with aura, four phases can be distinguished: the prodrome phase, the aura phase, the headache phase and the postdrome phase. The principal symptoms associated to each one of the four phases are listed. Figure based on information from [2, 8, 14]. 6

2.2 Schematic representation of the relationship between a transient increase in neural activity and the corresponding BOLD signal. Neuronal activity causes increased cerebral metabolic rate of oxygen consumption ($CMRO_2$), leading to alterations in the tone of the surrounding vasculature through neurovascular coupling. Such vascular adjustments lead to changes in the cerebral blood flow (CBF) and cerebral blood volume (CBV). The interaction between these 3 parameters leads to the blood oxygenation level dependent (BOLD) signal as measured in fMRI. Figure adapted from [97]. 16

2.3 Example of a 4D fMRI dataset. For easier illustration, a single slice of each 3D volume is shown, but the 4D data contains a full 3D image sampled throughout time. Extracting the intensities over time from a single voxel gives a timeseries (a set of intensities over time), as illustrated on the bottom right. Figure extracted from [98]. 16

2.4 Standard pipeline for fMRI data preprocessing steps. 17

2.5 Depiction of the General Linear Model (GLM) approach applied in first-level analysis. The data from an imaginary voxel with timeseries Y is predicted by a design matrix X including 10 effects (3 regressors of interest and 7 regressors of no interest - e.g., 6 motion parameters and 1 linear drift) of unkwown amplitude β, and an error term ε. Figure adapted from [100]. 18

2.6 Illustration of the canonical double-gamma hemodynamic response function (HRF). It depicts the change in BOLD signal as a function of time, as would be expected in response to a very short stimulus. Figure adapted from [98]. 21

2.7 (Left) Illustration of the major arteries of the human brain: the common carotid arteries (with two divisions - the external and internal carotid arteries -), and the vertebral arteries. Figure adapted from [125]. (Right) Illustration of the Circle of Willis, emphasizing the anterior cerebral arteries (ACA), the middle cerebral arteries (MCA), the posterior cerebral arteries (PCA), and the vertebrobasilar artery (VBA). Figure adapted from [126]. 25

4.1 Illustration of the three fMRI paradigms used in this work. (Top) Motor task paradigm. (Center) Visual stimulation paradigm. (Bottom) Breath-holding task paradigm. 34

4.2 Representative design matrix and contrasts used in subject-level GLM to assess brain activation in response to the motor task for one illustrative subject and session. 38

4.3 Representative design matrix and contrasts used in subject-level GLM to assess brain activation in response to the visual task for one illustrative subject and session. 39

4.4 Representative design matrix and contrasts used in subject-level GLM to assess brain activation in response to the breath-holding challenge for one illustrative subject and session. 40

4.5 Schematic representation of the computation of the CVR metrics from the sinusoidal modelling obtained from the GLM. BOLD percentage signal change consists in the amplitude of the model's maximum (point *a*) relative to the average signal during the first baseline period (initial 25 seconds) multiplied by 100. Time-to-peak (TTP) consists in the time of the model's maximum (point *a*) relative to the onset of the BH. 41

4.6 Cerebral lobes masks used for the region-specific group-level analysis performed in this study: frontal, occipital, parietal and temporal lobe masks. The masks were defined in the standard MNI152 space. All masks are represented in the sagittal, coronal and axial planes (from left to right) for better representation. A and P mark the anterior and posterior sides in the sagittal and axial representations. R and L mark the right and left sides in the coronal and axial representations. S and I mark the superior and inferior directions in the sagittal and coronal representations. 44

4.7 Arterial flow territories masks used for the region-specific group-level analysis performed in this study: internal carotid arteries (ICA) and vertebrobasilar artery (VBA) masks. The lighter red corresponds to the overlap of both masks. The masks were defined in the standard MNI152 space. All masks are represented in the sagittal, coronal and axial planes (from left to right) for better representation. A and P mark the anterior and posterior sides in the sagittal and axial representations. R and L mark the right and left sides in the coronal and axial representations. S and I mark the superior and inferior directions in the sagittal and coronal representations. 45

4.8 Vertebrobasilar artery (VBA) flow territory mask overlapped with four respective segmented regions masks: brainstem, cerebellum, occipital lobe, and thalamus (from left to right) used for the region-specific group-level analysis performed in this study. The masks were defined in the standard MNI152 space. All masks are represented in the sagittal, coronal and axial planes (from left to right) for better representation. A and P mark the anterior and posterior sides in the sagittal and axial representations. R and L mark the right and left sides in the coronal and axial representations. S and I mark the superior and inferior directions in the sagittal and coronal representations. 46

5.1 Representative brain activation maps in response to the motor task (top) and visual stimulation (bottom) for one illustrative subject and session. The map is represented as a thresholded Z-map ($Z>3.1$) in the standard MNI152 space. The z coordinate in the standard space is shown for the most inferior and most superior slices in the axial plane. . . . 50

5.2 Representative cerebrovascular reactivity (CVR, %BOLD) and time-to-peak (TTP, s) maps for one illustrative subject and session. The maps are represented in the standard MNI152 space. The z coordinate in the standard space is shown for the most inferior and most superior slices in the axial plane. 51

5.3 Group-level analysis of brain activation maps in response to visual stimulation: map of statistically significant differences between the ictal and interictal phases. Increased brain activation was found in the ictal vs. interictal phase ($p<0.05$). The map is represented in the standard MNI152 space. The z coordinate in the standard space is shown for the most inferior and most superior slices in the axial plane. 53

5.4 Boxplots representing the distributions across patients of the mean CVR and TTP values within the GM for each session. In the boxplots, the central mark is the median; the edges of the box are the 25th and 75th percentiles; the upper and lower extreme represent, respectively, the maximum and minimum values (excluding outliers). 54

5.5 Group-level analysis of CVR and TTP maps performed within the occipital lobe mask: maps of statistically significant differences between the ictal and interictal phases. Increased CVR and TTP were found in the ictal vs. interictal phase ($p<0.05$). The map is represented in the standard MNI152 space. The z coordinate in the standard space is shown for the most inferior and most superior slices in the axial plane. 56

5.6 Group-level analysis of CVR and TTP maps performed within the VBA flow territory mask: maps of statistically significant differences between the ictal and interictal phases. Increased CVR and TTP were found in the ictal vs. interictal phase ($p<0.05$). The map is represented in the standard MNI152 space. The z coordinate in the standard space is shown for the most inferior and most superior slices in the axial plane. 57

5.7 Group-level analysis of CVR and TTP maps performed within the VBA flow territory mask overlapped with the occipital lobe mask: maps of statistically significant differences between the ictal and interictal phases. Increased CVR and TTP were found in the ictal vs. interictal phase ($p<0.05$). The map is represented in the standard MNI152 space. The z coordinate in the standard space is shown for the most inferior and most superior slices in the axial plane. 58

5.8 Boxplots representing the distributions across patients of the mean ictal and interictal CVR and TTP values within the ictal>interictal regions-of-interest (ROIs) found by the region-specific, voxelwise group-level analysis shown in figures 5.5, 5.6 and 5.7. In the boxplots, the central mark is the median; the edges of the box are the 25th and 75th percentiles; the upper and lower extreme represent, respectively, the maximum and minimum values (excluding outliers). The ANOVA test revealed significant differences ($p<0.05$) for the CVR and TTP differences between the ictal and interictal phases within all the three ROIs, which are marked with an asterisk. 62

Acronyms

ACA Anterior Cerebral Arteries.

ANOVA Analysis of Variance.

ASL Arterial Spin Labeling.

BA Basilar Artery.

BBR Boundary-Based Registration.

BET Brain Extraction Tool.

BH Breath-Holding.

BOLD Blood Oxygenation Level Dependent.

BOLD-fMRI Blood Oxygenation Level Dependent-functional Magnetic Resonance Imaging.

CBF Cerebral Blood Flow.

CBV Cerebral Blood Volume.

CM Chronic Migraine.

$CMRO_2$ Cerebral Metabolic Rate of Oxygen consumption.

CO_2 Carbon Dioxide.

COPEs Contrast of Parameter Estimates.

CSF Cerebrospinal fluid.

CVR Cerebrovascular Reactivity.

EM Episodic Migraine.

EPI Echo-Planar Imaging.

EVs Explanatory Variables.

FAST FMRIB's Automated Segmentation Tool.

FDR False Discovery Rate.

FE Fixed Effects.

FEAT FMRIB's Expert Analysis Tool.

FILM FMRIB's Improved Linear Model.

FIX FMRIB's ICA-based Xoiseifier.

FLAME FMRIB's Local Analysis of Mixed Effects.

fMRI Functional Magnetic Resonance Imaging.

FMRIB Functional Magnetic Resonance Imaging of the Brain.

FNIRT FMRIB's Non-Linear Registration Tool.

FSL FMRIB Software Library.

FUGUE FMRIB's Utility for Geometrically Unwarping EPI.

FWE Family-Wise Error.

FWHM Full Width Half Maximum.

GE-EPI Gradient Echo-Echo Planar Imaging.

GLM General Linear Model.

GM Grey Matter.

GUIs Grapgical User Interfaces.

HbO$_2$ Oxyhemoglobin.

HC Healthy Controls.

HHb Deoxyhemoglobin.

HIT Headache Impact Test.

HRF Hemodynamic Response Function.

ICA Internal Carotid Arteries.

ICHD-3 International Classification of Headache Disorders, 3rd edition.

MCA Middle Cerebral Arteries.

MCFLIRT Motion Correction FMRIB's Linear Registration Tool.

ME Mixed Effects.

MNI Montreal Neurological Institute.

MPRAGE Magnetization-Prepared Rapid Gradient Echo.

MR Magnetic Resonance.

MRI Magnetic Resonance Imaging.

MwA Migraineurs with Aura.

MwoA Migraineurs without Aura.

O$_2$ Oxygen.

PaCO$_2$ Arterial blood partial pressure of CO_2.

PCA Posterior Cerebral Arteries.

PEs Parameter Estimates.

PET Positron Emission Tomography.

PETCO$_2$ End-tidal CO_2 Partial Pressure.

rCBF regional Cerebral Blood Flow.

ROI Region of Interest.

ROIs Regions of Interest.

RRF Respiratory Response Function.

RSFA Resting State Fluctuation Amplitude.

RVT Respiration Volume per Time.

SD Standard Deviation.

SNR Signal-to-Noise Ratio.

SPECT Single-Photon Emission Computed Tomography.

SUSAN Smallest Univalue Segment Assimilating Nucleus.

TCD Transcranial Doppler Ultrasound.

TD Temporal Derivative.

TE Echo Time.

TFCE Threshold-Free Cluster Enhancement.

TR Repetition Time.

TTP Time-To-Peak.

VAS Visual Analogue Scale.

VBA Vertebrobasilar Artery.

WHO World Health Organization.

WM White Matter.

Chapter 1

Introduction

This Master's Thesis aims to investigate neurovascular changes of migraine by investigating differences in cerebrovascular reactivity (CVR) and brain activation in distinct periods of this cyclic disease. To do so, analysis of blood oxygen level dependent functional magnetic resonance imaging (BOLD-fMRI) data from a group of patients with episodic migraine without aura was conducted. Each participant was scanned under two different conditions: during a spontaneous migraine attack (ictal phase) and during an attack-free period (interictal phase). In both conditions, data were acquired during a breath-holding (BH) challenge, visual stimulation, and a motor task.

This chapter starts by describing the motivation behind this study (section 1.1), followed by the main objectives aimed to be achieved by this work in section 1.2 and publications arising from this thesis (section 1.3) and the last section (1.4) provides a thesis outline, with an overview of the several chapters.

1.1 Motivation

Migraine is one of the most prevalent and disabling diseases worldwide [1]. It was ranked second in terms of disability in a global scale, and presented no association with sociodemographic development, which means that it affects both low- and high-income countries [1]. It is a brain disorder that affects predominantly young and middle-aged women, in particular when they are highly active in the professional area, therefore causing a significant loss of productivity [1]. Thus, it not only causes a general reduction of quality of life with consequent societal concern, but it also represents a significant financial burden on economies worldwide [2]. Migraine is a complex cyclic disorder, characterized by intermittent attacks of throbbing head pain alternated with attack-free periods. The headache attack is usually accompanied by neurological symptoms including increased sensitivity to movement, light (photophobia), sound (phonophobia) and any other sensorial inputs [2]. Additionally, the fact of resulting from a combination of genetic predisposition and environmental factors adds greater complexity to this disorder.

Adding to the enormous impact caused by the disease itself, it has been observed that migraineurs are at increased risk for cardiovascular disease, including conditions such as stroke, myocardial infarction, and cardiovascular mortality [3, 4]. Cerebrovascular reactivity (CVR) measurements have great

potential as a way to detect cerebrovascular pathophysiology and possible consequent vascular events in migraineurs' brain. CVR is commonly assessed using transcranial Dopller ultrasound (TCD) combined with hypercapnia-inducing stimuli to measure vasodilation and blood flow changes in the main cerebral arteries. More recently, BOLD-fMRI has been used to obtain more accurate CVR measurements across the whole-brain with high spatial resolution. It has been observed that CVR is impaired in the posterior circulation of migraineurs, and suggestions arose of reduced CVR being a key link between migraine and stroke [5]. However, only a few studies have investigated CVR in migraine. Almost all of them used TCD, assessing specific large arteries of the brain thus lacking regional information. fMRI appears as an indispensable tool for a whole-brain CVR evaluation. Furthermore, the majority of studies reported interictal (between attacks) measurements compared to healthy controls (HC). No study to date has used fMRI to measure CVR during migraine attacks. Being migraine a cyclic disorder, great potential is achieved by studying the brain activity of patients along different phases of the migraine cycle, as it is conducted in this study. Comparing to analysing migraine patients versus HC, studying migraineurs in a longitudinal approach allows the investigation of attack-specific neurovascular alterations [2]. This examination could allow a better description of migraine-specific characteristics, the identification of imaging biomarkers, the stratification of patients according to cardiovascular disease risk, the development of therapeutic agents and the evaluation of treatment response.

1.2 Thesis objectives

In this study, the main goal is the investigation of vascular reactivity changes during migraine attacks compared to attack-free periods through the analysis of BOLD-fMRI data. As a secondary objective, we also analysed neurovascular changes in response to brain activation associated with visual stimulation and with the performance of a motor task. With this purpose, previously collected data from a group of migraine patients during an attack and in an attack-free period was analyzed, including BOLD-fMRI data during visual stimulation, motor task, and a BH challenge. Information regarding the participants' migraine clinical features was also collected, allowing the investigation of how such parameters relate to CVR differences.

In order to successfully accomplish these objectives, specific goals were defined:

1. To process the functional data from all participants in both sessions, through appropriate preprocessing steps followed by a General Linear Model (GLM) approach and subsequent statistical inference. This allowed the attainment of individual maps showing the brain regions that activated in response to BH, motor task, and visual stimulation for the two sessions.

2. To obtain whole-brain maps describing the CVR for each subject and each session. CVR and time-to-peak (TTP) maps were constructed from the GLM referent to the BOLD response to the BH challenge, and CVR was characterized by the BOLD percent signal change and by the TTP of the BOLD signal.

3. To identify brain regions showing altered CVR, TTP, and brain activation during migraine attacks when compared to attack-free periods, by conducting a group-level analysis. This allowed the definition of regions of interest (ROIs), i.e. brain regions showing significant CVR and/or TTP differences between both sessions. Furthermore, the relationship between the averaged CVR and TTP within the ROIs and several migraine clinical features was also matter of investigation.

1.3 Publications arising from this thesis

The work developed in this thesis resulted in an abstract submission, which was selected for an oral presentation in the European Society for Magnetic Resonance in Medicine and Biology (ESMRMB) congress, that took place online between the Semptember 30th and October 1st 2020 [6].

1.4 Thesis Outline

This dissertation is organized in 6 main chapters. The first and current chapter consists in a brief introduction to this work, where the motivation for the study and main objectives to be accomplished have been described. Next, chapter 2 introduces the theoretical background behind this work, covering a description of migraine and its associated vasculopathy in section 2.1. Section 2.2 contains relevant information about the concept of CVR, along with the vasoactive stimuli and neuroimaging techniques that can be used to assess it. Following, section 2.3 comprises pertinent material on functional magnetic resonance imaging, such as the contrast used in this study and common data preprocessing and processing methods. In addition, it also focuses on specific topics regarding CVR, in particular the way CVR and TTP maps can be obtained, as well as specific brain regions that are more interesting to evaluate. Chapter 3 consists in the State of the Art, where a literature review can be found, focusing on previous studies assessing CVR in migraine, directly or indirectly related to the present work. Afterwards, chapter 4 starts with a description of the participants recruited for this work, the study design and the acquired fMRI data. Next, section 4.2 presents the methodology applied in order to achieve this dissertation's objectives: starting with information regarding preprocessing steps, going through subject-level analysis and computation of CVR and TTP maps, and ending with a group-level BOLD-fMRI data analysis and correlation with migraine clinical features. Chapter 5 focuses on the description of the results achieved at both the subject-level and group-level analysis (sections 5.1 and 5.2, respectively). Simultaneously with results' exposure, these are discussed and interpreted along with their comparison with findings from previous studies.

This dissertation ends with chapter 6, where the main conclusions to be drawn from this work are exposed, together with its main limitations and suggestions for future work.

Chapter 2

Theoretical Background

2.1 Migraine

Migraine is a severe and disabling neurological disorder, causing significant individual and societal burden due to pain, resulting disability with lost productivity, and an overall decreased quality of life [7].

In 2016, out of 328 diseases and injuries considered by the World Health Organization (WHO), migraine was the sixth most prevalent, and it was ranked second globally in terms of years lived with disability by the first study in subjects under 50 years old [1].

This disease is a relevant health problem in both genders and all age groups, but predominantly affects young and middle-aged females: there is a 3:1 female-to-male ratio, and it is most prevalent between the ages of 15 and 49, a time when most people are highly active in the professional area [1].

Importantly, unlike many other diseases, headache presents no clear relation to sociodemographic development, meaning that it is not limited to the high-income countries, but instead being an important cause of disability worldwide [1].

Migraine is a clinical syndrome characterised by headache with specific features and associated symptoms. It is a disease of cyclical nature, where intermittent headache attacks - ictal phase - alternate with attack-free periods - interictal phase. Typical characteristics of the headache are its unilateral location, pulsating quality, moderate to severe intensity, and variability in duration (between 4 and 72 hours). The headache attacks are usually aggravated by routine physical activity and are normally accompanied by a variety of autonomic symptoms (nausea, vomiting, nasal/sinus congestion, lacrimation, yawning), affective symptoms (depression and irritability), cognitive symptoms (attention deficit, difficulty finding words, transient amnesia, and reduced ability to navigate in familiar environments), and sensory symptoms (photophobia, phonophobia, osmophobia, muscle stiffness, and cutaneous allodynia) [8–11].

In around 70-80% of migraine patients, the headache is preceded by a prodromal phase, where symptoms such as fatigue, irritability, reduced concentration, neck stiffness, photo-/phonophobia, nausea and yawning appear up to 48 hours before the headache [8].

Most headaches are followed by up to 48 hours of feeling tired, together with difficulty with concentration and neck stiffness, called the postdrome phase [8].

In addition, approximately 20 to 40% of migraine patients suffer from migraine aura just before and/or during the headache phase. Migraine aura includes a variety of visual (most common), sensory, speech, and/or other neurological symptoms that usually develop gradually. The accepted duration for most aura symptoms is one hour [8, 12]. Positive (gain of function) and negative (loss of function) symptoms can take place, such as scintillating lights when affecting the visual cortex; paresthesia and numbness of the face and hands when affecting the somatosensory cortex; tremor and unilateral muscle weakness when affecting the motor cortex; and aphasia (difficulty saying words) when affecting the speech area [13]. Figure 2.1 represents the migraine cycle, with the ictal phase consisting of a whole migraine attack, where the duration of the four phases and principal associated symptoms are shown.

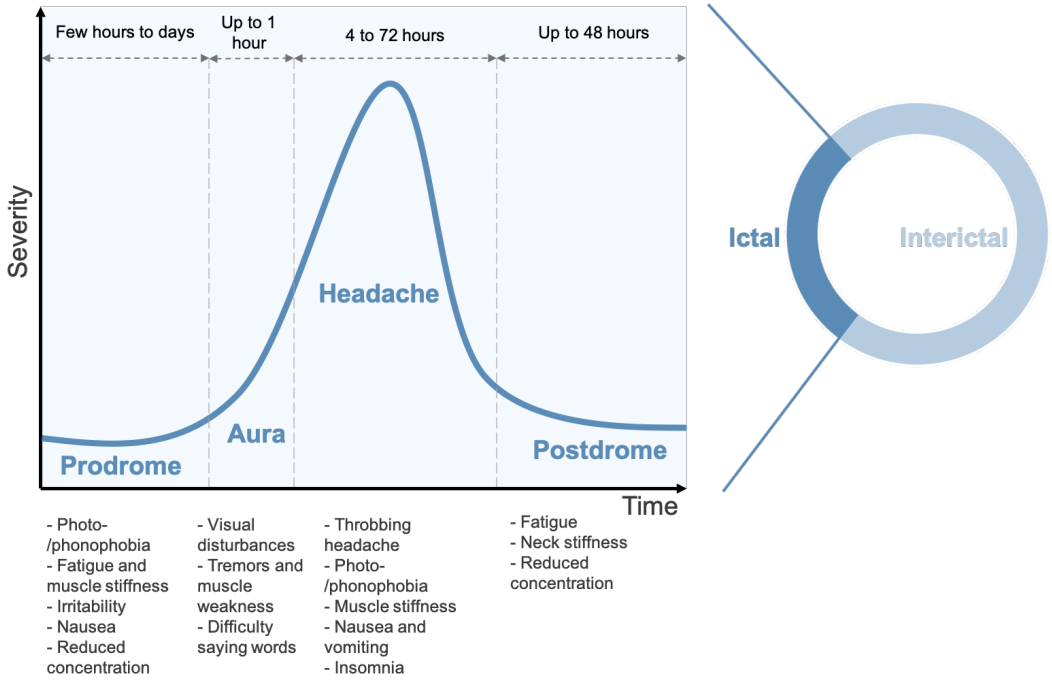

Figure 2.1: Graphical representation of the migraine cycle, with the ictal phase representing a whole attack and the interictal corresponding to the between-attack phase. Within a complete classic migraine attack with aura, four phases can be distinguished: the prodrome phase, the aura phase, the headache phase and the postdrome phase. The principal symptoms associated to each one of the four phases are listed. Figure based on information from [2, 8, 14].

The extent of the described symptoms suggests that migraine is more than just a headache, but instead it is a complex and multifaceted disorder which can last over several days. Although it is possible to distinguish four main phases of a migraine attack (prodrome, aura, headache, and postdrome), these do not usually follow a sequential order, but instead overlap with each other. Besides, the clinical manifestations of migraine probably depend upon a complex relationship between genetic, environmental and endogenous cognitive and emotive factors (migraine susceptibility), which enhance migraine complexity [2, 15].

According to the third edition of the International Classification of Headache Disorders (ICHD-3) [8], migraine can be subtyped as episodic migraine (EM) or chronic migraine (CM) based on the frequency of headache days. EM refers to a diagnosis of migraine with frequency of headache occurring on fewer than 15 days per month on average. CM is defined as a diagnosis of migraine with 15 or more

headache days per month, for more than 3 months, of which at least eight days have the features of migraine headache.

2.1.1 Migraine pathophysiology

The debate over the pathophysiology of migraine extends back to the middle decades of the 20th century, and has always been centered on neural versus vascular mechanisms that may be involved in triggering and driving the attacks.

Until the 1980s, the predominant explanation for migraine was the vasogenic theory, which held that migraine was a form of cerebrovascular dysregulation. It assumed that vasodilation of extracranial arteries and also intracranial blood vessels produced mechanical activation of perivascular nerve fibers that innervate the vessels, resulting in head pain [16].

The alternative neurogenic theory viewed migraine as a disorder of the brain, and considered that vascular changes were the result of neuronal dysfunction. In the late 1980s it was proposed that migraine pain may be due to a neurogenically induced inflammation of the dura matter [17, 18]. However, the use of specific proteins as migraine treatments failed, which called for new explanations [19, 20]. Further studies suggested the role of brainstem regions in migraine attacks, and even named brainstem as the “migraine generator” [21, 22]. This brainstem ”generator” theory has been debated over the last years, and resulted in the concept of a unique migraine generator being abandoned. Instead, much research has focused on other specific brain structures that may be involved. For example, it was observed hypothalamic activation during the prodromal phase [23] and during spontaneous migraine headache [24]. In addition, functional neuroimaging has detected altered functional connectivity between the hypothalamus and the areas of the brainstem “generator” during the 24h preceding a migraine attack, which led the authors to think that this network’s connectivity change might be the driver of attacks [25]. The thalamus has also been a matter of discussion, showing structural and functional alterations in migraineurs during the ictal and interictal phases of migraine which might influence the onset of the migraine attack [26–28]. Furthermore, the thalamus is a central area for the processing and integration of pain stimuli and its connection to a wide variety of cortical areas could explain part of the complexity of several migraine symptoms such as sensory hypersensitivity to visual stimuli [29]. Finally, several migraine therapies are thought to act centrally through the modulation of thalamic neurons [30, 31].

Having said that, migraine is currently recognized as a complex brain disorder that involves multiple brain regions - from cortical, subcortical, to brainstem regions - to account for both the pain and the variety of symptoms characterizing the attack. Simultaneously, there is evidence that migraine is associated with vascular dysfunction, both as a cause and a consequence [32]. Supporting this vascular involvement in migraine pathophysiology, there is evidence that the trigeminovascular pathways (neurons in the trigeminal nerve that innervate cerebral blood vessels) which specifically innervate the dural vasculature are activated and sensitized during a migraine attack, and studies show that vasodilators such as nitric oxide and CGRP (most potent vasodilator transmitter identified in the cerebral circulation [33]) are able to trigger migraine attacks. Additionally, CGRP-based drugs have shown a vasoconstrictive and

therapeutic effect, which also support the view that vascular changes are certainly involved in migraine attacks.

Having said, although the full pathophysiology of migraine is still incompletely understood, the consensus nowadays is of the neurovascular hypothesis being the most likely explanation, as it emphasizes the coupling between neural and vascular mechanisms: the condition is viewed as an inherent disorder of the brain, but vascular mechanisms are clearly implicated.

2.1.2 Migraine-associated vasculopathy

As presented, vascular changes are assumed to be an important pathophysiological factor in migraine disorder.

Migraine and cerebral ischemia have been linked for around 30 years, with reports of ischemic stroke (obstruction of a vessel supplying blood to the brain) occurring during and between migraine attacks [3, 34–38]. A hospital study suggested that, of all unusual causes of first-ever ischemic stroke, migraine accounted for 13% [39]. Adding to this, in a more recent meta-analysis of 21 observational studies regarding the association between migraine headache and ischemic stroke, migraine was reported as a significant risk factor for stroke, being independently associated with a 2-fold increased risk of ischemic stroke, with no significant differences between migraine with and without aura [40]. Importantly, the association between migraine and ischemic stroke showed to be independent of other cardiovascular risk factors, supporting the idea that there is a subgroup of people with migraine and vasculopathy even in the absence of atherosclerotic disease. Besides ischemic stroke, migraine was also associated with higher risk of hemorraghic stroke (rupture and bleeding of a blood vessel in the brain) [41], transient ischemic attacks (TIA) (temporary blockage or decreased blood flow to the brain) [42], and subclinical brain infarction (asymptomatic cerebral infarction, also called ”silent cerebral infarction”) [43]. Additionally, imaging evidence for the migraine-stroke association showed a high incidence of infarct-like lesions and white matter lesions in migraineurs [44–46], and imaging studies in migraine patients suffering from stroke have confirmed that infarct progression is accelerated, with reduced size of potentially salvageble brain tissue when compared to those stroke patients without a history of migraine [47]. Moreover, migraine has been associated not only with cerebral vasculopathy, but also with more widespread vascular changes, such as ischemic heart disease and myocardial infarction [3]. In addition, patients with migraine were found to be more likely to develop cardiovascular disease than those reporting no migraine history [4], which led the American Heart Association to provide specific recommendations for stroke prevention in women suffering from migraine [48].

Migraine and cardiovascular disease are among the most prevalent and disabling diseases in the world [49]. Because of their high prevalence and consequences on morbidity and mortality in the general population, a potential association between migraine and stroke/cardiovascular disease would have a substantial impact on public health.

Several proposed mechanisms have been suggested to be involved in this association, such as genetic risk factors, cardiac abnormalities, and atherosclerotic and nonatherosclerotic causes. Aiming to

investigate this possible connection, particular interest has been raised in the role of vasculature in migraineurs. In recent years, it has been proposed that the vasculopathy in migraine is thought to reflect endothelial dysfunction. The endothelium is the monolayer of endothelial cells lining the lumen of all blood vessels. It acts as a key regulator of vascular homeostasis, playing a direct role in the balance of tissue oxygen supply and metabolic demand via regulation of vessel tone and diameter [50]. Endothelial dysfunction is a pathological state of the endothelium resulting in impaired endothelium-dependent vasodilation, impaired vascular reactivity, hypercoagulability and inflammation. Subsequently, endothelial dysfunction is predictive of an increased rate of cerebrovascular and cardiovascular events, and is frequently referred as ”the ultimate risk of the risk factors” [51]. There is mounting evidence that migraine is linked to endothelial dysfunction. This includes decreased vasodilation, lower levels of inflammation markers, and increased thickness of the carotid intima media in migraine patients compared to healthy subjects [52], as well as fewer circulating endothelial-precursor cells in migraineurs compared to healthy controls [53, 54]. Importantly, while there have been controversial reports on systemic endothelial dysfunction, with studies not unanimously suggesting an impairment of systemic endothelial function in migraine, cerebral endothelial dysfunction has been reported to be impaired in migraineurs even in the absence of the systemic endothelial dysfunction [55]. All together, these results strongly support the idea of a dysfunctional cerebral endothelium playing an important role in the association between migraine and cardiovascular disease.

2.2 Cerebrovascular Reactivity (CVR)

Considering the above mentioned, especially the fact that endothelial dysfunction can be characterised by impaired vascular reactivity, it is of great interest to study changes of cerebrovascular regulation in migraine, as a way of identifying endothelial dysfunction and potential consequent vascular events in migraineurs' brain, this way shedding light into possible mechanisms of the migraine-stroke relationship.

Cerebrovascular reactivity, or CVR, is an intrinsic regulatory brain mechanism whereby blood vessels adjust their calibre in response to a vasoactive stimulus, in order to increase or decrease regional cerebral blood flow (CBF). Thus, this physiological parameter is an important index of the brain's vascular health. Measuring CVR variations within the brain has been able to detect cerebrovascular pathophysiology such as arterial stenosis [56], increased stroke risk [57, 58], brain tumours [59], and traumatic brain injury [60].

CVR is usually measured by applying a challenge to the vasculature and assessing the associated CBF changes. Thus, as it usually represents the unit change in CBF per unit change in a vasoactive stimulus, it is important that both of these variables are measured accurately and applied consistently across study subjects. Failure to do so can lead to differences in CVR measurements within subjects and between subject groups that are due to the methodological limitations and variability in techniques and not the disease processes under investigation.

2.2.1 Vasoactive stimuli

In order to obtain an accurate measure of CBF, it is important that the vasoactive stimulus produces a quantifiable and reliable effect on the cerebral vasculature. In addition, this standardized stimulus has to be applied across subjects and during assessments within the same subject. Otherwise, it will be impossible to conclude whether the differences in CVR are due to disease mechanisms or technique variability [61].

The most common approach involves the induction of hypercapnia, whereby the arterial blood partial pressure of carbon dioxide ($PaCO_2$) is increased, leading to vasodilation and increased CBF. The main hypercapnia-inductive stimuli fall into two categories: (i) administration of exogenous vasodilating agents, or (ii) manipulation of respiratory gases. A summary comparison of these approaches is presented on Table 2.1.

Acetazolamide falls into the first category. It is a selective inhibitor of the enzyme carbonic anhydrase, which decreases the conversion rate of CO_2 to bicarbonate, inducing an intracellular and extracellular acidosis (due to the increase of CO_2) and producing a vasodilatory effect. This technique was first used to measure CVR in 1986 [62], and has the advantages of allowing precise control of the amount of acetazolamide that is injected and requiring little subject adherence, which make it reproducible independent of subject cooperation. However, the injection of acetazolamide can be considered an invasive procedure, as it requires intravenous access, and can elicit variable side effects in different individuals: while low doses of acetazolamide can provoke dizziness, nausea, headache and fatigue lasting 0.5-72h [63], higher doses can lead to more severe effects, which may require treatment and even imply the terminus of the study [64]. Moreover, the most significant disadvantage of this technique for use in CVR studies is the acetazolamide's unpredictable pharmacokinetics and resultant effects on CBF: it has been found that a standardized dose does not generate the reproducible stimulus required for standardizing the measurement. More precisely, the same dose lead to different serum concentrations and cerebrovascular responses in different individuals [65], and even using large enough doses of acetazolamide did not produce a maximal CBF response in many normal subjects [64].

Administration of the aminoacid L-arginine has also been used to induce hypercapnia, since it has shown to induce vasodilation through enhanced production of nitric oxide in the cerebral endothelium [5]. Likewise acetazolamide, L-arginine requires intravenous infusion, thus being considered an invasive procedure.

The alternative approach of inducing hypercapnia consists in the manipulation of respiratory gases. This includes CO_2 inhalation: subjects are given a gas mixture with an increased CO_2 partial pressure, normally consisting of approximately 21% O_2 and 4-5% CO_2 with balanced nitrogen ("room" air contains 0.04% CO_2). More important than the CO_2 composition of the inspired gas is the resulting level of end-tidal CO_2 partial pressure ($PETCO_2$) (at the end of expiration), as this is thought to be representative of the $PaCO_2$ (the actual stimulus) [65]. Different techniques have been developed with the goal of manipulating the end-tidal pressure of respiratory gases [66–69]. This precise manipulation can be achieved despite variable ventilatory responses, which make these methods reliable [70]. However, they require complex and expensive experimental setups together with trained on-site personnel. Also, the

inhalation mask can be uncomfortable, and some individuals have experienced anxiety or panic attack symptoms [71]. Not only these symptoms cause discomfort to the subject, but they also can confound the measurement of CBF.

Alternative strategies have been proposed, based on respiratory tasks such as hyperventilation/paced deep breathing and breath-holding (BH). The BH technique involves short-duration periods of apnea, typically in the range of seconds, that lead to CO_2 increase and consequent vasodilation and CBF increase, alternated with periods of normal breathing. The primary advantage of this technique is its total noninvasiveness and relatively simple and inexpensive implementation (it requires no breathing circuits or equipment). Unfortunately, the BH technique is less controlled and, when used alone, it lacks the ability to measure delivered or expired gases. Even so, BH tasks showed to lead to mild hypercapnia and consequent vasodilation, and have been validated to be comparable to CO_2 inhalation, with studies founding no significant differences between CVR measurements obtained with both methods [72]. Moreover, the mild hypoxia that BH was shown to provoke has not significantly influenced CVR results when compared to methods that control respiratory gases levels [73, 74]. Hyperventilation or paced deep breathing methods, although equally as feasible, lead to hypocapnia-associated vasoconstriction and could be less intuitive in measuring cerebral blood vessel function [75]. Both of these strategies rely solely on the subject's ventilatory response and are well tolerated by healthy volunteers and patients. However, a potential drawback is that they may bring participant-related variability in adherence to the protocol. For example, some participants may find it difficult to follow the instructions and consequently perform hyperventilation or BH differently, which can affect the data quality and reliability of the methods. Nevertheless, several studies have proved that the BH task has many advantages over CO_2 administration due to its simplicity, especially when used with clinical populations [76–78].

Recently, resting-state fMRI, which is often used for functional connectivity mapping, has been shown to provide an estimation of CVR maps [79–81]. This approach exploits spontaneous fluctuations in the breathing pattern, and thus the CO_2 level, to extract CVR information from the resting-state BOLD signal changes. Good agreement between resting-state CVR results and hypercapnia CVR results has been reported [79, 81]. In general, the resting-state CVR method requires minimal subject compliance, overcoming task-related measurement inconsistencies, which makes it easier to perform by patients with more severe conditions. A limitation of the resting-state method is that, if the subject breathes regularly with minimal fluctuation in CO_2 level, there will not be enough CO_2-related signal variations for CVR evaluation. One study found that modelling the Resting State Fluctuation Amplitude (RSFA)-induced CVR was significantly worse than modelling for BH-CVR [82], and another one concluded that BH-based based vascular reactivity assessment was more reproducible than resting-state-based estimates [83], which indicate that the method needs some further investigations in order to become reliable and even possibly replace the BH task.

Having said, despite BH acknowledged limitations, this task offers significant advantages over the other existing methods, in particular its noninvasiveness and simplicity. In addition, BH-derived CVR measurements were seen to be similar or even superior to those obtained with other vasoactive stimuli. As such, BH stands as a widespread vasoactive stimulus to be employed in CVR studies.

Table 2.1: Advantages and disadvantages of several vasoactive stimuli for hypercania induction (acetazolamide injection, CO_2 inhalation, and breath-holding).

Vasoactive stimulus	Advantages	Disadvantages
Acetazolamide	- Precise control of the amount injected - Requires little subject adherence	- Invasive (intravenous administration) - Large variability in side effects between individuals - Unpredictable pharmacokinetics and effects on CBF
CO_2 inhalation	- Precise control of the amount delivered/expired (despite variable ventilatory responses) - Requires little subject adherence	- Invasive (inhalation mask) - May induce anxiety and/or panic attack symptoms - Fixed fraction amount of inspired CO_2 does not lead to equal $PaCO_2$ (actual stimulus) between and within subjects - Requires complex and expensive experimental setup, as well as trained personnel
Breath-holding	- Non-invasive - Safe - Simple and easy to implement (does not require complex equipment) and inexpensive - Possible to use a nasal cannula to measure $PETCO_2$ (although it lowers the ease of implementation)	- Less controlled and alone lacks the ability to measure delivered/expired gases - Variability in subject adherence - Equal apnea lengths does not lead to equal $PaCO_2$

2.2.2 Neuroimaging techniques for CBF assessment

Regarding the neuroimaging techniques to measure CBF, various have been used in CVR studies. These include Transcranial Doppler Ultrasound (TCD), Positron Emission Tomography (PET), Single-Photon Emission Computed Tomography (SPECT), and functional Magnetic Resonance Imaging (fMRI). A summary comparison of CBF measurement methods is found in Table 2.2.

TCD, first described by Markwalder et al. [84], can be used to measure blood flow velocities by taking advantage of the Doppler effect [85]. It is easily applied to large cerebral arteries and it allows the detection of changes in their mean velocity before and after applying the vasoactive stimulus, which are then used to calculate a reactivity (CVR) index. TCD is a simple, readily available, portable, inexpensive and completely non-invasive method; however, its poor spatial resolution i.e. the fact of only being possible to study large arteries, being user dependent, together with the fact of only allowing the measurement of global blood flow changes and not regional tissue perfusion limit its value [85].

Radiotracer imaging techniques, such as SPECT and PET, explore the properties of radioactive materials, or radiotracers. These materials target different organs in the body and images of their distribution give information about how much, how quickly, and where the radioactive material uptake occurs, which can determine whether tissue is healthy or diseased [85]. To obtain a map of CBF (and hence CVR), appropriate CBF radiotracers are needed. These modalities provide accurate and quantitave regional/tissue CBF measurements, thus enabling whole-brain mapping of CVR, are extremely sensitive (are able to detect nanograms of injected radioactive material) and specific (there is no natural radioactivity from the body). However, these techniques are quite expensive and invasive as they require the administration of radioactive tracers, which can limit their usage in many situations [85].

Alternatively, MRI techniques overcome the limitations of the supra mentioned methods, and allow improved temporal and spatial resolutions. MRI provides a spatial map of the hydrogen nuclei (water and lipid) in different tissues. Among the most common MRI sequences that are used to assess CVR are

blood oxygen level-dependent (BOLD) and arterial spin labeling (ASL). A more detailed explanation of BOLD-fMRI will be given further in Section 2.3.1. Regarding ASL, this is a perfusion imaging technique that provides truly quantitative measurements of CBF. To accomplish this, incoming blood water protons to the brain are labeled and can be measured once the blood reaches the perfusion bed of the target tissue. The balance between labeled intravascular water (reaching the tissue) and non-labeled water in the tissue is proportional to the CBF [86].

The main advantages of both of these MRI techniques are: (i) they are non invasive, with no ionizing radiation being required, (ii) they provide whole-brain scans (the images can be acquired in any two- or three-dimensional plane), and (iii) they allow high spatial resolution (order of 1 mm or less can be achieved). However, MR image acquisition scans might last 30-40 minutes; a significant number of patients have to be excluded due to metallic implants or because they are required to be in a small enclosed space; and they are moderately expensive [85]. Furthermore, and specifically for ASL, its intrinsic low signal-to-noise ratio (SNR) and relatively poor temporal resolution hamper its value and make it less useful for CBF quantification [86].

Despite the mentioned disadvantages, functional magnetic resonance imaging (fMRI) (in particular, BOLD-fMRI) is currently considered the most promising measurement technique of CVR, mainly because it provides whole-brain scans with high spatial resolution.

Table 2.2: Advantages and disadvantages of several neuroimaging techniques for CBF assessment: Transcranial Doppler Ultrasound (TCD), radiotracer imaging techniques (SPECT and PET), and functional Magnetic Resonance Imaging (fMRI).

Neuroimaging technique for CBF measurement	Advantages	Disadvantages
Transcranial Doppler Ultrasound (TCD)	- Non-invasive - Safe - Readily available and inexpensive	- Low spatial resolution (can only measure large arteries) - Only allows the measurement of global blood flow changes, not regional tissue perfusion
Radiotracer imaging techniques (SPECT and PET)	- Provide whole-brain scans - Sensitive (able to detect nanograms of injected radioactive material) - Specific (there is no natural radioactivity from the body) - Accurate and quantitative regional/tissue CBF measurements	- Moderate spatial resolution - Low temporal resolution - Invasive (requires administration of radioactive contrast agents) - Expensive - Less available than TCD
functional Magnetic Resonance Imaging (fMRI)	- Non-invasive - Safe - Readily available - Provides whole-brain scans - High spatial resolution - High temporal resolution - Accurate (and potentially quantitative) regional/tissue CBF measurements	- Long image acquisition scans - Excludes claustrophobic subjects or using metallic implants - Moderately expensive

2.2.3 Breath-holding data acquisition parameters

Several protocol parameters have to be adjusted regarding the use of a breath-holding task in order to assure that it produces a reliable effect and that its consequent CBF changes can be properly measured.

The BH protocols normally consist of a standard block design, with alternating periods of ceasing respiration and normal breathing. The parameters that need to be adjusted include the duration of the BH and normal breathing periods, the number of BH challenges, and choosing between performing the breath-hold after inspiration or expiration.

Regarding the BH period duration, this must be short enough in order to be well performed and tolerated by the participant, but long enough to induce sufficient hypercapnia and CBF response. Although it has been reported that BOLD responses can be detected with breath-holds as short as 3 seconds [87], the brain greatly responds to longer block durations, leading to more activated voxels (plateau at BH duration of 20s [88]) and to an increase in the measured imaging signal amplitude [89]. Longer BH also produce more robust and reproducible BOLD responses across scanning sessions spanning weeks [90]. A literature review observed that clinical studies typically have BH lengths around 15s, probably due to being easier to implement, and that methodological studies averaged BH period duration of around 20s [91]. 20s BH duration has shown to lead to a more sharp increase in CVR [88] and to express significantly higher CVR values than using 15s [90]. Thus, the authors have suggested that the best BH protocol would most likely consist of a BH block of 20s. Normal breathing periods need to have a longer duration in order to allow blood gas levels to return to baseline.

Regarding the number of BH challenges, one expects that a higher number of challenges enables more averaging and consequent higher SNR. However, more challenges also implies longer protocol durations which may bring patient fatigue and increase motion artifacts. Common number of challenges in BH-CVR studies is between 3 and 7 [91].

Finally, it is required to choose between performing the BH after an inspiration or expiration. This is an important question to address because CBF responses and consequent BOLD signal changes present different shapes depending on end-inspiration or end-expiration BH protocols. CBF (and consequent BOLD signal) has been found to present a biphasic change (decrease followed by increase) when the BH is performed after inspiration [92], whereas BH after expiration has lead to an immediate rise in CBF (and BOLD signal) [93]. However, more complex responses have been observed, with end-inspiration BH protocols producing a triphasic shape and end-expiration a biphasic one [90]. Thus, when analyzing BOLD signal changes induced by BH, one should expect different shapes depending on the moment when BH was performed by the subject. Furthermore, end-inspiration BH is a more comfortable and natural form of holding one's breath, especially considering the ease of implementation of this task; however, it has been shown that subjects have different levels of inspiration depth, which can be a confounding variable [94]. BH after expiration, although more difficult to perform, offers better reproducibility: following normal exhalation, the lungs return to the state of "functional reserve capacity" at which the lungs, chest and diaphragm are resting at equilibrium, which is a more repeatable starting point for BH challenges [95]. Moreover, end-expiration based protocols have shown a quicker CVR peak (reached peak signal about 10 seconds earlier [96]), although both methods reached the same signal peak.

Having said, it is evident that several variables have to be taken into consideration when constructing the BH procotol to be used. In addition, this protocol has to be equally applied to all subjects in the study,

otherwise it will be impossible to reach correct conclusions regarding the observed CVR measurements.

2.3 Functional Magnetic Resonance Imaging

Since its development in the early 1990s, fMRI has become a standard tool for mapping brain activation, both in health and in disease. The reason for this is that fMRI allows to safely and noninvasively image brain activity, with very good spatial resolution, good temporal resolution, robustness and reproducibility [86]. fMRI provides information about the activity of the neurons in the brain, either in response to specific stimuli or tasks that the experimenter applies to the participant - task-based fMRI -, or in relation to the spontaneous activity of the participant's neurons - resting-state fMRI-, which is commonly used to investigate brain's functional connectivity.

2.3.1 The BOLD contrast

Functional brain mapping most commonly measures the blood oxygenation level dependent (BOLD) signal, based on the fact that an increase in neuronal activity in the brain stimulates higher energy consumption and increased blood flow through the activated area.

This underlying mechanism is called neurovascular coupling: the regular interplay between neural activity changes and corresponding vascular changes to alter cerebral blood flow to maintain metabolic support. More specifically, an increase in electrical and synaptic activity of an assembly of neurons in the brain results in an increased cerebral metabolic rate of oxygen ($CMRO_2$) and glucose, which ultimately results in an hemodynamic response characterized by larger cerebral blood flow (CBF), cerebral blood volume (CBV) and blood oxygenation. What is particularly interesting is that the amount of blood that is sent to the area is more than what is needed to replenish the oxygen that is used by the cells. Thus, the activity-related increase in blood flow caused by neuronal activity leads to a relative surplus in local blood oxygen. This oversupply of oxygen means an increase in the oxy-/deoxy-hemoglobin ratio. Oxy-hemoglobin (HbO_2) is diamagnetic, i.e. has the same susceptibility as surrounding tissues and therefore has minimal impact on the measured BOLD signal, while deoxyhemoglobin (HHb) is paramagnetic and degrades the BOLD signal. Consequently, higher HbO_2/HHb ratio leads to an increase in the MRI signal of the activated region compared to that of the surrounding tissues [86].

It is important to recognize that BOLD contrast is a consequence of a series of indirect effects. It results from changes in the magnetic properties of water molecules, which in turn reflect the influence of paramagnetic HHb, which is a physiological correlate of oxygen consumption, which itself is a correlate of a change in neuronal activity evoked by a given stimulus. Consequently, BOLD signal changes must be interpreted as a relative rather than a quantitative measure of activity.

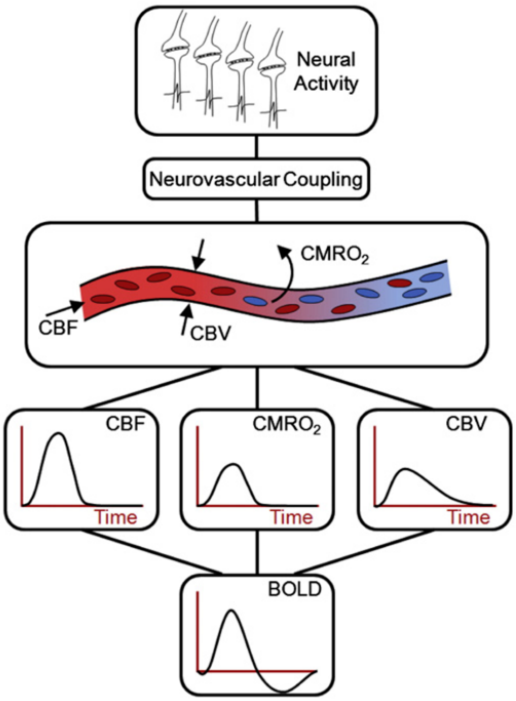

Figure 2.2: Schematic representation of the relationship between a transient increase in neural activity and the corresponding BOLD signal. Neuronal activity causes increased cerebral metabolic rate of oxygen consumption ($CMRO_2$), leading to alterations in the tone of the surrounding vasculature through neurovascular coupling. Such vascular adjustments lead to changes in the cerebral blood flow (CBF) and cerebral blood volume (CBV). The interaction between these 3 parameters leads to the blood oxygenation level dependent (BOLD) signal as measured in fMRI. Figure adapted from [97].

2.3.2 fMRI data preprocessing

fMRI data can be seen as 4D dataset consisting of a 3D matrix (a volume) of smaller volume elements (voxels) that is repeatedly sampled over time. The set of images can be considered to form a 4D image, where the fourth dimension is time. This enables the construction of a time course for each voxel, which translates its signal (arising from BOLD contrast) variation throughout time. This is represented in figure 2.3.

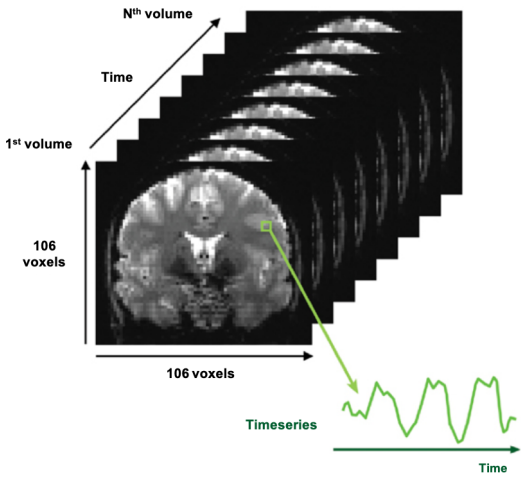

Figure 2.3: Example of a 4D fMRI dataset. For easier illustration, a single slice of each 3D volume is shown, but the 4D data contains a full 3D image sampled throughout time. Extracting the intensities over time from a single voxel gives a timeseries (a set of intensities over time), as illustrated on the bottom right. Figure extracted from [98].

However, only 1-3% of the change in the fMRI signal arises from underlying neuronal activity. Noise and artifactual sources of fluctuation considerably contribute to the BOLD signal. There are very forms of artifacts: they can be caused either by the MRI scanner itself, by the subject being scanned, or even a combination of both. Furthermore, all fMRI data suffers from spatial and temporal inaccuracy that, if uncorrected, may reduce or even eliminate the detection power of an experiment.

Consequently, MRI data directly from the scanner require a number of preprocessing operations in order to remove uninteresting variability from the data and prepare it for further processing steps. These include correcting for geometrical distortions, signal losses, different acquisition times between slices, as well as motion correction techniques and spatial and temporal filtering. A final preprocessing step consists of normalization of each individual data to a common standard space in order to be able to do comparisons between individuals. Figure 2.4 provides an overview of the principal preprocessing operations that are usually performed. Further in this dissertation (Section 4.2.1), preprocessing steps employed in this work will be described in more detail.

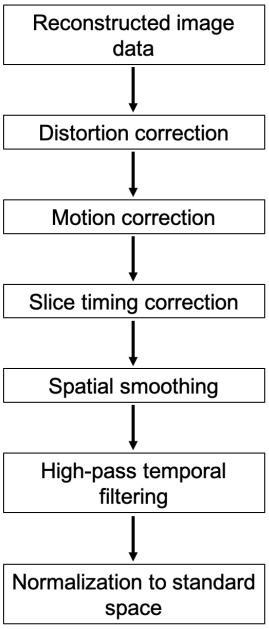

Figure 2.4: Standard pipeline for fMRI data preprocessing steps.

2.3.3 Subject-level fMRI data analysis

Following preprocessing, a separate first-level analysis of data from each individual subject is carried out. When using task-based fMRI data, the objective is to locate and analyze the brain activity in response to the task performed by the subject within the scanner.

2.3.3.1 The General Linear Model approach

The most employed method in task-based fMRI data analysis is the General Linear Model (GLM). This is fundamentally a linear model whose basic idea is that the observed signal can be described as a

weighted sum of one or more regressors, or Explanatory Variables (EVs). The EVs represent components expected to be found in the signal, but may or may not be meaningful: for example, they can represent the experimental task or express confounding factors. The aim is to estimate if, and to what extent, each EV contributes to the variability observed in the signal. Each EV is scaled by a Parameter Estimate (PE), which indicates how much each EV contributes to the observed signal.

Having said, the GLM can be expressed, for each voxel, as

$$Y = X\beta + \varepsilon \tag{2.1}$$

Y represents the observed BOLD signal timecourse. X is the design matrix, with each column representing the timecourse of a different EV (of interest are the columns representing experimental conditions, but the matrix also typically includes regressors of no interest). β is a vector of PEs setting the magnitude and direction of the association between each given EV and the signal Y (one PE for each EV). ε contains the residues associated with each observation (i.e. the amount of signal that is not explained by the weighted sum of EVs) [99]. Figure 2.5 depicts the GLM model for a given voxel with associated time-series Y, described as the linear combination of three explanatory variables (e.g., tasks A,B,C) and a number of non-interest regressors, each scaled by a parameter estimate β, plus a residue/error term ε [100].

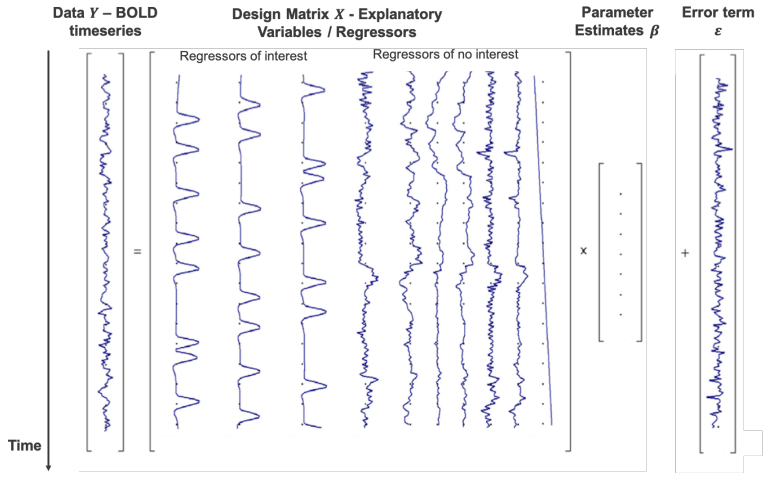

Figure 2.5: Depiction of the General Linear Model (GLM) approach applied in first-level analysis. The data from an imaginary voxel with timeseries Y is predicted by a design matrix X including 10 effects (3 regressors of interest and 7 regressors of no interest - e.g., 6 motion parameters and 1 linear drift) of unkwown amplitude β, and an error term ε. Figure adapted from [100].

The model fit is determined by the minimization of the residual error. This requires finding the best values for all the separate PEs. Several methods are available to do so, such as the ordinary least squares (OLS), which is the standard approach: in its form, the optimal PEs are defined as those that minimize the sum of squared residuals, i.e. the squared difference between the observed signal Y and the expected signal specified by the matrix X scaled by the β parameters [100].

As mentioned before, the goal is to determine which voxels show significant changes correlated with the pattern of stimulation or experimental manipulation. Thus, the GLM is applied separately for each voxel - a voxelwise analysis. Each voxel's time series is analyzed to see whether its BOLD signal

changes are related to some stimulus or task. Such a voxel-by-voxel approach is known as a mass univariate data analysis, which means that the same analysis is performed many times ("mass"), and is performed separately for every voxel in the brain ("univariate") (in contrast to a multivariate approach, which would take more than one voxel into account in the same analysis). Therefore, the estimated β values are different for every voxel.

The output of a subject-level analysis using the GLM is a whole-brain PE map for each regressor of interest. In these maps, the value in each voxel consists in the PE that scales the associated regressor in order to best explain the original signal from that voxel. Thus, the higher the β value at one voxel, the better that explanatory variable explains the original signal from that specific voxel [98].

Often, researchers are interested in understanding if one explanatory variable has a "bigger effect" in the data than another. In other words, if there is any stimulus leading to more activation than another in one particular voxel. This can be done through the use of contrasts of parameter estimates (COPEs). A COPE combines different regressors. In the GLM, it is defined by a set of weights, one for each PE, which are used to specify an inequality. For example, if there are three regressors explaining the signal at each voxel, then the inequality will take the form:

$$c1 * \beta_1 + c2 * \beta_2 + c3 * \beta_3 > 0 \tag{2.2}$$

If $c1 = 1$, $c2 = 0$, $c3 = 0$, then this results in $\beta_1 > 0$, which simply tests if the signal/effect size associated with the first regressor is positive. In the case of $c1 = 0$, $c2 = 1$, $c3 = -1$, this results in $\beta_2 - \beta_3 > 0$, or $\beta_2 > \beta_3$, which tests whether the effect associated with the second regressor is greater than the one associated with the third regressor. In the case of the regressors being different stimulus, this is equivalent to studying whether the activation of that voxel results more from stimulus 2 or stimulus 3. Each different COPE results in a different PE map. In this specific example, one PE map would reflect the voxel-wise values for the PE β_1, and the other for the PE combination $\beta_2 - \beta_3$ [98].

After voxelwise modelling, the PE maps arising from the contrasts are used for hypothesis testing. This starts with the assumption that there are no signals (effects) of interest in the data and that what we measure is random noise: the null hypothesis. Then, a test statistic is chosen, which is a quantity derived from the fitted GLM. Among the most common test statistics are *t*-statistics and F-statistics. The *t*-statistic is the ratio between the amplitude of the quantity of interest (the PE value associated with the contrast of interest) and its standard error (derived from the residual term ε after the complete model has been fit). An F-statistic combines the quantities formed by a set of *t*-statistics. For example, one contrast might form $\beta_1 - \beta_2$ and another might form $\beta_2 - \beta_3$, and an F-statistic can include both of these contrasts. The nature of an F-test is to ask a question like "is effect A or effect B or effect C, or any combination of them, significantly non-zero?". Thus, an F-test tests for both positive and negative effects, responding to any combination of non-zero effects, and can be induced by a single strong effect or several weaker ones together [98].

The chosen statistical test is performed for all voxels in the brain. If a *t*-statistic is chosen, then it results in a *t*-statistic image (a map of *t*-statistic values across all voxels). The *t*-values are converted

into probability values, usually a normal Z statistic, via standard statistical transformation (z is a "Gaussianised" *t*). Afterwards, this Z map is thresholded at a particular significance level to show which voxels or clusters of voxels are activated at that particular significance level [98].

This threshold is usually chosen at a *p*-value of 0.05, meaning that every individual test has a 5% chance of generating a false positive result. However, a typical fMRI dataset contains a very large number of voxels, with more than 100,000 statistical tests being performed. Therefore, a $p<0.05$ would result in up to 5000 voxels erroneously identified as significant. This is called the multiple comparisons problem. A way to quantify the likelihood of obtaining one or more false positive results in a family of tests is through the Family-Wise Error Rate (FWER). A commonly used approach to avoid such a high false-positive rate in fMRI is called the family-wise error (FWE) rate correction. This correction considers a family of tests instead of individual/voxel-wise ones, and the *p*-value is set to threshold the entire family. This way, instead of every single voxel having a 5% chance of generating a false positive result, the whole-brain has a 5% chance of having one or more false positives, and the remaining 95% have none [98].

As mentioned before, the X matrix contains the explanatory variables/regressors, which represent components expected to be found in the BOLD signal. The way that a regressor of interest is generated consists in convolving an hemodynamic response function (HRF) with the time course of the stimulus paradigm. This makes the choice of an appropriate HRF key in ensuring a good fit of the GLM regressors to the observed BOLD signal timecourse.

An HRF characterises the BOLD signal response to a stimulus, i.e. it is the measurement that would be expected in a perfect, noise-free MRI scanner when a subject received a short, sharp stimulus and the brain was only responding to that (neglecting all other neuronal and physiological changes). After neuronal activation, there is an intrinsic delay before regional vasodilation occurs and CBF increases. Thus, the BOLD signal does not increase instantaneously. Also, it does not return to baseline immediately after the stimulus ends. This has to be taken into account by the HRF.

In order to estimate and characterize the HRF, Fristion et al. [101] and Lange & Zeger [102] applied deconvolution models to BOLD data and found that, in general, the HRF could be approximately described by a gamma function. Later, it was realized that the model fit could be further improved by using a combination of two gamma functions. This function remains until now known as the canonical double-gamma HRF [103], illustrated in figure 2.6. It basically consists of a short onset delay (an initial dip), a gradual rise to peak 5-6s after the stimulus, followed by a return to the baseline and a small post stimulus undershoot before stabilizing again [99].

Although the HRF is of great value in most situations, the true shape of the HRF depends on the properties of the evoking stimulus and varies considerably across subjects and within subjects across different regions of the brain [104, 105]. By assuming that the HRF can be accurately described using a single canonical response function, we will only find responses similar to that function. Instead, it is possible to use a set of HRF basis functions that, when combined, express a wide range of hemodynamic responses, thus allowing to detect voxels whose activity does not follow the standard response, such as those with a wider response or with a later peak. The most commonly used basis set for fMRI analysis

is the “canonical HRF plus temporal derivative” approach developed by Friston et al. [103]. Adding the temporal derivative is equivalent to shifting the model slightly in time, and the rationale for doing so is that it can achieve a slightly better fit to the data, reducing unexplained noise and increasing resulting statistical significance.

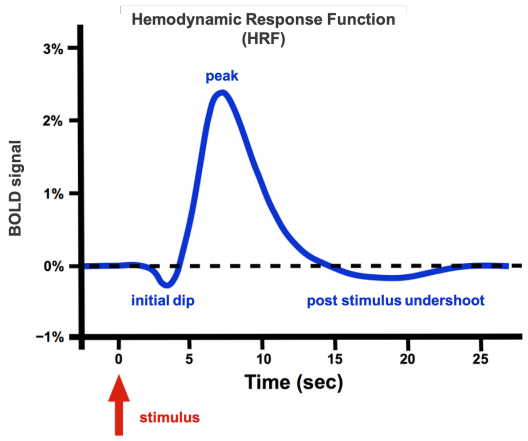

Figure 2.6: Illustration of the canonical double-gamma hemodynamic response function (HRF). It depicts the change in BOLD signal as a function of time, as would be expected in response to a very short stimulus. Figure adapted from [98].

2.3.3.2 Breath-hold fMRI data modelling

Analysis of BH BOLD data is easily accomplished using the GLM approach. As in for most task-based fMRI studies, the explanatory variable referent to the BH task could, in principle, be generated by convolving the paradigm time course with the canonical HRF [95, 106, 107], and even adding the regressor temporal derivative [103, 108, 109].

However, several aspects of BH-derived BOLD signal must be considered: (1) when performing respiratory tasks, the BOLD signal increases after a relatively longer delay when compared to other fMRI tasks [77]; (2) arterial CO_2 accumulates over time, and thus BOLD signal increases gradually throughout the duration of the BH [110]; and (3) increases in arterial CO_2 due to BH differ between subjects [111]. Consequently, the actual stimulus - $PaCO_2$ increase - most certainly does not match the simple BH square block paradigm.

In order to account for these differences, there have been several attempts to obtain more appropriate regressors to model the BOLD signal in response to a BH task. For example, in order to account for the longer delay observed in the BOLD response to respiratory tasks, one approach consists in introducing onset delays to the BH square block paradigm, before convolving it with the canonical HRF. As an example, a study compared four different stimulus paradigms: the standard square block paradigm, the block paradigm + temporal derivative (TD), the block paradigm delayed by 9 seconds, and the block paradigm delayed by 9 seconds + TD. The latter regressor, i.e. the block paradigm delayed by 9 seconds convolved with HRF + TD, revealed to be the most appropriate in modelling the BOLD signal in response to a BH task [110]. A wide range of delay values have previously been used, from 7s [112] up to 12s [113].

In order to account for the accumulation of CO_2 over time, another study used ramp functions, assuming a linear increase in the BOLD response with the BH duration [108]. However, these did not achieve acceptable repeatability and did not fully account for subject variability in BH performance.

Having in mind artifactual signal changes induced by the breathing cycle itself (image distortions caused by chest motion, variations in arterial CO_2 due to changes in the depth and rate of breathing), Birn et al. [114] developed a respiratory response function (RRF) to model the BOLD response. This response function correlated better with MRI signal changes induced by BH than the canonical HRF.

Lastly, and based on the fact that the change in arterial CO_2 levels associated with the BH challenge is the direct cause of the vascular response and consequent BOLD signal change, some studies have collected end-tidal CO_2 data ($PETCO_2$) simultaneously with BOLD-fMRI data. By convolving this data with an HRF, this new regressor provided more reproducible findings than ramp functions [108]. A study compared different $PETCO_2$-based regressors ($PETCO_2$ trace, $PETCO_2$ trace + TD, $PETCO_2$ trace convolved with the canonical HRF, $PETCO_2$ trace convolved with the canonical HRF + TD), and concluded that the last one provided the best fitting model [110].

Additionally, using $PETCO_2$ measures to normalize data showed to mitigate the effects of poor BH task performance, which is particularly useful when studying patient populations [108]. However, as mentioned before, measuring $PETCO_2$ in a clinical study requires an extra hurdle because a nasal cannula must be used and participants need to be instructed to breathe through their nose before and after the BH for proper measurement, which raises relevant compliance issues. In addition, some inaccuracies in the synchronization between $PETCO_2$ and fMRI recording can exist, which may pose an extra problem to the $PETCO_2$ model [83].

Nevertheless, all these modelling strategies apply a single global time lag for the entire brain, which is insufficient to explain variations of BOLD signal response across brain regions. This is a potential limitation not only in healthy subjects, but in particular in patients with cerebrovascular pathology, where regional BOLD signal changes are prone to be even more inhomogeneous due to reduced or delayed arrival of blood to the brain, thereby altering the accuracy of CVR interpretation. Thus, a voxelwise delay must be incorporated [115].

Several studies have attempted to take this into consideration when modelling the BOLD signal. One of these consisted in incorporating voxelwise delay maps into the analysis. These maps were obtained by temporally shifting the GLM and computing, in each voxel, the time shift that provided the highest cross-correlation with the BOLD signal [77].

Alternatively, an interesting approach is the use of a sinusoidal model, which consists of a sinusoid composed of the linear combination of a sine and cosine waves at the BH task frequency. This model accounts for the complex shape of the BH BOLD response and the periodicity of the BOLD signal variations at the paradigm frequency. Also, its inherent phase flexibility allows for different time delays across the brain, thus being able to model variations of BOLD signal across brain regions. When compared to other models, a study observed that the sine-cosine modelling was better at fitting the BH BOLD response than all the block-based approaches, and there was no significant difference in the variance explained by the $PETCO_2 * HRF$ + TD model (the best model so far) over the sine-cosine regressors

[110]. Another study showed that the sine-cosine model produced equal or even higher repeatability values than the $PETCO_2$ model [83]. An additional advantage of the sinusoidal modelling is that it only requires the BH task frequency and no further parameters or inputs, automatically performing delay estimation, this way avoiding time lag assumptions and optimizations.

Bearing in mind the complex shape that the BH BOLD response may have (especially when the BH is performed after an inspiration [90], as referred in Section 2.2.3) authors hypothesized that the inclusion of harmonics (higher order Fourier basis sets) could improve the sine-cosine modelling of the BH BOLD response, by allowing more flexibility to the amplitude, phase and shape of the model [116]. Thus, they compared linear combinations of sine-cosine pairs at the BH task frequency and its successive harmonics. They found that the 2nd order model (sine-cosine linear combination at the task frequency with its first two harmonics) explained significantly more variance, produced a greater number of responsive voxels, did not underestimate CVR amplitude, and showed better test-retest reproducibility than lower order methods.

Having all this in consideration, the sine-cosine pair at the BH task frequency and its two harmonics seem to be the most suitable model for BOLD-fMRI response to a breath-holding task.

2.3.3.3 Cerebrovascular Reactivity (CVR) and Time-To-Peak (TTP) maps

After modelling the BOLD response to the BH task, the CVR of the brain can be characterised. Quantification of CVR can be done in terms of amplitude and temporal responses: regarding the amplitude, CVR metrics is typically the BOLD percent signal change (for reasons of simplicity, we call this value "CVR"), while in terms of temporal response, the metrics is the time-to-peak (TTP) of the BOLD signal.

As previously mentioned, the GLM is applied separately to each voxel's BOLD timeseries. Thus, in each voxel, BOLD percent signal changes can be calculated as the amplitude of the model's maximum relative to the baseline/normal breathing signal (multiplied by 100), and TTP can be calculated as the time of the model's maximum relative to the beginning of the BH. This makes it possible to obtain a value of CVR and TTP for each voxel, resulting in whole-brain CVR and TTP maps for each subject.

2.3.4 Group-level fMRI data analysis

The main interest of most fMRI studies is to compare brain activity between different groups of subjects, such as patients vs controls, and/or between different sessions/conditions, such as comparison between different phases of the migraine cycle.

With this purpose, group-level analysis can be performed over the individual maps that were obtained in single subject data analysis, once these are registered to a common standard space.

There are two common statistical approaches for group-level fMRI data analysis: fixed-effects (FE) and mixed-effects (ME) analyses.

A FE analysis assumes that the experimental effect is fixed/constant across subjects, i.e. assumes that the experimental stimulus has the same effect in the BOLD signal in every subject. Thus, this anal-

ysis combines all data points from all subjects into a single analysis, and ignores inter-subject variance. This presents an important disadvantage: the differences in activation reported by a FE analysis are restricted to the particular sample of subjects present in the study, and are not representative of the wider population to which they belong [117].

In its turn, ME models the inter-subject variability, and it therefore allows to make inferences about the larger population from which the subjects were drawn. ME modelling options can be divided into parametric or non-parametric statistics. Parametric tests assume the data distribution to be normal/Gaussian, which is a strong assumption rarely met by fMRI data (most of the time, there is no normality of the distribution of PEs across subjects) [118, 119]. Non-parametric tests are often a better alternative because they make no assumptions regarding the data distribution. Instead, they estimate the null distribution from the data itself, under the assumption that the null hypothesis is true. One common non-parametric test is permutation testing. It creates the null distribution by repeatedly mixing up the subjects, i.e. shuffling the assignment of experimental labels to the subjects (they alternate between the correct and incorrect group). For each shuffle, data is analyzed to create a distribution of statistic values consisting in the null hypothesis. Afterwards, un-permuted data (subjects with the correct label) is used to calculate the real test statistic. By comparing the null distribution with the distribution of un-permuted data, the significance of the statistic expressing the experimental effect can be assessed. The higher the number of permutations, the more accurate is the test, since it gets closer to the true distribution, if all possible permutations were performed [119, 120]. An advantage of the permutation test is that it is based on a very small number of assumptions, thus being characterised by its accuracy and statistical power. The only assumption in non-parametric tests is exchangeability: subjects are exchangeable if the permutation does not change the distribution under the null hypothesis. For example, when studying the same subjects under two different conditions/sessions, it is only possible to permute the same subject between the two sessions.

2.3.4.1 Region-specific analysis

When looking for group differences in brain vascular reactivity in migraine, an initial approach may consist of a whole-brain analysis, meaning that a voxel-wise analysis will search for significant differences in all brain voxels. However, it may also be of great interest to focus the research into specific brain regions in order to identify threatened tissue areas in clinical patients.

2.3.4.1.1 Cerebral lobes

The cerebral cortex is generally divided into four lobes: frontal, occipital, parietal, and temporal lobes. Each of these lobes exists in both right and left hemispheres of the brain and has its specific functions. All together, cerebral lobes are responsible for most of the information processing taking place in the brain, from sensation to cognition. For example, the occipital lobes are the main center for visual processing. The visual information is sent to the parietal lobes, which are involved in receiving and processing sensory information, and to the temporal lobes, which are responsible for memory, emotion, hearing and language. In its turn, the frontal lobes control logical thought, personality, and voluntary movement

[121].

Having in mind the complexity of migraine and its associated symptoms, several studies have investigated differences in the activity of the cerebral lobes in patients with migraine. The rationale to do so is that it may allow the localization of atypical activations in migraine, including hypersensitivities or identification of brain regions that may contribute to abnormal processing of sensory stimuli.

One of the most influential migraine studies measured rCBF in migraineurs during spontaneous attacks and observed that, compared with the pain-free interval, there was an increase in rCBF during migraine headache in the brainstem, visual and auditory association cortices [122]. In another study, the temporal pole revealed to be hyperexcitable during a migraine attack in response to thermal pain-induced activation compared with interictal activation [123]. In addition, when processing olfactory stimuli, migraineurs had greater activation in the temporal pole, amygdala, cerebellum, and other brain regions, during spontaneous migraine attacks compared to the interictal state [124].

In the particular case of this work, focusing the study of CVR in the cerebral lobes may help to identify whether there is a particular cerebral lobe where cerebrovascular dysfunction is more prominent in migraine.

2.3.4.1.2 Arterial flow territories

Vascular changes are recognized as an important pathophysiological factor in migraine. In addition, CVR is an intrinsic brain mechanism whereby blood vessels regulate the cerebral blood flow. Thus, it makes sense to focus the study of cerebrovascular reactivity on the arterial flow territories of brain blood vessels.

Normal functioning of the brain is dependent upon adequate supply of blood through a dense network of blood vessels, which is partially represented in figure 2.7.

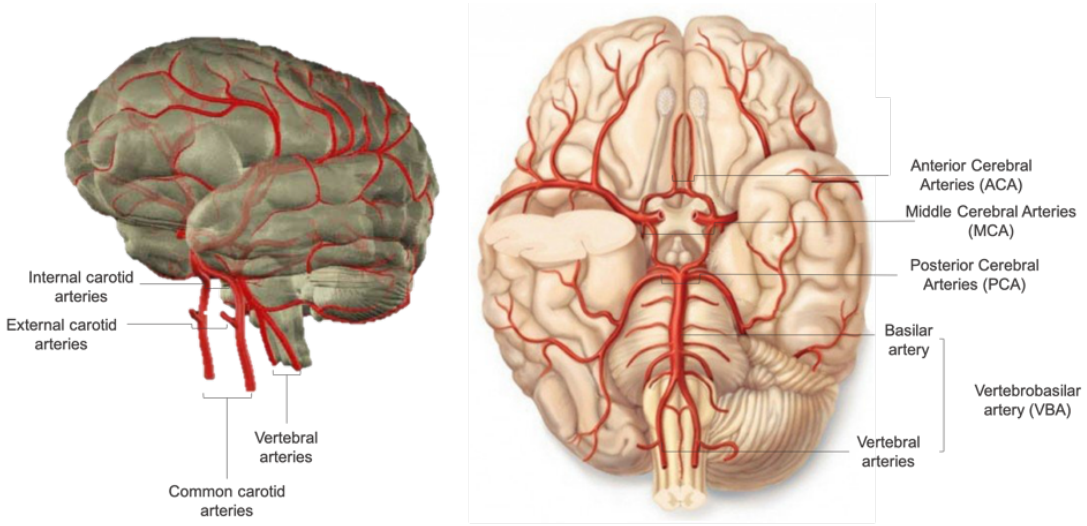

Figure 2.7: (Left) Illustration of the major arteries of the human brain: the common carotid arteries (with two divisions - the external and internal carotid arteries -), and the vertebral arteries. Figure adapted from [125]. (Right) Illustration of the Circle of Willis, emphasizing the anterior cerebral arteries (ACA), the middle cerebral arteries (MCA), the posterior cerebral arteries (PCA), and the vertebrobasilar artery (VBA). Figure adapted from [126].

The two major sets of arteries supplying the brain are the common carotid arteries and the vertebral arteries (both exist on right and left sides). The common carotid arteries have two divisions: the external carotid arteries, which supply the face and scalp, and the internal carotid arteries (ICA), which supply blood to most of the anterior portion of the brain. The vertebral arteries together with the basilar artery (BA) comprise the vertebrobasilar artery (VBA), which is illustrated in figure 2.7 (Right). The VBA serves as a critical arterial blood supply to the brainstem, cerebellum, thalamus, and occipital lobe [127].

At the base of the brain, the ICA and the VBA form a circle of communicating arteries known as the Circle of Willis. From this circle, other arteries - such as the anterior cerebral arteries (ACA), the middle cerebral arteries (MCA), the posterior cerebral arteries (PCA) - arise and travel to all parts of the brain. The ACA supply the frontal lobe, the MCA supply a portion of the frontal lobe and the lateral surface of the temporal and parietal lobes, and the PCA supply the temporal and occipital lobes. Investigating CVR in the territories of the arteries of this complex vascular network may serve to identify which blood vessels and respective supplied brain regions are mostly affected by impaired CVR and endothelial dysfunction in migraine disorder.

Chapter 3

State of the art

Few studies exist concerning investigation of CVR in migraine. The first evaluation of CVR in migraineurs dates back to 1979 [128]. The authors used SPECT to compare CBF changes associated with CO_2 inhalation between migraineurs and matched healthy controls. From then, mainly due to the exposure to radiation and potentially toxic radioactive contrast agents used in radiotracer imaging techniques, the majority of studies have used TCD, a more safe and non-invasive method. This technique, as previously said, directly assesses large cerebral arteries' velocity. In CVR studies of migraine, the most commonly studied arteries are the MCA, the PCA and the BA. Unfortunately, TCD studies are not able to provide regional information. Alternatively, fMRI scans overcome this limitation by providing whole-brain scans with high spatial resolution. Nevertheless, to our knowledge, there is only one study in migraine that assesses CVR through the use of fMRI [117].

Another important aspect in CVR studies of migraine is that the majority of them compare healthy controls versus migraine patients only in the interictal phase. As explained in Section 2.1, migraine is a cyclic disorder, where it is possible to distinguish four different phases. Thus, studying only one of them does not cover the cyclical nature of the disease. Instead, following a longitudinal approach, where brain activity of migraineurs is measured along the migraine cycle, holds greater potential because it allows for the investigation of differences across several phases of migraine, as well as neurophysiological mechanisms and even attack-specific alterations that may exist [2].

A literature review has been conducted, which is presented in table 3.1. Although the present work uses fMRI and adopts a longitudinal approach only focused in episodic migraine patients without aura, studies that use different techniques (mainly TCD) and compare healthy controls versus migraine patients (episodic and chronic; with and without aura) were also included, because they are comparable with this work to some extent, and especially because of the very few number of studies that exist. Contrarily, studies that did not include episodic migraineurs without aura and the ones evaluating CBF or CBV instead of CVR were excluded from this literature review.

Most studies included patients with both migraine subtypes (with and without aura), and five focused on migraine without aura (MwoA). All studies employed TCD to assess CVR, except from one study which employed SPECT and one that used fMRI. Regarding the vasoactive stimuli, the majority as-

sessed CVR to hypercapnia obtained by BH or CO_2 inhalation; two studies used infusion of chemical substances (acetazolamide and L-arginine) and other two measured CVR in response to hyperventilation. All studies assessed patients with migraine during the interictal, i.e. headache-free, phase, except from five studies which compared the ictal with the interictal phases.

Table 3.1: Cerebrovascular reactivity studies in migraine, presented in chronological order (most recent first).

	Cohort (N,gender)	CBF measurement technique	Vasoactive stimulus	Acquisition phase	Main findings
Chan (2019) [117]	Episodic MwoA (3, M) Episodic MwA (2, F; 1, M) HC (5, F)	fMRI	Inspired carbon dioxide (4-8 mmHg above the subject's resting $PETCO_2$)	Interictal	In MwoA, compared to HC: Similar CVR to CO_2 at the cortex and white matter tracts. In MwoA, compared to MwA and HC: Reduced (or even negative) CVR to CO_2 at the red nucleus of the midbrain.
Lee (2019) [129]	MwoA or MwA (201, F; 47, M) HC (86, F; 19, M)	TCD	Breath-holding	Interictal	In MwoA and MwA, compared to HC: Reduced CVR in the MCA, PCA and BA.
González-Quintanilla (2016) [52]	Episodic MwoA (12) Episodic MwA (25) Chronic MwoA (13) Chronic MwA (22) HC (41)	TCD	Breath-holding	Interictal	In MwoA and MwA, compared to HC: Reduced CVR in the MCA.
Rajan (2015) [55]	Episodic MwoA (30) Episodic MwA (15) HC (44)	TCD	Breath-holding	Interictal	In MwoA and MwA, compared to HC: Reduced CVR in bilateral PCA and BA; Similar CVR in bilateral MCA.
Perko (2011) [5]	MwoA (16, F; 4, M) MwA (16, F; 4, M) HC (16, F; 4, M)	TCD	Intravenous infusion of 100 ml of 30% L-arginine	Interictal	In MwoA and MwA, compared to HC: Reduced CVR in the PCA; Similar CVR in the MCA.
Arjona (2007) [130]	Episodic MwoA (36) HC (44)	TCD	Breath-holding	Interictal	In MwoA, compared to HC: No differences in CVR to CO_2 in bilateral MCA.
Silvestrini (2004) [131]	MwoA (15) MwA (15) HC (15)	TCD	Breath-holding	Interictal	In MwoA, compared to HC: Similar CVR in the BA. In MwoA and MwA, compared to HC: Similar CVR in the MCA.
Dora (2002) [132]	Episodic MwoA (22, F; 1, M) HC (9, F, 1, M)	TCD	Breath-holding	Interictal	In MwoA, compared to HC: Increased CVR to CO_2 of right and left MCA; CVR to CO_2 of MCAs reflected no side difference between the "headache" side and "non-headache" side.
Kastrup (1998) [133]	Episodic MwoA (18, -) Episodic MwA (2, -) HC (17, F; 13, M)	TCD	Inhalation of carbogen (95% O_2, 5% CO_2)	Interictal	In MwoA and MwA, compared to HC: Increased CVR to CO_2 of the ACA, MCA and PCA; The "headache" side revealed higher CVR to CO_2 than the "non-headache" side.
Totaro (1997) [134]	MwoA (28, F; 2, M) MwA (26, F; 4, M) HC (27, F; 3,M)	TCD	Inhalation of carbogen (95% O_2, 5% CO_2)	Interictal	In MwoA, compared to MwA and HC: Reduced CVR to CO_2 of the MCA.
Silvestrini (1996) [135]	MwoA (13, F; 2, M) MwA (11, F; 4, M) HC (15, -)	TCD	Breath-holding	Interictal	In MwoA and MwA, compared to HC: Similar CVR to CO_2 of the MCA; Migraineurs with unilateral headaches showed no asymmetry in CVR to CO_2 of the MCA.
Valilkovics (1996) [136]	MwoA or MwA (12) HC (19)	TCD	Injection of acetazolamide	Interictal	In MwoA and MwA, compared to HC: Similar CVR in bilateral MCA.
Silvestrini (1995) [137]	MwoA (10, F; 6, M) HC (10, F; 6, M)	TCD	Breath-holding	Interictal and ictal	In MwoA, compared to HC: Similar CVR in bilateral ACA, MCA and PCA. In MwoA, in ictal state compared to interictal state: Reduced CVR of the ACA, MCA and PCA.
Zwetsloot (1992) [138]	Episodic MwoA (17, F; 6, M)	TCD	Hyperventilation	Interictal and ictal	In MwoA, in ictal state compared to interictal state: No differences in CVR of the VBA.
Zwetsloot (1991) [139]	MwoA (48) HC (17)	TCD	Hyperventilation	Interictal and ictal	In MwoA, in ictal state compared to interictal state: No differences in CVR of the MCA and BA. In MwoA, compared to HC, in ictal and interictal states: No differences in CVR of the MCA and BA.
Harer (1991) [140]	MwoA or MwA (21, F; 9, M) HC (9, M; 21, F)	TCD	Inhalation of carbogen (95% O_2, 5% CO_2)	Interictal and ictal	In MwoA and MwA, compared to HC: **Ictal phase:** Reduced CVR to CO_2 of the MCA. **Interictal phase:** Nearly double CVR to CO_2 of the MCA ipsilateral to the headaches.
Thomas (1990) [141]	MwoA or MwA (7, F; 3, M) HC (3, F; 7, M)	TCD	Inhalation of carbogen (95% O_2, 5% CO_2)	Interictal	In migraineurs, compared to HC: Increased CVR to CO_2 of the MCA.
Sakai (1979) [128]	MwoA (32, F; 2, M) MwA (13, F; 5, M) HC (26, F; 22, M)	SPECT	Inhalation of carbogen (95% O_2, 5% CO_2)	Interictal and ictal	In MwoA and MwA, compared to HC: **Prodrome and headache phases:** Reduced CVR to CO_2 throughout both hemispheres. **Interictal phase:** Excessive CVR to CO_2; The cerebral hemisphere on the side of predominant head pain showed significantly greater CVR to CO_2 than the "non-headache" hemisphere.

fMRI = functional Magnetic Resonance Imaging; TCD = Transcranial Doppler; SPECT = Single Photon Emission Computed Tomography; CVR = Cerebrovascular Reactivity; MwoA = Migraineurs without Aura; MwA = Migraineurs with Aura; CO_2 = Carbon dioxide; $PETCO_2$ = End-tidal partial pressure of carbon dioxide; ACA = Anterior Cerebral Arteries; BA = Basilar artery; MCA = Middle Cerebral Arteries; PCA = Posterior Cerebral Arteries.

Chapter 4

Materials and Methods

4.1 Participants and data

4.1.1 Participants

The present work used data acquired from a population of 14 female episodic migraine patients without aura (MwoA) in the context of a previous project, which was carried out in accordance with the recommendations of *Comissão de Ética para a Investigação Clínica*, where all subjects filled an informed consent form. Volunteers were recruited among the staff of Hospital da Luz (Lisbon, Portugal) and patients from the acute care outpatient clinic.

Exclusion criteria included previous history of migraine with aura, other headache types and chronic migraine. Besides, pregnant or claustrophobia-suffering subjects, as well as subjects with ferromagnetic foreign bodies such as metallic implants, were excluded in order to ensure safety during data acquisition. To avoid any possible pharmacological interference with the investigation, only oral contraception was allowed as concomitant medication.

Table 4.1 presents participants' demographic data together with several clinical parameters regarding the participants' migraine attacks: usual attack frequency (number of attacks per month), usual duration of the attack (in hours), and usual headache intensity (assessed on a 0-10 visual analog scale (VAS), where 0 corresponds to "non-existing" and 10 to "very strong" pain).

Table 4.1: Demographics and clinical parameters, averaged across participants.

Parameters	mean ± SD
Age (y)	35.69 ± 7.35
Usual attack frequency (nr of attacks/month)	2.38 ± 1.56
Usual attack duration (h)	32.62 ± 25.27
Usual headache intensity (0-10 VAS)	7.38 ± 1.26

y = years; h = hours; VAS = Visual Analogue Scale

4.1.2 Study design

This study followed a longitudinal approach, where each participant was evaluated in two different phases of the migraine cycle. The first session (S1) corresponds to the ictal phase of the migraine cycle. All subjects were experiencing head pain during the scan, therefore, the acquired data corresponds to the headache phase of the ictal phase/migraine attack. The second session (S2) refers to the interictal period, i.e. outside a migraine attack.

Regarding the first session (headache phase), participants were not allowed to take any relief medication within the preceding 12 hours, and should report a minimal headache intensity of 4 on a 0-10 VAS before entering the scan. The second session was in all patients performed at least one month after the first evaluation and with a minimal 48 hours delay from the last attack, to assure that the participants were all in the interictal period (and not in the postdrome phase of the migraine attack).

Data were acquired in each session during a BH challenge, a motor task and visual stimulation. While the BH challenge allows for investigation of vascular changes in migraine, the rationale for the motor and visual data acquisitions was to investigate neuronal/brain activation differences between the two migraine phases. More specifically, if there are differences in activation of the brain regions specific to motor and visual functions between the ictal and interictal phases of migraine.

Several clinical parameters were reported during the first session, including the duration (time from the beginning of the migraine attack until data acquisition onset) and headache intensity of the ongoing attack. Also, participants rated the expression of several migraine-related symptoms using a 0-10 VAS. This information is presented in table 4.2.

Table 4.2: Clinical parameters characterising the ongoing attack in S1, averaged across participants.

Parameters	mean ± SD
Attack/Pain duration (h)	15.31 ± 18.94
Headache intensity (0-10 VAS)	6.81 ± 1.18
Nausea (0-10 VAS)	4.27 ± 1.54
Photophobia (0-10 VAS)	4.88 ± 1.66
Phonophobia (0-10 VAS)	5.00 ± 2.35

h = hours; VAS = Visual Analogue Scale

Given that information in table 4.1 refers to the usual attacks and table 4.2 refers to symptoms that patients were experiencing at the time of the report, the latter are believed to be the most reliable since they do not rely on patients' memory of the details of the attacks. Furthermore, since the data acquisition was performed at the time participants were experiencing the symptoms described in the table 4.2, this may be of great use to study the neural mechanisms underlying these symptoms.

4.1.3 Image acquisition

All images were acquired with a 3 Tesla Siemens Verio MRI system using a 12-channel head radiofrequency coil. Both structural and functional images were acquired in each session. The structural anatomic scans were performed using a T1-weighted magnetization-prepared rapid gradient echo

(MPRAGE) series with the following repetition time (TR), echo time (TE) and voxel size: TR=2250ms, TE=2.26ms, and voxel size of 1mm x 1mm x 1mm. Regarding functional data, in each session participants were given three different stimuli: a motor task, visual stimulation, and a BH challenge. All functional scans were acquired using a T2*-weighted gradient echo-echo planar imaging (GE-EPI) sequence.

BOLD data acquisition parameters are presented in table 4.3. BOLD data referent to the motor task and visual stimulation were acquired with the following parameters: TR=3000ms, TE=30ms, and voxel size of 4mm x 4mm x 3.75mm. BOLD images referent to the BH task were obtained with the following parameters: TR=2500ms, TE=50ms, and voxel resolution of 3.5mm x 3.5mm x 3.5mm.

Table 4.3: Acquisition parameters referent to the three BOLD datasets (breath-holding challenge, motor task, and visual stimulation).

BOLD image acquisition parameters	**Breath-holding (BH)**	**Motor task**	**Visual stimulation**
Resolution (mm^3)	3.5 x 3.5 x 7	4 x 4 x 3.75	4 x 4 x 3.75
Number of slices	21	37	37
Number of volumes	110	140	90
TR (ms)	2500	3000	3000
TE (ms)	50	30	30

The motor stimulus consisted of a bimanual finger tapping task cued by auditory instructions. The protocol comprised three cycles of alternating periods of 60s of baseline condition (rest) and 60s of motor task performance. At the end of the three cycles, a final 60s period of baseline condition was added, resulting in a total protocol duration of 420s (7 minutes), presented in figure 4.1 (Top). The visual protocol comprised four cycles of alternating periods of 30s of baseline condition and 30s of flashing checkerboard visualization (frequency of 4Hz). At the end, a period of 30s of baseline condition (fixation cross) was performed. The total visual protocol duration was of 270s (4.5 minutes), shown in figure 4.1 (Center). Only 12 of the 14 participants were able to perform both sessions of the motor task and visual stimulation, therefore, only these were considered for subject- and group-level analysis of motor and visual data. Regarding the BH task, the protocol comprised two 25s periods of self-paced breathing (baseline) at the beginning and end of the protocol and three 75s cycles of alternating periods of 20s apnea (BH) cued by auditory instructions and preceded by a preparatory inspiration, and followed by 55s of self-paced breathing (total duration of 275s, approximately 4.5 minutes). This protocol is presented in figure 4.1 (Bottom). Only 11 of the 14 participants were able to perform both sessions of BH, therefore, only these were considered for subject- and group-level analysis of BH data.

All three paradigms are represented in figure 4.1.

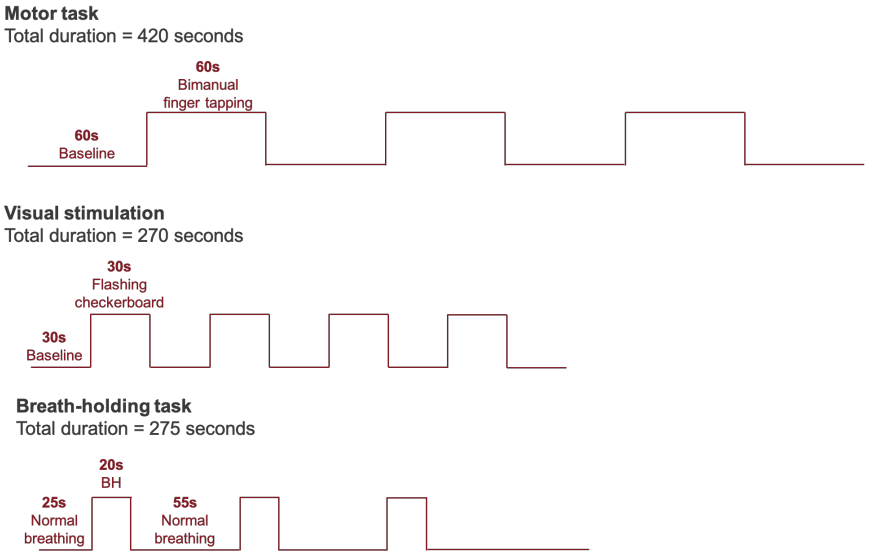

Figure 4.1: Illustration of the three fMRI paradigms used in this work. (Top) Motor task paradigm. (Center) Visual stimulation paradigm. (Bottom) Breath-holding task paradigm.

4.2 BOLD-fMRI data processing and analysis

As previously referred, only 12 of the 14 participants were able to perform both sessions of the motor task and visual stimulation, and only 11 could perform both sessions of the breath-holding task. Therefore, only data from these patients were considered for data processing and analysis.

Processing of BOLD-fMRI and further analysis was conducted using both the FMRIB Software Library (FSL, `https://fsl.fmrib.ox.ac.uk/`) and the MATLAB software (`https://www.mathworks.com/products/matlab.html`). The FSL built-in tools were run both from the command line and graphical user interfaces (GUIs) [142].

4.2.1 Preprocessing and registration

4.2.1.1 Preprocessing

As previously explained in Section 2.3.2, the first step in data analysis consists in applying preprocessing methods. In this work, these methods and respective FSL tools were the following:

(i) Removal of non-brain tissues, using the Brain Extraction Tool (BET, `https://fsl.fmrib.ox.ac.uk/fsl/fslwiki/BET`) [143]. This tool uses the mean volume of the fMRI data, creates a brain mask, and applies it to all volumes to eliminate unwanted voxels, such as the ones in the skull.

(ii) Segmentation of the brain, which delineates where different tissues or structures are. Using the FMRIB's Automated Segmentation Tool (FAST, `https://fsl.fmrib.ox.ac.uk/fsl/fslwiki/FAST`), brain was segmented into different tissue types including the grey matter (GM), white matter (WM) and cerebrospinal fluid (CSF).

(iii) Distortion correction, also called B0 unwarping, using the FUGUE tool (`https://fsl.fmrib.ox.ac.uk/fsl/fslwiki/FUGUE`).

The echo planar imaging (EPI) sequence used for functional data acquisition is affected by magnetic field inhomogeneities, which cause geometric distortions and signal losses. Once the data have been acquired, there is no way to retrieve areas where signal loss has occurred. Only geometric distortions can be corrected. A common method to do so is called B0 unwarping, which is based on the acquisition of a field map image characterizing the location of field inhomogeneities (where distortions are more critical) [99]. The FUGUE tool here applied makes use of this fieldmap image to calculate the geometric distortions and compensate for (not completely remove) these artefacts in the functional images.

(iv) Motion correction, using the Motion Correction FMRIB's Linear Registration Tool (MCFLIRT, `https://fsl.fmrib.ox.ac.uk/fsl/fslwiki/MCFLIRT`) [144] and nuisance regression of motion parameters.

Head motion occurs in every fMRI data acquisition scan. One of its critical consequences is the mismatch between the location of subsequent images in the time series, which results in a discordant spatial correspondence between voxels and anatomical areas over time. In order to correct for this mis-alignment between images, we must perform volume registration, also known as realignment. The MCFLIRT tool here applied relies on optimization and registration techniques to align different volumes acquired for one subject. This is done by defining a common reference scan (the middle volume) and realign each image to it. MCFLIRT estimates 6 motion parameters (3 rotations and 3 translations along the axis x, y and z) for each volume and applies a rigid body geometrical transformation based on these parameters to each volume in order to align every single one with the template [145].

In addition to realignment, nuisance regression of motion parameters was performed. This helps in reducing the influence of additional signal intensity changes/disruption caused by head motion (due to movement, a voxel that has no brain tissue in it at one time point, suddenly contains tissue) and further clean up the signal. The correction method for these artifacts begins by creating a multiple regression linear model to model the observed signal in each voxel in terms of the motion parameters, which means that the motion parameters will be the regressors/EVs. Then, these motion parameters are included as nuisance regressors in each voxel's GLM. The term *nuisance* is used to describe regressors that do not contribute to the signal of interest but are included in the GLM to pick up extra variability in the data. Thus, they are regressed out from the GLM that models the fMRI time series, leaving only the signal of interest [118]. Moreover, instead of considering only 6 regressors, it is often beneficial to include the derivatives of the motion parameters, or even squared or delayed versions of them, as they can help model motion-related noise and spikes in the data [120].

(v) Nuisance regression of motion outliers, using the FSLMotionOutliers tool (`https://fsl.fmrib.ox.ac.uk/fsl/fslwiki/FSLMotionOutliers`).

The motion parameter nuisance regression in (iv) only accounts for signal changes induced by small motions. In order to account for artifacts induced by strong and large head motion, nuisance regression of motion outliers is performed.

The FSLMotionOutliers tool detects timepoints in an fMRI dataset that have been corrupted by rapid and large motion. To achieve this, it starts by performing motion correction and calculating metric values for each timepoint that indicate how much it is affected by motion. After this calculation, the metric values are thresholded to look for outliers. A confound matrix is then generated, with a separate column for each timepoint that is considered to be an outlier. Within each column, the values are all zeros except for the timepoint that is considered to be the outlier, whose value is one. This confound matrix is added to the GLM, where the influence of each outlier will be modeled with a separate parameter estimate (PE). This means that the intensities at that timepoint (in any voxel) have no influence on any of the other PEs, effectively removing the effect of these timepoints from the estimation of all the effects of interest.

(vi) Spatial smoothing, using the SUSAN tool (`https://fsl.fmrib.ox.ac.uk/fsl/fslwiki/SUSAN`) [146].

This consists in the application of low-pass spatial filters to the images in order to reduce the high-frequency spatial components, i.e. removing small-scale changes from the image. The principal reason to do so is the resulting increase in the signal-to-noise ratio (SNR).

The standard spatial smoothing procedure consists of convolving the fMRI signal in each voxel with a Gaussian kernel. This Gaussian spatial filter will spread the intensity at each voxel in the image over nearby voxels. The distance of its effects, i.e. the amount of smoothing, is determined by the width of the Gaussian distribution (Full Width at Half-Maximum, FWHM): the larger the FWHM, the greater the smoothing. This value should be the minimum necessary to achieve the desired results. A reasonable starting point is a FWHM of 1.5x the voxel dimension [120]. The chosen FWHM for this work was of 5 mm.

(vii) High-pass temporal filtering, using the FEAT tool.

Temporal filtering is performed in order to remove the effects of confounding signals with known or expected frequencies. This helps attenuate noise and thus increase the SNR, substantially improving the quality of fMRI data [99]. Very-low frequency changes are observed in fMRI experiments, such as those related to scanner drifts ($\approx<$0.01 Hz), which are induced by hardware imperfections. These changes often appear as near linear increases or decreases in absolute signal over the experiment (last regressor of no interest in figure 2.5), and can be extremely problematic for fMRI experiments. The most commonly used filters to address this issue in task-based fMRI are high-pass filters, with a cutoff value of about 2 times that of the task-frequency (the interval between one trial start and the next one) [118].

The cutoff frequency used in this work was 0.01 Hz, which succeeded in eliminating scanner-related drifts from the signal, consequently increasing SNR.

4.2.1.2 Registration and normalization

The last preprocessing step after subject-level data analysis was the registration of the subjects' functional images to the structural images, and normalization to the standard space. This was performed in a two-step process.

The first step consisted in registering the functional images of each subject to the respective structural space (T1-weighted images) through FLIRT boundary-based registration (BBR, https://fsl.fmrib.ox.ac.uk/fsl/fslwiki/FLIRT_BBR). This registration is a linear registration (with 6 degrees of freedom, like in motion correction (iv)) in which the cost function to minimize is based on EPI (functional) intensity difference between voxels inside and outside of white-matter/grey-matter boundaries (that were previously defined by T1-weighted segmentation in (ii)).

The second step is the normalization from the structural space to a common anatomical template. The standard space used was the Montreal Neurological Institute (MNI) 152 standard space T1-weighted average structural template image (2mm) [147]. The normalization to the MNI152 template was performed through a non-linear registration using FMRIB's Non-Linear Registration Tool (FNIRT, https://fsl.fmrib.ox.ac.uk/fsl/fslwiki/FNIRT). A non-linear registration is able to translate, rotate, zoom and shear one image to match it with another, thus accounting for the alignment of internal structures. These local deformations often do a better job than using a simple linear registration. The cost function (that defines the difference between the images) used by FNIRT was the sum-of-square difference, and the intensity values between grid points were interpolated using a trilinear approach.

Finally, the two transformations (registration and normalization) were combined, defining a single transformation from the functional space to the standard space.

4.2.2 Subject-level BOLD-fMRI data analysis

Regarding subject-level data, the first step of the analysis was to use the GLM approach, as explained in Section 2.3.3.1. This was performed using FEAT (https://fsl.fmrib.ox.ac.uk/fsl/fslwiki/FEAT), a software tool contained in FSL for high quality model-based fMRI data analysis. The model represents what we expect to see in the data: changes in BOLD hemodynamic response to neural activity in response to a certain stimulus. Thus, the explanatory variables included in the model were derived from the stimuli paradigms that were applied to the subject in the MRI scanner, i.e. motor, visual and BH tasks.

4.2.2.1 Function-specific BOLD fMRI data analysis

The explanatory variables representing the paradigms of the motor task and visual stimulation were obtained in the standard way: convolving a square box function at the timing of the stimulus presentation with the canonical double gamma HRF, and adding its temporal derivative.

Regarding the **motor** task, as stated in Section 4.1.3, the task consisted of three and a half cycles of 60s of baseline condition followed by 60s of bimanual finger tapping. The regressor of interest used in the GLM to model the hemodynamic response to this task was a square box at the timing of the paradigm convolved with the canonical double gamma HRF, along with its temporal derivative. In order to regress out noise components, the motion parameters and motion outliers estimated by the MCFLIRT and FSLMotionOutliers tools, respectively, were also included in the model. An example of the design matrix and contrasts used for a specific subject and session is represented in figure 4.2. The first EV

corresponds to the regressor of interest, the second to its temporal derivative, and the remaining ones refer to the confound regressors, meaning that they are ignored in the sense that no PEs maps will be constructed for such regressors. The last five regressors consist of the motion outliers detected, and the remaining ones to the motion parameters. The contrast C1 (with a 1 for EV1 and 0 elsewhere) tests for voxels where activation follows the motor task (activation of interest).

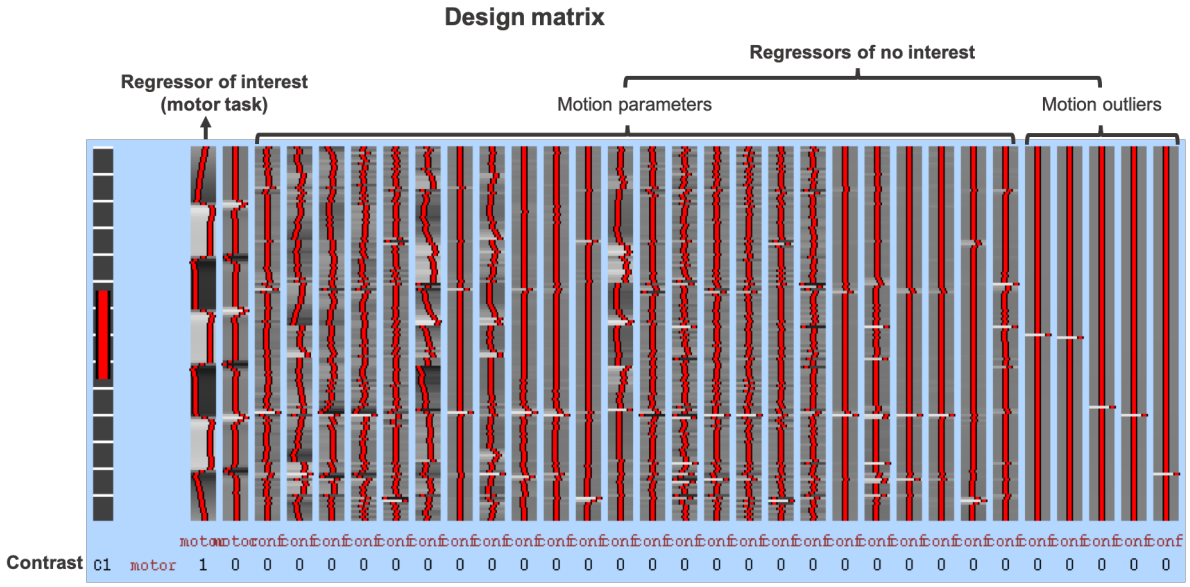

Figure 4.2: Representative design matrix and contrasts used in subject-level GLM to assess brain activation in response to the motor task for one illustrative subject and session.

The **visual** protocol comprised four and a half cycles of alternating periods of 30s of baseline condition and 30s of flashing checkerboard visualization. Accordingly, the regressor used to model the response to the visual stimulation was a simple square block timing convolved with the double-gamma HRF, along with its temporal derivative. Motion parameters and motion outliers obtained during the preprocessing were also added to model noise present in the data. An example of the design matrix and contrasts used for a specific subject and session is represented in figure 4.3. The first EV corresponds to the regressor of interest, the second to its temporal derivative, and the remaining ones refer to the non-interest regressors: the last two regressors consist of the motion outliers detected, and the remaining ones to the motion parameters. The contrast C1 (with a 1 for EV1 and 0 elsewhere) tests for voxels where activation follows the visual stimulation (activation of interest).

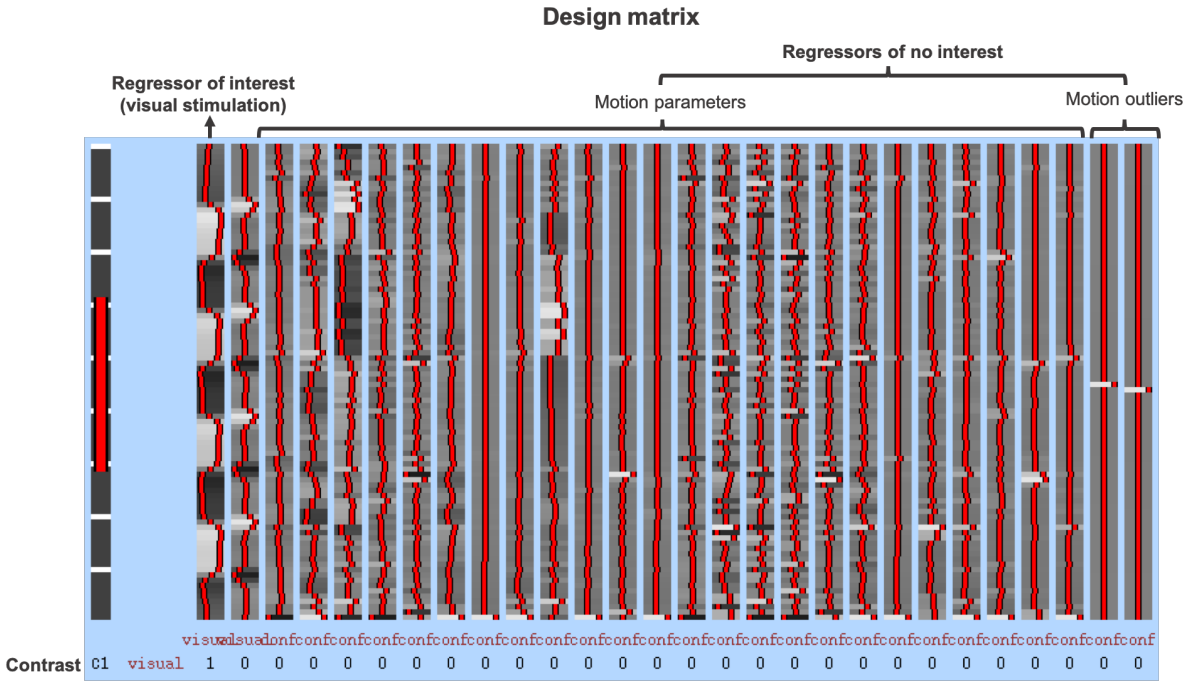

Figure 4.3: Representative design matrix and contrasts used in subject-level GLM to assess brain activation in response to the visual task for one illustrative subject and session.

4.2.2.2 Breath-hold BOLD fMRI data analysis

Concerning the **breath-holding** data, as explained in detail in Section 2.3.3.2, the most satisfactory modelling approach of the BOLD-fMRI response to a BH task is the use of a sine-cosine pair at the BH task frequency and its first two harmonics. In this work, the BH protocol included three 75s cycles of alternating periods of 20s apnea and 55s of normal breathing (baseline). Thus, the regressors consisted in sine and cosine waves at task frequency (75s) and their first and second harmonics. Motion parameters and motion outliers were also included in the model. An example of the design matrix and contrasts used for a specific subject and session is represented in figure 4.4. The first and fourth EVs correspond to the sine and cosine waves at task frequency, the second and fifth to their 1st harmonics, and the third and sixth to their 2nd harmonics, respectively. The last two regressors consist of the motion outliers detected, and the remaining ones to the motion parameters. As an example, the contrast C1 (with a 1 for EV1 and 0 elsewhere) tests for voxels where activation follows the sine waveform. For the BH task, five different F-tests were constructed: F4 combined the contrasts referring only to the sine and cosine waves (C1 and C4), F5 combined the sine and cosine waves and their 1st harmonics (C1, C2, C4 and C5), F2 combined the sine wave and its 1st and 2nd harmonics (C1, C2 and C3), F3 combined the cosine wave and its 1st and 2nd harmonics (C4, C5 and C6), and finally, F1 combined all the regressors of interest - sine and cosine waves and their 1st and 2nd harmonics (C1, C2, C3, C4, C5 and C6).

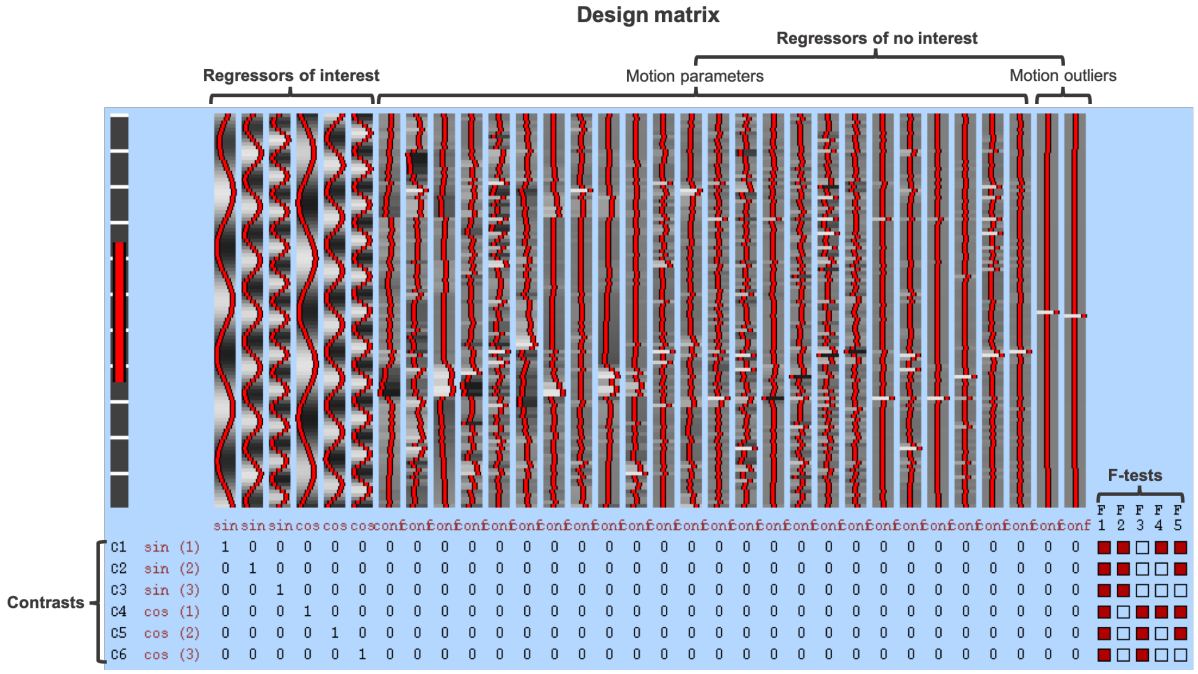

Figure 4.4: Representative design matrix and contrasts used in subject-level GLM to assess brain activation in response to the breath-holding challenge for one illustrative subject and session.

For each stimulation type, the GLM was fit to the data in each voxel. The method that FEAT uses to do this on first-level data is FILM (FMRIB's Improved Linear Model). Among the outputs are several Z statistic maps, one for each contrast (and each F-test in the case of the BH data). Cluster thresholding (cluster $p<0.05$ and voxel Z-score>3.1) was then performed on these statistic maps in order to identify brain regions with stimulus-related activation.

4.2.2.2.1 Cerebrovascular reactivity (CVR) and time-to-peak (TTP) maps computation

The next step of the analysis was to obtain whole-brain maps describing the CVR. CVR can be characterised quantitatively in terms of amplitude and temporal responses. In terms of amplitude, the metric is typically the BOLD percent signal change (PSC), while in terms of temporal responses, it is the time-to-peak (TTP) of the BOLD signal/response. As the general linear model obtained in FEAT recreates the BOLD signal/response, the values of CVR and TTP were computed from it.

First, the six regressors of interest (sine and cosine waves, and their 1st and 2nd harmonics) and respective parameter estimates values were used in MATLAB in order to recreate the GLM of the BOLD response at each voxel. The GLM recreates the BOLD response of a particular voxel to the entire BH protocol performed by each subject, i.e. to the three BH cycles. In order to obtain just one CVR and TTP value for each voxel, we computed the mean of the three BH cycles' models and computed CVR and TTP values from this single averaged model. BOLD percentage signal changes were computed in each voxel as the amplitude of the model's maximum relative to the average signal during the first baseline period (first 25 seconds) multiplied by 100 (% BOLD). Outlier voxels were identified as having PSC values 2 standard deviations above the mean value and were removed from further analysis. Time-to-peak (TTP) values were also computed in each voxel as the time of the model's maximum relative to

the onset of the BH. An exemplification of CVR and TTP computation from the sinusoidal modelling is demonstrated in figure 4.5.

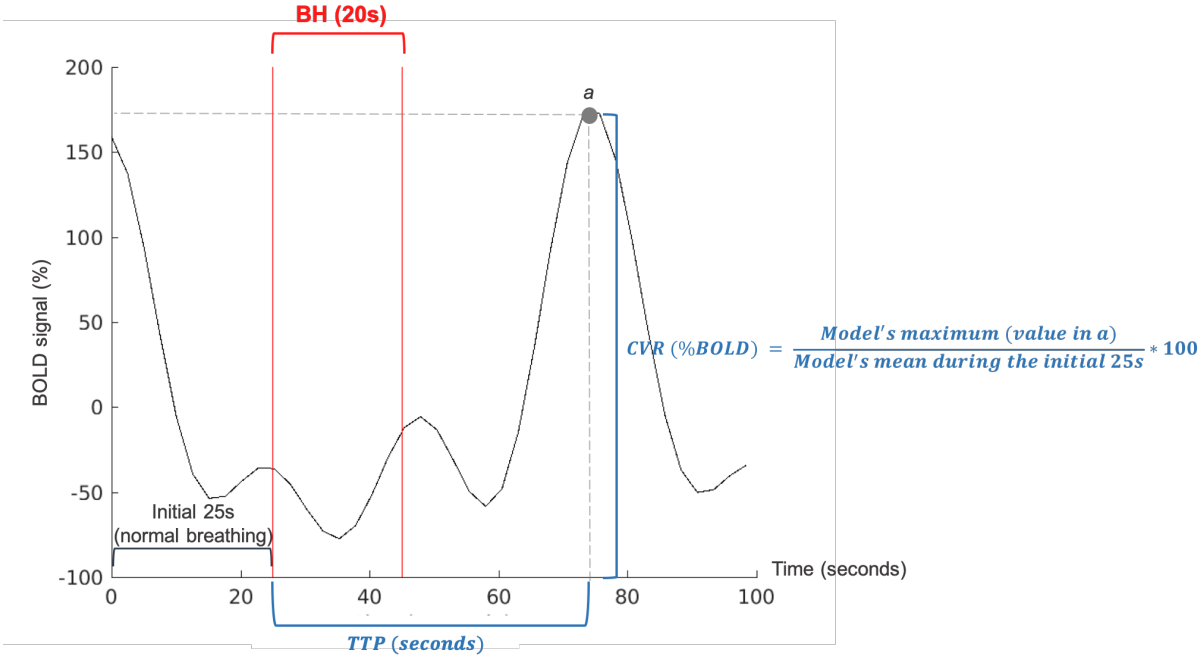

Figure 4.5: Schematic representation of the computation of the CVR metrics from the sinusoidal modelling obtained from the GLM. BOLD percentage signal change consists in the amplitude of the model's maximum (point *a*) relative to the average signal during the first baseline period (initial 25 seconds) multiplied by 100. Time-to-peak (TTP) consists in the time of the model's maximum (point *a*) relative to the onset of the BH.

The next step was to obtain two distinct brain maps for each subject: one with the value in each voxel being the CVR in %BOLD, and another with the value in each voxel being the TTP in seconds.

These maps were created only within the brain regions presenting significant activation to the BH task. To do so, we created masks of these regions: we binarized the thresholded Z statistic images referent to the F-test 1 (all regressors of interest - sine and cosine waves and their 1st and 2nd harmonics) resulting from each subject-level analysis. This resulted in a whole-brain binary mask for each subject and session, with a value of 1 in voxels showing significant activation in response to the BH task, and 0 elsewhere. These individual binary masks were imported to MATLAB and used as a template to create the CVR and TTP maps for each subject and session.

In addition, CVR and TTP maps were only assigned non-zero values for voxels belonging to the grey matter (GM). The rationale for this was that, within the brain, the distribution of blood flow is heterogeneous. GM is a very much vascularized area, that receives several times more flow than white matter (WM) (comparable to that in heart muscle) [86]. Additionally, in BH-CVR studies, greater BOLD signal change is usually seen in GM while nonsignificant changes are usually observed in WM [91, 93, 148]. A study aiming to investigate the distribution of CVR within the brain observed a three times higher percent signal change in GM compared to WM [149]. Also, it revealed a hemispherically symmetrical and homogeneous distribution of CVR over the entire GM. Hence, we decided to obtain these maps only within the GM.

To do so, GM masks had to be created for each individual. Resulting from the tissue segmentation

of the structural images performed during the preprocessing (Section 4.2.1.1), there were GM whole-brain images for each subject. Voxel values of these images represent the probability of that particular voxel belonging to the grey matter. In order to create binary masks (a value of 1 for voxels belonging to GM, and 0 elsewhere), these images were thresholded at a probability value of 0.5 and binarized, meaning that only voxels with $>$50% probability of belonging to GM were given a value of 1. Then, they were registered to the individual's functional image in each subject and session, by using the spatial transformation from functional to structural spaces that had been obtained during the preprocessing registration step.

The GM masks were imported to MATLAB and the whole-brain CVR and TTP maps were obtained only within them for each subject and session.

4.2.3 Group-level BOLD-fMRI data analysis

At this stage, resulting from the subject-level data analysis were CVR and TTP maps, as well as motor and visual activation maps, for each subject and for each session.

In order to compare brain activity between the two sessions (ictal versus interictal phases of the migraine cycle), the individual maps were registered to the standard MNI152 space making use of the spatial transformation obtained during preprocessing, and group-level analysis was performed.

4.2.3.1 Voxel-wise analysis

The group-level analysis started with a voxel-wise investigation of ictal versus interictal differences in motor and visual activation maps, and CVR and TTP maps. This means that every single voxel was individually tested for significant differences between S1 and S2.

To do so, non-parametric permutation testing was implemented using the *randomise* tool from FSL (`https://fsl.fmrib.ox.ac.uk/fsl/fslwiki/Randomise`).

Randomise performed group-level analyses in a very straightforward way: it began by computing for each subject the difference between the two conditions (S1$-$S2) for each one of the stimuli (motor, visual, BH); then, these within-subject differences were entered into a one-sample (group) *t*-test.

As an example, for the group-level analysis performed on CVR maps, there were 22 separate 3D brain maps (11 subjects, with 2 maps per subject) resulting from the subject-level analysis. The first step was to use *fslmaths* (`https://fsl.fmrib.ox.ac.uk/fsl/fslwiki/Fslutils`) to calculate the difference between S1 and S2 for each subject, ending up with one 3D image per subject. Then, *fslmerge* (`https://fsl.fmrib.ox.ac.uk/fsl/fslwiki/Fslutils`) was used to create a single 4D volume with the 11 individual difference images (along the 4th dimension).

This 4D volume was given as an input to *randomise*. *Randomise* conducted 5000 permutations of the data to build up the null distribution to test against, and output a whole-brain map with the value in each voxel being the 1p-value. Once thresholded voxel-wise, these maps show the voxels in which activation between the two conditions (S1 vs S2) was significantly different.

Randomise performs multiple comparisons correction with the Threshold-Free Cluster-Enhancement

(TFCE) method. Therefore, in the output 1p-value images, only FWE-corrected p-values less than 0.05 are accepted, meaning that the chance of having one or more false positives over the entire brain is no more than 5%.

4.2.3.1.1 Whole-brain

This sequence of steps was conducted for the CVR and TTP maps, as well as for the motor and visual brain activation maps. This resulted in four whole-brain images representing the differences in reactivity and brain activation between ictal and interictal phases of the migraine cycle.

4.2.3.1.2 Region-specific

Assessing CVR and TTP differences in global GM provides insight into the overall variations of the responsiveness of the cerebrovasculature to the BH hypercapnia stimulus. However, after the whole-brain group-level analysis, we were interested in regional variations in vascular reactivity within the brain. With that purpose, we proceeded to investigate CVR and TTP differences in particular brain regions, i.e. a region-specific group-level analysis.

This next step required the creation of brain masks to define those specific regions. These masks consisted of whole-brain images with a value of 1 in voxels that belong to the brain region being masked, and 0 in voxels that do not belong. These masks were given as an input to the *randomise* command, which investigated ictal versus interictal differences in CVR and TTP maps only in the voxels included in the masks.

4.2.3.1.2.1 Cerebral lobes

First, we focused on the structural cerebral lobes: frontal, occipital, temporal, and parietal lobes. Masks of these regions were obtained from the Harvard-Oxford Cortical structural atlas, which already comes with FSL [150].

This atlas is normalized to the MNI152 standard space, and partitions the brain into different labels, each one representing a different brain region. The intensity in each voxel corresponds to its probability of belonging to a specific brain structure.

In order to obtain a binary mask (0's and 1's) instead of a probabilistic map of each cerebral lobe, we must threshold the probabilistic map at a certain probability value. We chose a value of 10%, meaning that every voxel with $>$10% probability of belonging to the cerebral lobe being masked was included in the binary mask.

We created four different masks for each one of the cerebral lobes, which are presented in figure 4.6.

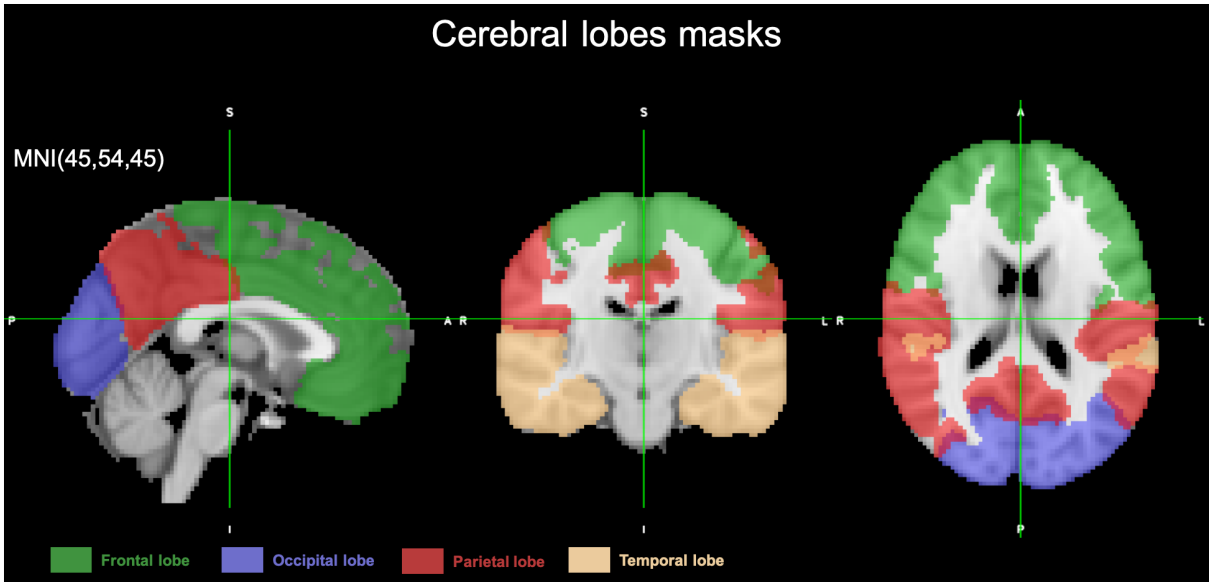

Figure 4.6: Cerebral lobes masks used for the region-specific group-level analysis performed in this study: frontal, occipital, parietal and temporal lobe masks. The masks were defined in the standard MNI152 space. All masks are represented in the sagittal, coronal and axial planes (from left to right) for better representation. A and P mark the anterior and posterior sides in the sagittal and axial representations. R and L mark the right and left sides in the coronal and axial representations. S and I mark the superior and inferior directions in the sagittal and coronal representations.

4.2.3.1.2.2 Arterial flow territories

We then focused our attention on blood flow territories.

Ready-to-use arterial flow territory probability atlas are available online [151]. They were developed from brain images of 158 subjects, and correspond to probability maps of the left and right internal carotid arteries (ICA) and vertebrobasilar artery (VBA) flow territories. The intensity in each voxel represents the probability (0-1) of that particular voxel belonging to the artery flow territory.

In order to obtain a binary mask, the threshold chosen was 0.3, meaning that every voxel with $>$0.3 (30%) probability of belonging to the arterial flow territory was included in the masks. The final ICA and VBA masks are presented in figure 4.7. The goal of creating these two different masks was to obtain distinct masks for the anterior and posterior cerebral circulations: the ICA flow territory mask represents the anterior cerebral circulation, thus including more anterior regions of the brain as well as regions supplied by the ACA and MCA (frontal lobe and lateral surfaces of the temporal and parietal lobes); the VBA flow territory mask represents the posterior cerebral circulation, thus including posterior brain regions as well as the regions supplied by the PCA (including some regions of the temporal lobe).

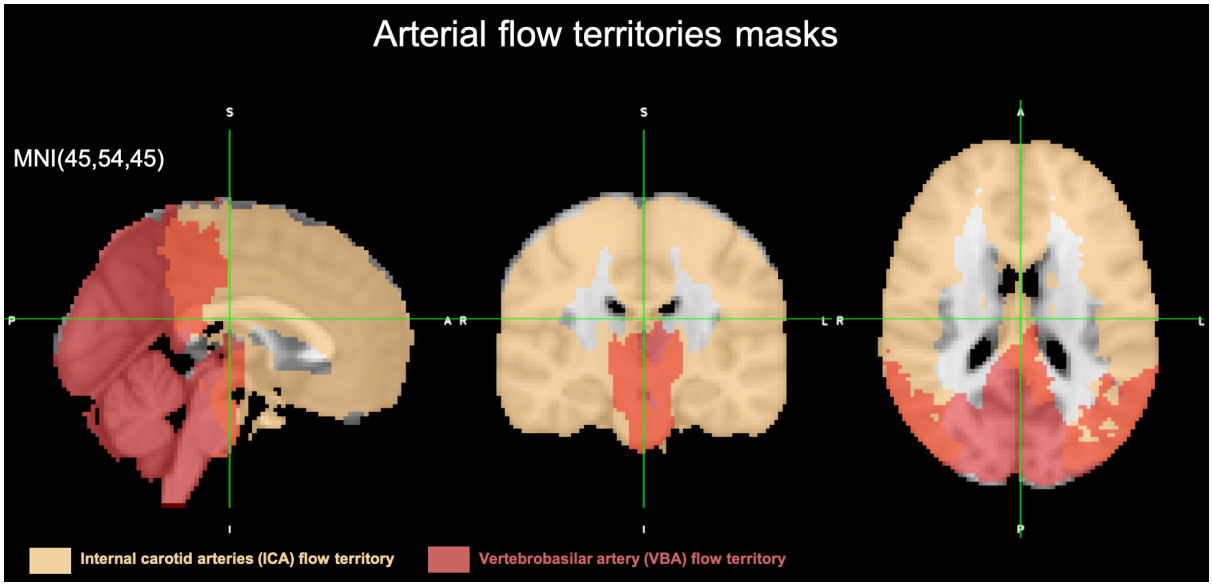

Figure 4.7: Arterial flow territories masks used for the region-specific group-level analysis performed in this study: internal carotid arteries (ICA) and vertebrobasilar artery (VBA) masks. The lighter red corresponds to the overlap of both masks. The masks were defined in the standard MNI152 space. All masks are represented in the sagittal, coronal and axial planes (from left to right) for better representation. A and P mark the anterior and posterior sides in the sagittal and axial representations. R and L mark the right and left sides in the coronal and axial representations. S and I mark the superior and inferior directions in the sagittal and coronal representations.

As explained earlier in Section 2.3.4.1.2, the VBA supplies posterior regions of the brain. More specifically, it serves the brainstem, the cerebellum, the occipital lobe, and the thalamus. In order to be more specific in the investigation, we also wanted to assess if there was a particular region included in the VBA flow territory that presented ictal versus interictal CVR differences in migraine. To do so, we created masks of these regions by overlapping the VBA flow territory mask with masks of the brainstem, the cerebellum, the occipital lobe, and the thalamus, which were obtained from the FSL atlases [150] (similar to what was done with the cerebral lobes masks). These four additional masks are presented in figure 4.8.

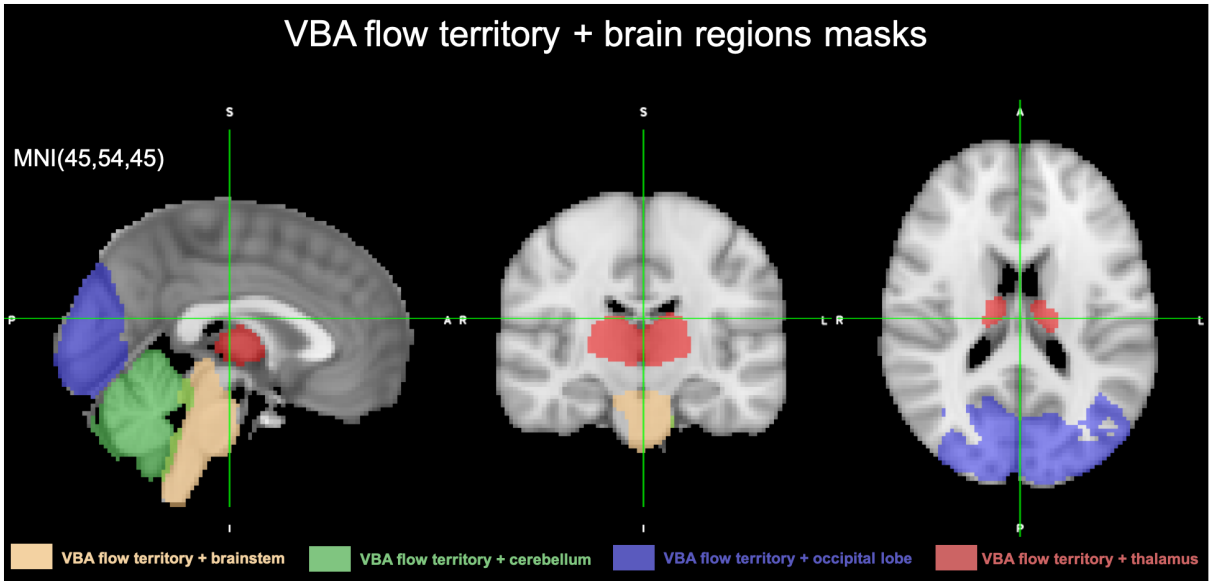

Figure 4.8: Vertebrobasilar artery (VBA) flow territory mask overlapped with four respective segmented regions masks: brainstem, cerebellum, occipital lobe, and thalamus (from left to right) used for the region-specific group-level analysis performed in this study. The masks were defined in the standard MNI152 space. All masks are represented in the sagittal, coronal and axial planes (from left to right) for better representation. A and P mark the anterior and posterior sides in the sagittal and axial representations. R and L mark the right and left sides in the coronal and axial representations. S and I mark the superior and inferior directions in the sagittal and coronal representations.

4.2.3.2 Region-of-interest (ROI) analysis

The next step of this investigation focused on the regions identified by the group-level analysis, i.e. the regions that presented statistically significant CVR and TTP differences between the ictal and interictal phases of the migraine cycle. We call this ”Region-of-Interest (ROI) analysis”.

4.2.3.2.1 Correlation with clinical features

In order to search for possible relationships between the values of CVR and TTP within the ROIs and several clinical features, a post-hoc analysis was performed.

For each subject and session, mean values of CVR and TTP within these regions were computed and Pearson correlation analysis [152] was performed between the individual mean CVR and TTP values and several migraine clinical features. For testing the null hypothesis (no correlation) against the alternative hypothesis of a significant correlation, a significance threshold of 5% was applied.

The clinical parameters considered for correlation were either general, i.e. characterizing participants' usual attacks, or referring to the ongoing attack on the day of S1. The clinical features are presented for each subject in the table 4.4. The only general feature (the headache intensity) was correlated with CVR and TTP values from both S1 and S2, while the clinical features characterising the ongoing migraine attack were correlated with CVR and TTP values only from S1.

Table 4.4: General migraine clinical parameters and migraine clinical parameters characterizing the ongoing attack in the day of S1, for each participant.

Subject	General clinical parameter	Clinical parametes in S1		
	Usual headache intensity (0-10 VAS)	**Attack/Pain duration (h)**	**Headache intensity (0-10 VAS)**	**Photophobia (0-10 VAS)**
1	7.5	7.38	8	3
2	10	22.25	6	3
3	6	1.23	6	2
4	7.5	67.8	5	4
5	7	9.2	7	8
6	8	41.27	7	5
7	6	12.33	6	5
8	8	7.07	8	7
9	6.5	6	9	5
10	9	3.33	8	6.5
11	5.5	11.12	6	5

h = hours; VAS = Visual Analogue Scale

Chapter 5

Results and Discussion

The main goal of the present work was the investigation of CVR differences between the ictal and interictal phases of the migraine cycle. With this purpose, data referred to a BH task from 11 migraine patients, who underwent two fMRI sessions (S1, ictal and S2, interictal), was preprocessed and afterward analyzed to construct CVR and TTP maps. Afterwards, the statistical analysis of these maps allowed for the detection of significant vascular reactivity group differences between S1 and S2.

5.1 Subject-level BOLD-fMRI data analysis

5.1.1 Function-specific BOLD fMRI data analysis

Apart from a BH task, patients were also subjected to a motor task and visual stimulation in both sessions S1 and S2. Analysis of the data referred to these tasks for each subject and session was carried out and resulted in whole-brain maps showing the clusters of voxels with significant activation in response to visual and motor stimuli. Representative motor and visual brain activation maps are represented in figure 5.1.

After going through all the individual motor and visual brain activation maps (for all subjects and sessions), it was observed that the clusters of activated voxels were all located in the brain regions specific to motor and visual functions, i.e. motor and visual cortices, as expected.

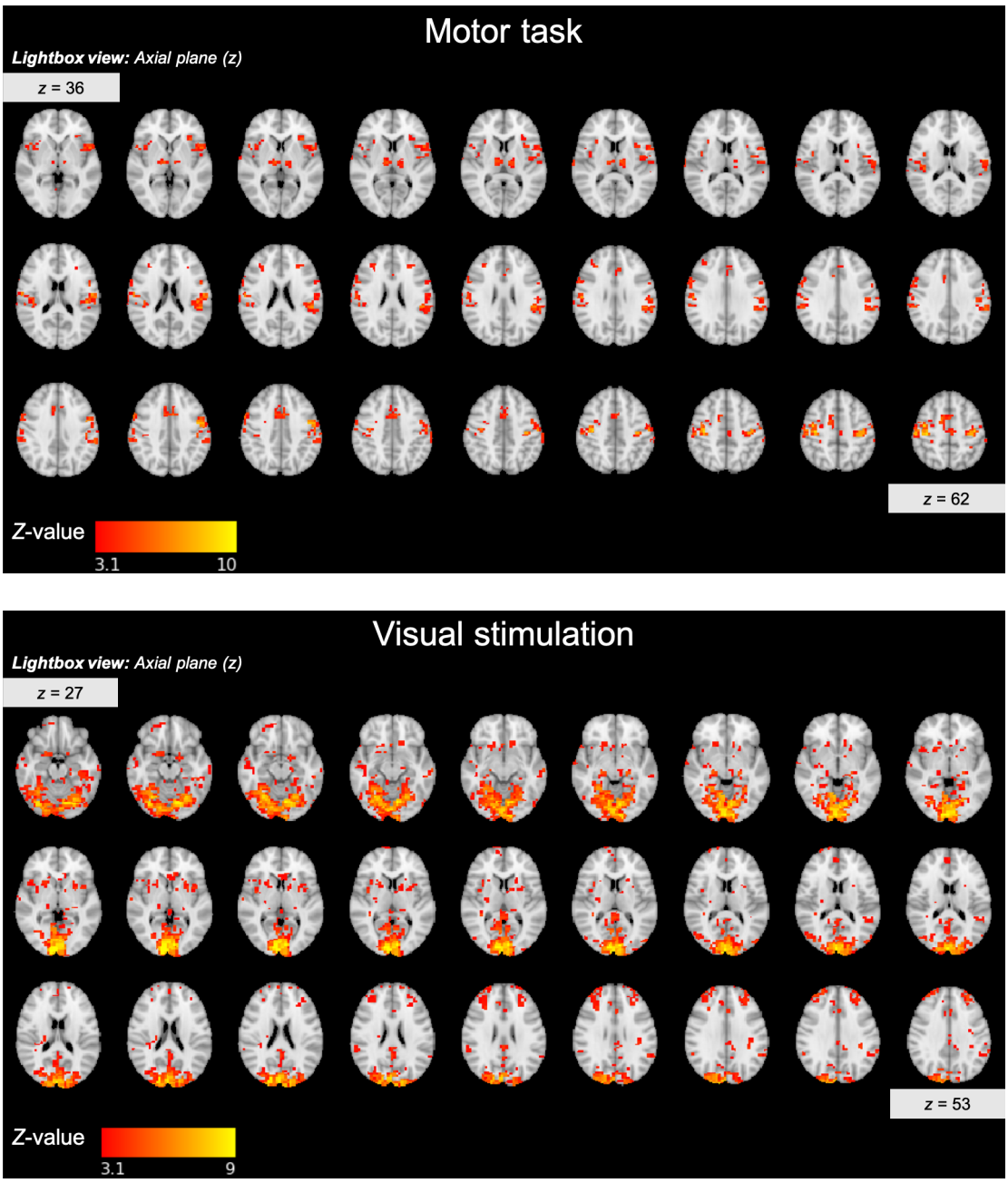

Figure 5.1: Representative brain activation maps in response to the motor task (top) and visual stimulation (bottom) for one illustrative subject and session. The map is represented as a thresholded Z-map ($Z>3.1$) in the standard MNI152 space. The z coordinate in the standard space is shown for the most inferior and most superior slices in the axial plane.

5.1.2 Breath-hold BOLD fMRI data analysis

5.1.2.1 Cerebrovascular reactivity (CVR) and time-to-peak (TTP) maps computation

Regarding the CVR and TTP maps, these were only obtained (for each individual and each session) within the voxels belonging to each individual's GM. Representative CVR and TTP maps are shown in figure 5.2. For all subjects and for both sessions, virtually the entire GM presented significant activation in response to the BH task. This result is not surprising since GM is a highly vascularized area within the brain and in most CVR studies using a breath-holding task, GM presents a very large signal change [86, 91, 153].

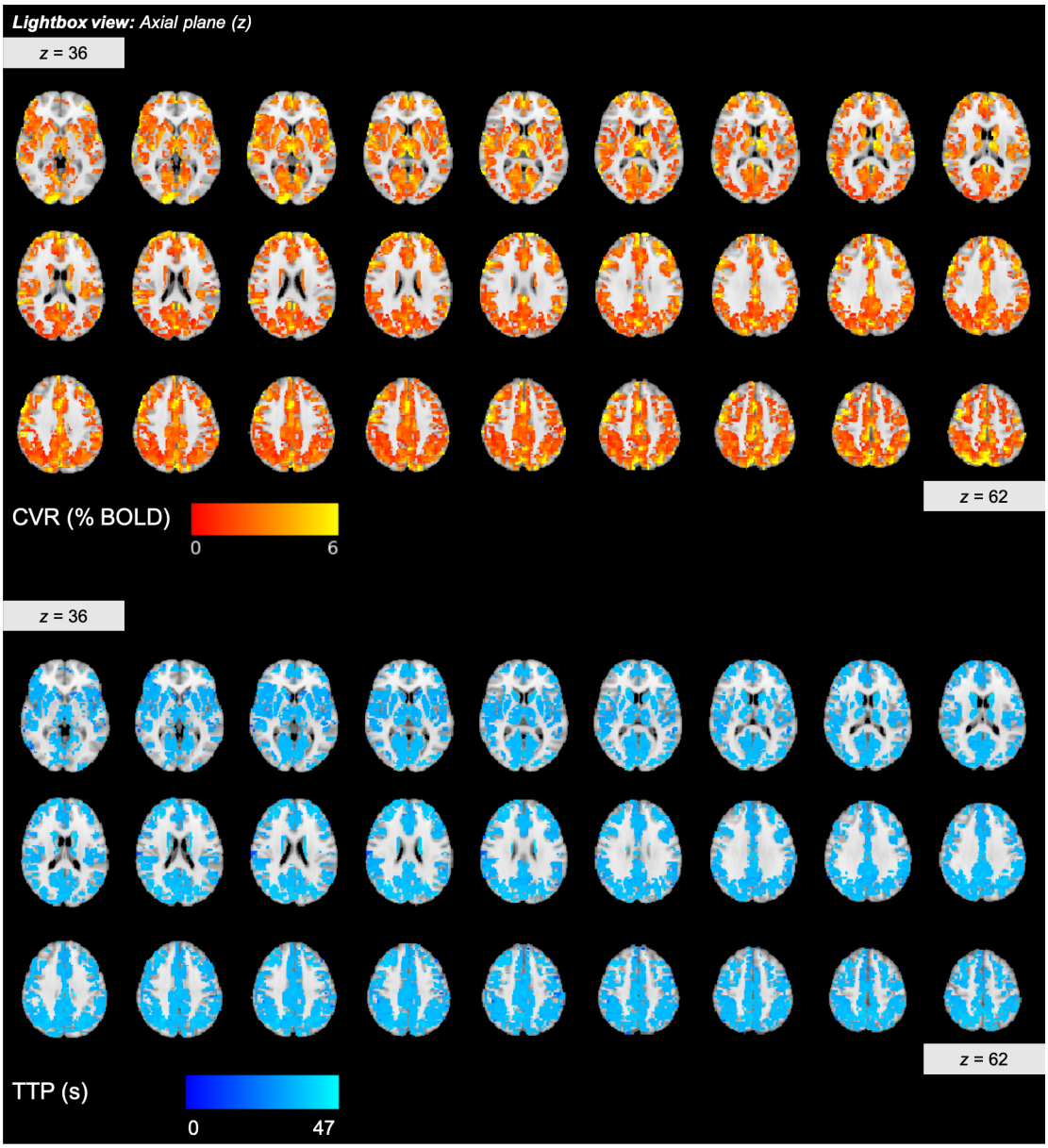

Figure 5.2: Representative cerebrovascular reactivity (CVR, %BOLD) and time-to-peak (TTP, s) maps for one illustrative subject and session. The maps are represented in the standard MNI152 space. The z coordinate in the standard space is shown for the most inferior and most superior slices in the axial plane.

5.2 Group-level BOLD-fMRI data analysis

Group-level analysis was performed on motor, visual, and reactivity (CVR and TTP) data in order to study differences in brain activation and reactivity between the ictal and interictal phases of the migraine cycle.

5.2.1 Voxel-wise analysis

5.2.1.1 Whole-brain

A whole-brain analysis was performed for each one of the different group of maps (motor, visual, CVR and TTP) in order to assess voxel-wise differences concerning brain activation and reactivity between S1 and S2. These differences were estimated using non-parametric permutation testing. Statistically relevant voxels were the ones surviving to a significance threshold of 0.05, FWE-corrected with the TFCE method.

Motor fMRI data group-level analysis

Regarding the motor task, no voxel has survived the significance threshold of 0.05, meaning that no significant group differences between S1 and S2 were found. The maximum 1p-value of the output map of the group-level analysis was of 0.63. Thus, it is possible to conclude that migraineurs do not present any neuronal alterations in motor function-specific brain regions between the ictal and interictal phases of the migraine cycle.

Visual fMRI data group-level analysis

The voxel-wise group-level analysis of the visual data revealed significant differences in brain activation between S1 and S2, which are presented in figure 5.3. It is possible to observe that these differences were not in brain regions involved in visual functions, as they did not occur in occipital/visual cortex regions.

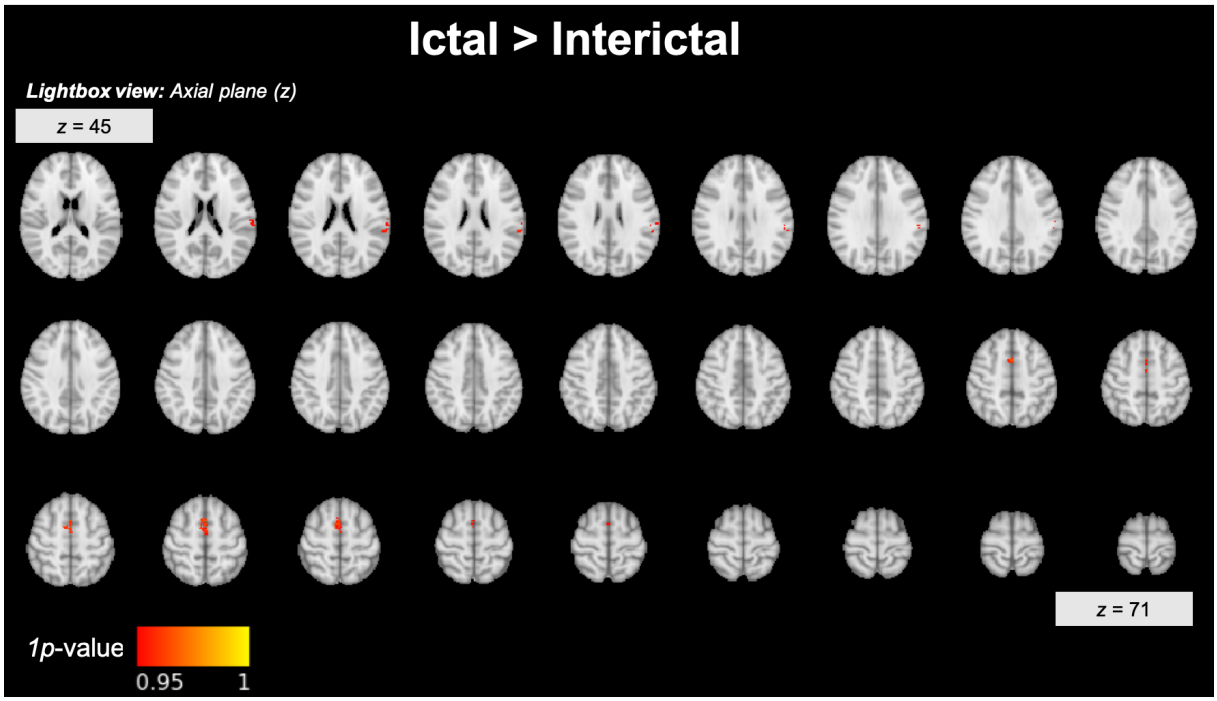

Figure 5.3: Group-level analysis of brain activation maps in response to visual stimulation: map of statistically significant differences between the ictal and interictal phases. Increased brain activation was found in the ictal vs. interictal phase ($p<0.05$). The map is represented in the standard MNI152 space. The z coordinate in the standard space is shown for the most inferior and most superior slices in the axial plane.

In order to investigate these clusters of voxels, in particular their location, the FSL tool *cluster* (`https://fsl.fmrib.ox.ac.uk/fsl/fslwiki/Cluster`) was used. A threshold of 0.95 was given, meaning that this tool reported information only about the clusters with 1p-values higher than 0.95 (equivalent to threshold at $p<0.05$). The output provided by *cluster* was a table reporting the different clusters, together with their size and information about their location and contents (in this case, the maximum 1p-value within each cluster). The clusters of voxels identified as presenting activation differences between S1 and S2 were predominantly located in the right premotor cortex (Brodmann area 6) and Broca's area (Brodmann areas 44 and 45).

Table 5.1: Characteristics of the two larger clusters showing significant ictal > interictal brain activation differences in response to visual stimulation.

Cluster index	Number of voxels	Peak MNI coordinate			Brain region(s)
		x	y	z	
1	115	44	67	64	Right premotor cortex (Brodmann area 6)
2	53	75	67	36	Left Broca's area (Brodmann areas 44 and 45)

Nevertheless, brain regions normally involved in and responsible for visual functions showed no differential activation to visual stimulation between S1 and S2. The same results were observed regarding brain regions involved in motor functions. Together, these observations allowed us to assume that the neuronal brain response was not altered between the ictal and interictal phases of migraine.

Thus, we proceeded into a group-level analysis on reactivity data (CVR and TTP maps) assuming that neuronal changes did not occur in these patients between S1 and S2, and hoping to be able to

identify alterations in brain vascular responses during ictal versus interictal phases.

Cerebrovascular reactivity fMRI data group-level analysis

CVR data group-level analysis started by averaging the values of CVR and TTP maps (within the GM) for each subject and session, in order to obtain individual mean values of CVR and TTP, regardless of the voxelwise group analysis. The boxplots representing the distributions of the mean CVR and TTP values (within the GM) for each session are represented in figure 5.4. Afterwards, an analysis of variance (ANOVA) was performed over the individual S1 and S2 averaged CVR and TTP values in order to analyze paired differences between the ictal and interictal phases. The ANOVA test revealed no significant difference in the mean CVR and TTP between the ictal and interictal periods (p>0.05).

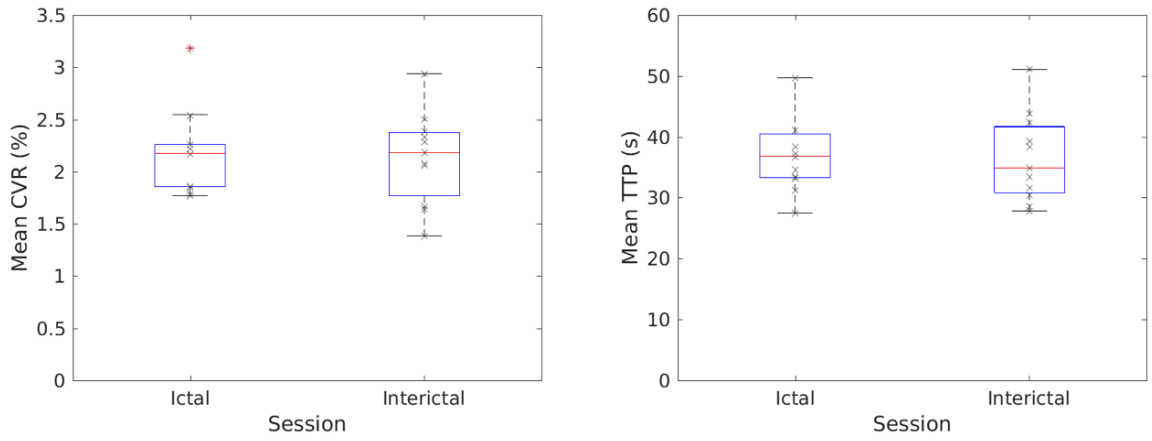

Figure 5.4: Boxplots representing the distributions across patients of the mean CVR and TTP values within the GM for each session. In the boxplots, the central mark is the median; the edges of the box are the 25th and 75th percentiles; the upper and lower extreme represent, respectively, the maximum and minimum values (excluding outliers).

Following, a non-parametric permutation testing was performed over the CVR and TTP maps in order to investigate group differences between the ictal and interictal phases. The brain maps resulting from these group-level analyses revealed a very small cluster of voxels in occipital regions surviving the significance threshold of 0.05 (FWE-corrected with the TFCE method) for both CVR and TTP differences. The maximum 1p-value reported for CVR and TTP group-level analysis was of 0.97 and 0.96, respectively. However, we did not consider these clusters to be relevant due to their very small size. In fact, they were barely detected when thresholding the outpup 1p-value map at 1p>0.95 (equivalent to p<0.05).

In this analysis it would be expected to find bigger clusters of voxels showing alterations in vascular reactivity between the ictal and interictal phases of migraine. The absence of significant results may be partially explained by the low number of participants in the study and consequent lack of statistical power, not enough to survive a strict corrected threshold, together with the fact of the brain region being investigated in this group analysis being relatively large (the entire GM).

5.2.1.2 Region-specific

Following the whole-brain (more specifically, GM) group-level analysis of CVR and TTP maps, a region-specific voxel-wise analysis was performed in these maps in order to assess voxel-wise differences of particular brain regions between S1 and S2. These differences were estimated using non-parametric permutation testing. Statistically relevant voxels were the ones surviving to a significance threshold of 0.05, FWE-corrected with the TFCE method.

5.2.1.2.1 Cerebral lobes

The first brain regions to be studied in closer detail were the cerebral lobes. After defining masks representing these regions, CVR and TTP group differences between S1 and S2 were assessed within each one of the four cerebral lobes: frontal, occipital, parietal and temporal lobes.

Concerning the frontal, parietal, and temporal lobes, no voxel has survived the significance threshold of 0.05, meaning that no significant group differences between S1 and S2 were found. This result enabled to conclude that there is no vascular reactivity differences in the frontal, parietal, and temporal lobes between the ictal and interictal phases of episodic migraine without aura. As previously referred, an abnormal CVR is a downstream marker of impaired endothelial function. Therefore, finding no CVR and TTP differences means that there is no endothelial impairment in these brain regions between S1 and S2.

As for the occipital lobe mask, the group-level analysis revealed an increased CVR and TTP during the ictal phase compared to the interictal phase of migraine, as shown in figure 5.5. Specifically, these differences were located in the primary visual cortex (V1), and in the visual areas 2, 3 and 4 (V2, V3, and V4).

One important aspect to mention is that the voluntary act of breathing, which is present when performing a BH challenge, is able to induce neuronal activation and consequent local cerebral blood flow and oxygenation changes. These CBF changes could influence the results, i.e. it could be possible that some of the BOLD signal changes time-locked to the BH challenge were neuronal in origin. Previous studies have investigated the brain regions involved in the conscious control of breathing and identified the primary sensory and motor cortices, the supplementary motor area, the cerebellum, thalamus, caudate nucleus, globus pallidum, and medulla [154]. By looking at the maps in figure 5.5, it is possible to observe that the group-level analysis results of this work did not reveal significant differences in any of these regions. Thus, it can be assumed that neuronally-induced BOLD response is unlikely to have contributed to the group differences found in occipital regions of the brain.

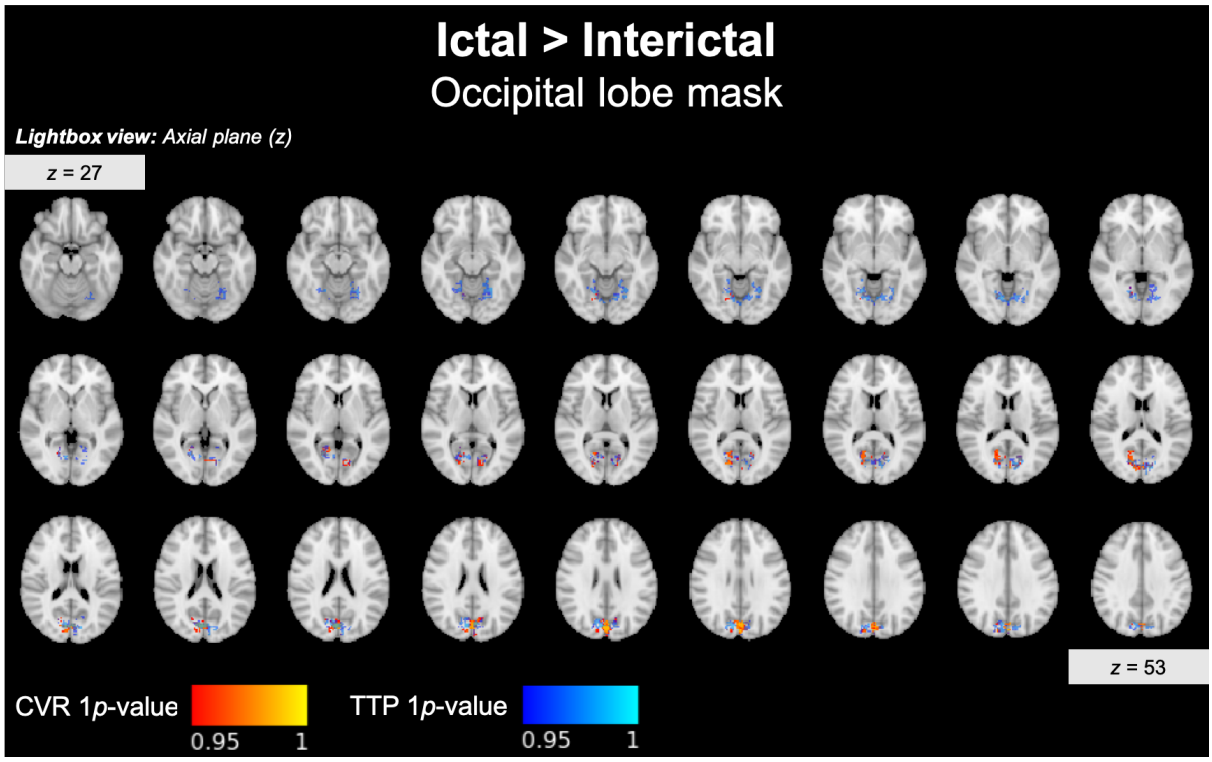

Figure 5.5: Group-level analysis of CVR and TTP maps performed within the occipital lobe mask: maps of statistically significant differences between the ictal and interictal phases. Increased CVR and TTP were found in the ictal vs. interictal phase ($p<0.05$). The map is represented in the standard MNI152 space. The z coordinate in the standard space is shown for the most inferior and most superior slices in the axial plane.

5.2.1.2.2 Arterial flow territories

Afterwards, we focused our search for reactivity differences on blood flow territories, in particular the territories of the internal carotid arteries (ICA) and vertebrobasilar artery (VBA).

Regarding the group analysis performed within the ICA flow territory mask, no voxels survived the significance threshold of 0.05, which means that no differences in CVR and TTP between S1 and S2 were found in this region. The ICA flow territory mask represented the anterior cerebral circulation, including the regions supplied by the ICA as well as by the ACA and MCA, i.e. frontal and lateral surfaces of the temporal and parietal lobes. Thus, the fact that no group differences were found within this brain mask is concordant with the previous result reported in section 5.2.1.2.1 of no group differences in frontal, parietal and temporal lobes.

Revisiting the literature review, the vast majority of studies have used TCD to evaluate CVR in middle cerebral arteries (MCA). Moveover, most of them compared patients in the interictal phase of migraine with matched healthy controls. The results have yielded both hyperreactivity [132, 133, 141] and hyporeactivity [52, 129, 134], but most of them found no reactivity differences of the MCA between migraineurs in the attack-free interval and controls [55, 130, 131, 135, 136]. Thus, it can be declared that the MCA in the interictal phase of migraine are not affected by an abnormal vascular reactivity, and hence no cerebral endothelial dysfunction. Regarding comparison of ictal versus interictal phases of migraine, the first study performing this comparison used SPECT imaging and focused predominantly in MwoA patients. It observed a reduced CVR to hypercapnia during the attack, which returned to normal 6-20 hours after

the headache had subsided, and was excessive during the interictal/headache-free phase [128]. These observations were supported by a further TCD study by Harer et al. [140], who observed a reduced CVR of the MCA during the headache attack, followed by nearly CVR in the interictal phase. Contrary to these results, one study showed no difference in CVR of these arteries in migraineurs between the attack and the attack-free interval [137]. The results of the present work are consistent with these last findings and extent them to the anterior cerebral circulation (not only the MCA), showing similar vascular reactivity (CVR and TTP) of this circulation between the ictal and interictal phases of migraine.

Thus, previous studies' results of normal interictal CVR in the MCA in migraine patients (compared to controls), together with this work's result of similar CVR of the ICA flow territory between the ictal and interictal phases of migraine, suggest that the anterior cerebral circulation is not affected by impaired vascular reactivity in migraine.

As for the VBA flow territory mask, group-level analysis revealed increased CVR and TTP within this region during the ictal compared to the interictal session. These results are presented in figure 5.6, where it is possible to observe that the statistically significant clusters of voxels are essentially located in the same regions as the ones found within the occipital lobe mask (figure 5.5).

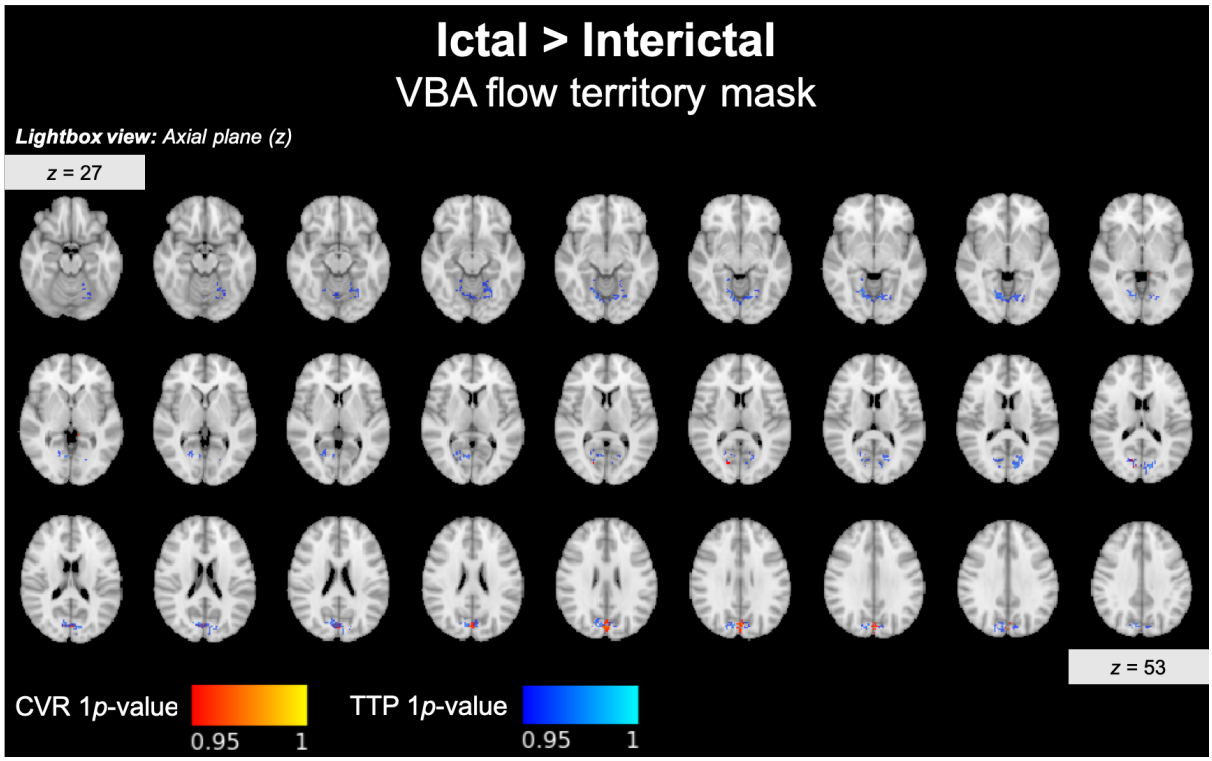

Figure 5.6: Group-level analysis of CVR and TTP maps performed within the VBA flow territory mask: maps of statistically significant differences between the ictal and interictal phases. Increased CVR and TTP were found in the ictal vs. interictal phase ($p<0.05$). The map is represented in the standard MNI152 space. The z coordinate in the standard space is shown for the most inferior and most superior slices in the axial plane.

As explained back in section 2.3.4.1.2, the VBA serves as a blood supply not only to the occipital lobes, but also to the brainstem, the cerebellum, and the thalamus. In order to be able to draw more robust conclusions regarding occipital regions of the brain, and also to assess whether any of the remaining brain regions supplied by the VBA presented CVR differences between S1 and S2, group-level analyses were performed in four additional masks (VBA flow territory mask overlapped with these four brain regions' masks). From these, only the VBA flow territory + occipital lobe mask presented statistically significant group differences between S1 and S2, that can be seen in figure 5.7. It is possible to observe that the statistically significant clusters of voxels are essentially the same as the ones identified in the group-level analysis performed within the occipital lobe mask (figure 5.5).

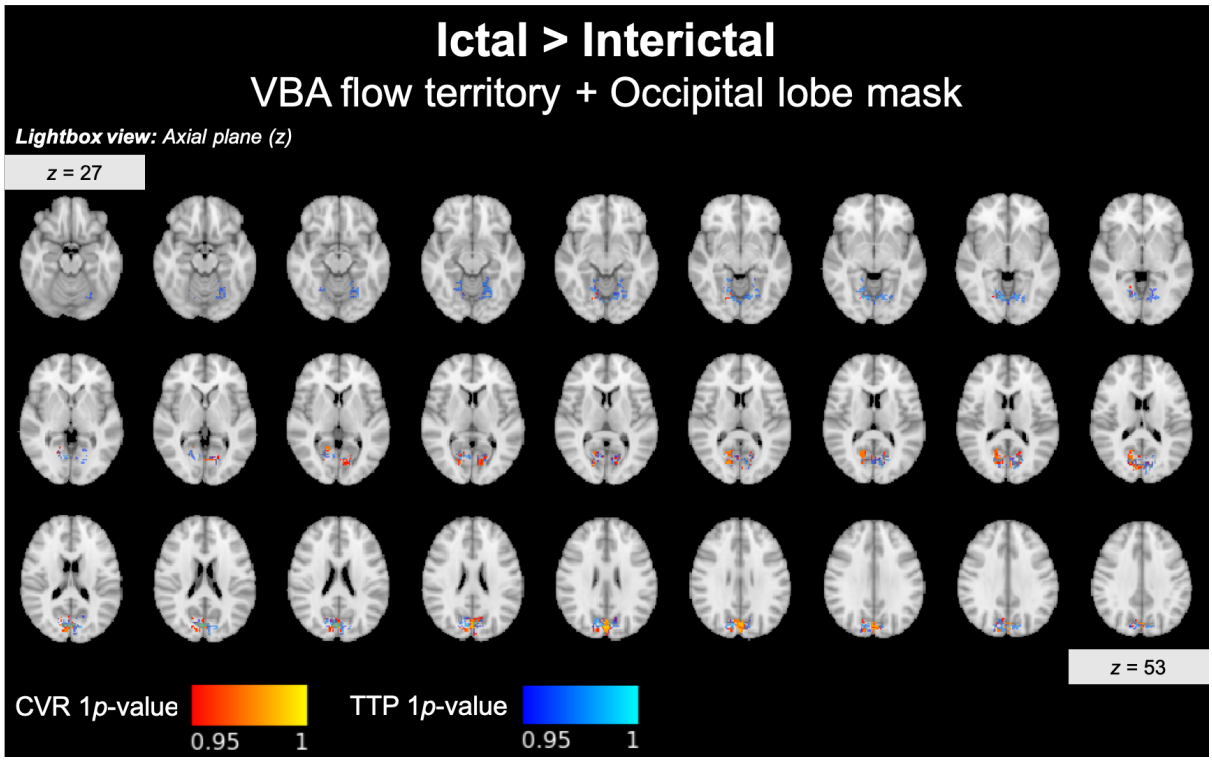

Figure 5.7: Group-level analysis of CVR and TTP maps performed within the VBA flow territory mask overlapped with the occipital lobe mask: maps of statistically significant differences between the ictal and interictal phases. Increased CVR and TTP were found in the ictal vs. interictal phase ($p<0.05$). The map is represented in the standard MNI152 space. The z coordinate in the standard space is shown for the most inferior and most superior slices in the axial plane.

All together, these results showed that patients with episodic migraine without aura have increased CVR and TTP within the posterior cerebral circulation (represented by the VBA territory mask), more specifically within occipital regions, during the headache phase of a spontaneous migraine attack compared to the interictal phase.

Regarding the literature review, the vast majority of studies regarding CVR of the posterior cerebral circulation in migraine compared patients during the interictal/attack-free period with healthy subjects. Contradictory results have been achieved, ranging from reduced [5, 55, 129] to normal [131, 139] and even exaggerated [133] interictal vascular responses of migraineurs' brain in comparison with controls.

In the first study back in 1979, reactivity to CO_2 inhalation was reduced during the attack, returned to normal values 6-20 hours after the attack, and was excessive during the interictal/headache-free interval

[128]. Later on, Kastrup et al. [133] achieved the same result: increased CVR to CO_2 inhalation of the PCA during the interictal phase of migraine compared to healthy controls. Two other studies found no differences in CVR between migraineurs and healthy controls [131, 139].

Perko et al. were the pioneers in using L-arginine infusion as the vasoactive stimulus to induce hypercapnia. They evaluated vascular reactivity of the PCA in migraine patients during the interictal phase in respect to healthy subjects [5]. Rajan et al. [55] performed the same comparison in the PCA as well as in the BA, using BH as the vasoactive stimulus. Both studies observed reduced CVR of the posterior circulation arteries outside the migraine attack compared to healthy subjects. Importantly, both studies also assessed the MCA and found no difference in their reactivity. Thus, these results showed for the first time an impairment of the CVR restricted to the posterior cerebral circulation in migraine patients during the interictal phase compared to healthy subjects. A more recent study confirmed these results by observing a reductal interictal CVR in the PCA compared to HC [129].

Regarding the investigation of ictal versus interictal differences in posterior cerebral circulation's reactivity, to the best of our knowledge, there are only three TCD studies performing this comparison. The first evaluated the basilar artery (BA) [139] and the second study both the BA and VBA [138], during and outside a migraine attack without aura. No differences in vascular reactivity between both periods were detected, which lead the authors to declare that the functional integrity of these posterior circulation's arteries was not affected during migraine attacks without aura. The third study observed a lower reactivity during the migraine attack than the migraine-free interval, suggesting a failure of cerebrovascular regulation during attacks of migraine without aura [137].

The results of the present work contribute with new evidence to the literature. They demonstrated for the first time that migraine patients during spontaneous attacks had increased CVR of the posterior cerebral circulation restricted to occipital regions compared to the interictal period. In addition, vascular reactivity was examined not only in terms of percent signal change, but also in terms of the amount of time to reach the peak of response/CVR. To the best of our knowledge, this was the first time that the latency/delay of the response was evaluated in migraine patients, since previous studies mostly used TCD and hence were uncapable of assessing this information. Both CVR and TTP of the posterior cerebral circulation showed to be increased during the ictal versus interictal phases of migraine, which is consistent with the reduced reactivity of this circulation reported in the interictal phase of migraineurs relative to controls. It is important to refer that this work did not perform any comparison between migraineurs and healthy controls. Thus, it is impossible to infer whether our results indicate an above normal reactivity during the ictal phase or a below normal interictal reactivity. Nevertheless, a reduced CVR of occipital regions during the interictal phase observed in this work may indicate a potential endothelial dysfunction of these areas, which would somehow be alleviated in the ictal phase.

Plenty of evidence exists that considers endothelial dysfunction an index of increased susceptibility to cerebrovascular events, in particular ischemic stroke [58]. In migraine, it is known that there is a 2-fold increased risk of ischemic stroke [40] and it has been observed that migraine accounted for 13% of all first-ever ischemic stroke of unusual cause [39]. This connection between migraine and stroke is recognized as being complex and multi-factorial. Heterogeneous mechanisms may contribute to the

increased risk of stroke in migraineurs. At this point, proposed linking mechanisms include genetic predisposition, coagulation abnormalities such as platelet hyperaggregability and consequent cerebral microembolism, and/or cardiac abnormalities [47, 155–157]. In order to further elucidate the association between migraine and stroke, it is of great value to study vasculature in this disease, in particular the CVR. In fact, and although not a single cause directly causes stroke, reduced CVR and endothelial dysfunction can predispose migraine patients to ischemic stroke by several manners. Firstly, reduced CVR may explain the lower ischemic threshold reported in experimental models of migraine, additively or synergistically with cortical excitability and spreading depolarization [158]. Endothelial dysfunction can not only impair the detection and rapid vasodilatory response to hypoxia or hypercapnia, but it can also hamper the development of collateral channels in response to ischemia [129]. Having said, the reduced interictal versus ictal CVR and inferable endothelial dysfunction found in this work may suggest that migraine patients are at increased risk of an ischemic stroke during the interictal phase of migraine. This is consistent with the finding of strokes rarely developing during a migraine attack [158].

One could argue that migraineurs were more prone to cardiovascular risk factors and hence cerebral infarcts. However, no significant differences in cardiovascular risk factors were observed between migraine patients with and without posterior circulation territory infarct-like lesions, and migraineurs did not present increased predisposition to atherosclerosis [55]. These facts suggest that these lesions are not atherosclerotic. Thus, endothelial dysfunction of the posterior cerebral circulation assumes the greatest importance as a potential mechanism to explain higher risk of cerebral infarcts in these brain regions in migraineurs. Nevertheless, no assumptions can be undoubtedly made due to the evident heterogenous relationship between migraine and stroke. Future studies are needed to further untangle the complex migraine-stroke association.

Importantly, several studies have focused on characterising the ischemic strokes occurring in migraine, aiming to investigate the vasculopathy associated to them. Initial studies promptly reported the occipital lobe as the main site involved in infarcts ocurring in migraine patients [159–163]. Later on, a population-based study suggested that migraineurs were at increased risk of cerebellar posterior circulation territory infarcts [45]. Adding to this, ischemic-like lesions have been found in the territory of the posterior cerebral circulation in migraine patients [44, 164, 165], and especially the PCA territory has shown to be significantly involved in cerebral infarcts associated with migraine [165, 166]. All together, these results provide evidence to a particular vulnerability of the posterior cerebral circulation regarding cerebral infarcts in migraine. Our findings of decreased interictal versus ictal CVR restricted to occipital brain regions of migraineurs are consistent with the increased vulnerability of these areas regarding cerebral infarcts and ischemic-like lesions in migraine.

Why reduced vascular reactivity and deducible endothelial dysfunction have been frequently limited to the posterior circulation in migraine is not clear. Kruit et al. [44] investigated infarct-like lesions in migraine and suggested an explanation for silent infarcts occurring in the posterior circulation territory: they proposed a combination of hypoperfusion (low cerebral blood flow) during migraine attack and artery to artery embolism [44]. Specifically, they postulated that a decrease in cerebral perfusion pressure and associated changes in cerebral haemodynamics may affect the clearance and destination

of embolic particles; simultaneously, narrowing of the arteries and endothelial anomalies may provoke the formation of thrombi, and occlusive thrombi further reduce blood flow and brain perfusion. Another study observed a strong association between migraine and hypoplastic/underdeveloped arteries of the posterior circulation [167], which could be an additional agent on the specificity of CVR impairment in posterior brain regions.

5.2.2 Region-of-interest (ROI) analysis

The spatial maps of the ictal versus interictal differences identified within the occipital lobe, VBA flow territory and VBA flow territory overlapped with the occipital lobe were used to define masks representing the ROIs within which the values of CVR and TTP were averaged for each subject. The boxplots representing the distributions of the mean CVR and TTP values for each session and ROI are represented in figure 5.8. Median of mean ictal CVR across subjects in the occipital lobe, VBA flow territory, and VBA flow territory + occipital lobe was 2.3%, 2.6%, and 2.3%, respectively. Median of mean interictal CVR across subjects in the occipital lobe, VBA flow territory, and VBA flow territory + occipital lobe was 1.3%, 1.3%, and 1.3%, respectively. Median of mean ictal TTP across subjects in the occipital lobe, VBA flow territory, and VBA flow territory + occipital lobe was 36.8 s, 36.8 s, and 36.6 s, respectively. Median of mean interictal TTP across subjects in the occipital lobe, VBA flow territory, and VBA flow territory + occipital lobe was 24.6 s, 22.6 s, and 24.8 s, respectively.

Afterwards, in order to investigate paired differences between the ictal and interictal phases, an analysis of variance (ANOVA) test was performed over the within ROI-averaged CVR and TTP values, for each ROI. The ANOVA test revealed a significant paired difference in the mean CVR and TTP of all ROIs between the ictal and interictal periods ($p<0.05$). This was an expected result since CVR and TTP showed to be increased during the attack when compared to the attack-free period within these three ROIs in the voxelwise analysis.

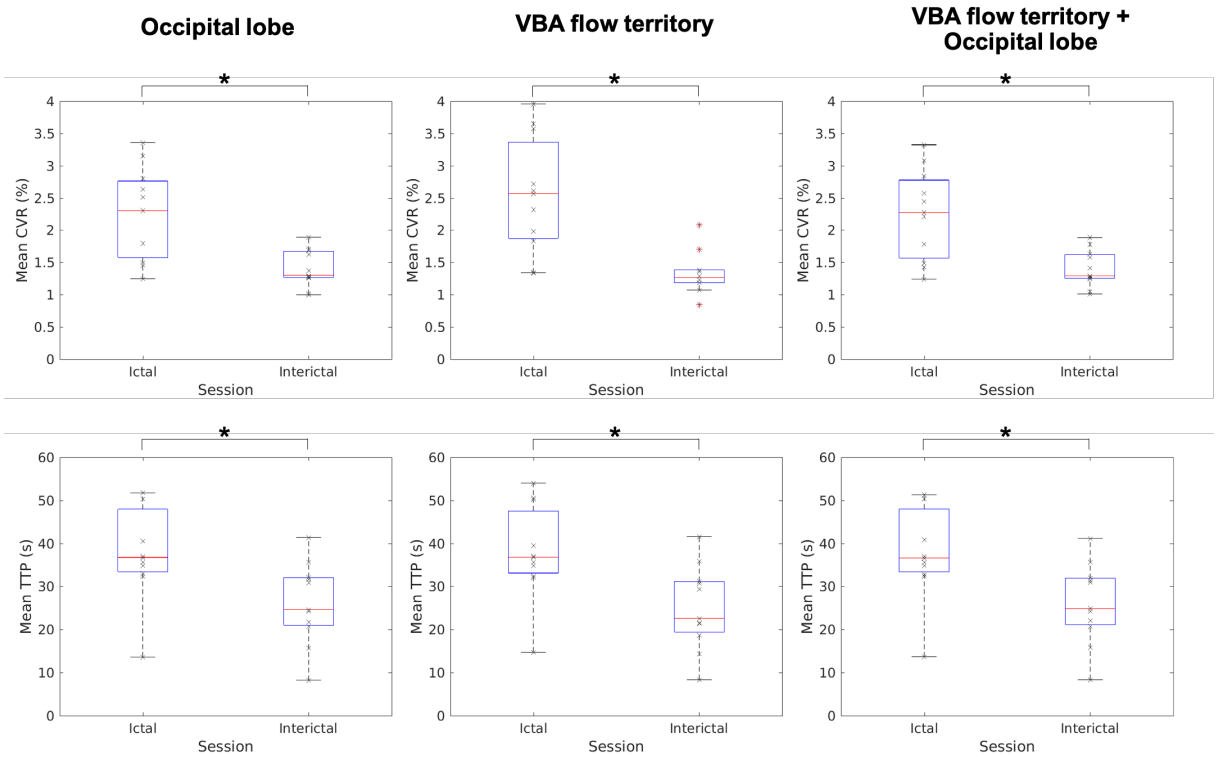

Figure 5.8: Boxplots representing the distributions across patients of the mean ictal and interictal CVR and TTP values within the ictal>interictal regions-of-interest (ROIs) found by the region-specific, voxelwise group-level analysis shown in figures 5.5, 5.6 and 5.7. In the boxplots, the central mark is the median; the edges of the box are the 25th and 75th percentiles; the upper and lower extreme represent, respectively, the maximum and minimum values (excluding outliers). The ANOVA test revealed significant differences ($p<0.05$) for the CVR and TTP differences between the ictal and interictal phases within all the three ROIs, which are marked with an asterisk.

5.2.2.1 Correlation with clinical features

A post-hoc analysis was performed regarding CVR and TTP values within the ROIs. The relationship between the individual mean CVR and TTP within the ROIs and several migraine clinical parameters was assessed through Pearson correlation analysis. The results are displayed in table 5.2.

No *p*-value was below the significance threshold of 0.05, which means that no significant correlations were found between any of the migraine clinical parameters and mean CVR and TTP values.

Boxplots in figure 5.4 reveal a higher dispersion of ictal CVR and TTP values within the ROIs than interictal ones. It was hypothesized that this could be explained by the fact that patients in S1 were studied at different times during the attack, and hence it was expected to observe some correlation between the time from attack onset to data acquisition (attack/pain duration) and CVR and TTP values. However, this was not observed and therefore we cannot support this assumption.

Table 5.2: Pearson correlation analysis between mean CVR and TTP values within the regions-of-interest (ROIs) in each session and participants' general clinical parameter and clinical parameters characterizing the ongoing attack. The ρ corresponds to the Pearson correlation coefficient.

ROI	Cerebrovascular reactivity index	Session	General clinical parameter	Clinical parameters in S1		
			Usual headache intensity	**Attack/Pain duration**	**Headache intensity**	**Photophobia**
Occipital lobe	CVR	S1	ρ=0.21 (p=0.56)	ρ=-0.55 (p=0.10)	ρ=0.28 (p=0.44)	ρ=0.26 (p=0.46)
		S2	ρ=-0.32 (p=0.37)	-	-	-
	TTP	S1	ρ=-0.33 (p=0.35)	ρ=-0.35 (p=0.32)	ρ=-0.18 (p=0.62)	ρ=-0.39 (p=0.27)
		S2	ρ=-0.33 (p=0.35)	-	-	-
VBA flow territory	CVR	S1	ρ=0.02 (p=0.95)	ρ=-0.54 (p=0.11)	ρ=0.16 (p=0.65)	ρ=0.21 (p=0.56)
		S2	ρ=-0.10 (p=0.78)	-	-	-
	TTP	S1	ρ=-0.35 (p=0.33)	ρ=-0.36 (p=0.30)	ρ=-0.18 (p=0.61)	ρ=-0.37 (p=0.29)
		S2	ρ=-0.30 (p=0.39)	-	-	-
VBA flow territory + Occipital lobe	CVR	S1	ρ=0.21 (p=0.56)	ρ=-0.55 (p=0.10)	ρ=0.29 (p=0.42)	ρ=0.29 (p=0.41)
		S2	ρ=-0.37 (p=0.29)	-	-	-
	TTP	S1	ρ=-0.33 (p=0.36)	ρ=-0.34 (p=0.34)	ρ=-0.19 (p=0.61)	ρ=-0.39 (p=0.26)
		S2	ρ=-0.32 (p=0.37)	-	-	-

Chapter 6

Conclusions

In the present study, a group of patients was studied during the ictal and interictal phases of migraine. In both scanning sessions, BOLD-fMRI data were acquired during a BH challenge, a motor task and visual stimulation. Analysis of data referent to the sensory stimuli (motor and visual) revealed unaltered neuronal response of the motor and visual functions specific brain regions between both migraine periods. BOLD-fMRI data referent to the BH task were analysed within the entire brain, the four cerebral lobes, and anterior and posterior cerebral circulations' flow territories. The group-level analysis revealed increased CVR and TTP in the posterior cerebral circulation restricted to occipital brain regions in the ictal versus intercital phase, pointing to an endothelial dysfunction of the posterior cerebral circulation in migraine.

Regions that reported increased ictal versus interictal CVR and TTP in the present work are associated with cerebral ischemia. Ischemic-like lesions have been found in the territory of the posterior cerebral circulation, and especially the occipital lobe and the posterior cerebral artery (PCA) have been consistently identified as the main brain regions involved in cerebral infarcts associated with migraine. Altered CVR within occipital regions might explain, to some extent, the vulnerability of the posterior cerebral circulation regarding migrainous infarcts: impaired CVR reflects endothelial dysfunction, which is a risk factor for vascular events such as cerebral infarcts.

The present work contributes with new evidence to the limited literature. Most CVR studies in migraine make use of TCD to compare migraineurs in the interictal phase with healthy controls. In addition, they mostly assess CVR in MCA. To our knowledge, only one fMRI study has investigated CVR in migraineurs, and this again focused only on the interictal period. The present study is therefore the first using fMRI to report on CVR differences between spontaneous migraine attacks and pain-free periods.

6.1 Limitations and future work

The first limitations worth mentioning regard the study design. The small number of participants strongly limits the statistical power of the findings, possibly limiting the generalisability of the results. The fact that patients were scanned during the headache phase of migraine can also be seen as a pitfall. First, some

patients may have declined their participation in the study because they had to be scanned during pain; second, the ones who enrolled in the study were not so collaborative in session 1 which may have caused inter- and intrasubject variations in task performance. Additionally, patients during the ictal session were not scanned at exact same time from attack initiation, i.e. the time from attack onset until acquisition (pain duration) was not the same for all the participants. Although this variation may be seen as useful to investigate possible relationships between CVR and pain duration, equal periods of time between attack onset and scanning would probably strengthen this investigation and allow even more attack specific features to be found. In addition, it would have been of great value to include healthy controls in the study in order to investigate whether migraine patients present an above the normal CVR during the ictal phase or a below the normal CVR during the interictal phase, this way testing the hypothesis of a reduced interictal CVR that increases during attacks. Furthermore, migraine patients during other phases of the ictal period, such as the prodrome and postdrome, could also be investigated, as a means to increase the limited knowledge on mechanisms involved in these phases.

Regarding the imaging technique used (BOLD-fMRI), some limitations could be pointed out: BOLD contrast depends on and is influenced by CBF, cerebral blood volume (CBV), and cerebral metabolic rate of oxygen ($CMRO_2$) [86]. Thus, it does not provide a direct measure of CBF, but rather measures a complex combination of vascular and metabolic parameters. Even so, BOLD-fMRI is superior to the alternative techniques, since it provides high spatial resolution and regional information of the brain.

Considering the CVR metrics achieved using BH BOLD-fMRI, these are relative metrics, mainly qualitative in nature, because the baseline values are unaccounted for and the signal is expressed in percent change. This is unlike Arterial Spin Labeling (ASL), a true perfusion imaging technique which gives a direct quantitative measurement of CBF. ASL has shown to be superior to BOLD in terms of spatial localization (because it reflects a single physiological process, namely CBF, it yields better spatial correlations with the actual site of regional involvement than BOLD), signal quantification, and susceptibility effects [168]. However, ASL scans have also been reported to activate one third less voxels [92]. Additionally, its intrinsically low signal-to-noise ratio (SNR) and additional technical difficulty have limited its applicability to studies of CVR. Nonetheless, a recent report found that CVR measurements are similar when using ASL and BOLD contrasts, suggesting that both techniques can provide consistent information and are suitable for studying vascular dysfunction [169].

Another possible pitfall of this study could be the vasoactive stimuli used to induce hypercapnia. The breath-holding (BH) task is a very simple technique with significant advantages over the other existing methods, namely its noninvasiveness and being easy to implement, in particular when studying patient populations. Also, it is capable to produce similar increases in arterial CO_2 levels and resultant BOLD CVR maps as those achieved by using gas-inhalation techniques [73]. However, being a respiratory challenge, BH can simultaneously alter oxygen levels in addition to the intended CO_2 levels, i.e. it can result not only in the desired hypercapnia, but also in mild hypoxia. A relevant concern is that changes in arterial oxygen could possibly influence the BOLD contrast [170]. Fortunately, the role of arterial O_2 pressure in CBF regulation seems to be minor: hypoxic ranges of 60-80mmHg PaO_2 are needed to induce significant CBF changes, which are very unlikely with the 20s BH duration used in this work

[171]. Also, CO_2 cerebral reactivity has shown to be 60/150 times larger than to O_2 [172]. Having said, we are confident to declare that the hypoxic component of BH challenges did not influence our work's results.

Regarding the acquisition guidelines, findings to date suggest that preferred parameters for a standardized approach to BH-CVR may include 20s BH duration, end-expiration, controlled breathing during rest, and normalization to end-tidal CO_2 levels [91]. The BH tasks performed by the subjects in this study were 20s long, preceded by a preparatory inspiration and followed by periods of self-paced breathing. In general, the preparatory inspiration leads to a more complex BOLD response. Also, the end-expiration BH technique with computer-paced breathing has shown to offer superior repeatability [95]. However, end-inspiration protocols tend to be easier to perform, and therefore are recommended when dealing with potentially less cooperative patients (which is the case of this work, in which patients during S1 were experiencing pain) [173]. As for using computer-paced normal breathing instead of self-paced breathing, this could reduce possible inter- and intra-subjects CBF differences arising due to CO_2 variations caused by subjects' ventilation (breathing rate and breathing depth) and lung function [95]. Nevertheless, we used self-paced normal breathing because it minimizes deep breathing and its associated hypocapnia, and mainly because it was better accepted by the volunteers.

The direct cause of the vascular response and BOLD signal changes is the change in arterial CO_2 levels associated with the BH challenge. Thus, measuring $PETCO_2$ could provide a full model of the hypercapnia stimulus, and could be used as a regressor of the GLM analysis instead of the sine-cosine regressor employed in this study. At the same time, it would increase the reproducibility of results and reduce inter- and intrasubject variability caused by respiratory and BH-task compliance differences [108]. In addition, it would be possible to obtain a quantitative interpretation of CVR results if the BOLD ratio was normalized by $PETCO_2$. However, CO_2 tracing requires complex experimental setups that are in general uncomfortable for the subjects. Furthermore, it has been shown that absolute BOLD signal intensity changes after an hypercapnic challenge hold better reproducibility and lower between-subject variability than BOLD ratios normalized by $PETCO_2$ [174].

Lastly, this study holds the great advantage of following a longitudinal approach, i.e. comparing the same migraine patients in the ictal and interictal phases of the disease. This makes the observed CVR and TTP alterations possibly specific to migraine. In particular, migraine without aura patients were found to have increased CVR and TTP in occipital regions during the ictal phase of migraine compared with the interictal state.

In summary, this work showed that BH-CVR using fMRI is a promising and practical measure to assess CVR, and one that is sensitive to group differences when comparing migraineurs in different phases of the migraine cycle. We could conclude that migraine patients without aura might have impaired CVR and cerebral endothelial dysfunction in the posterior cerebral circulation, which could associate migraine and cerebral infarcts that are more common in the PCA distribution in these patients. To the best of our knowledge, it has not been yet documented whether endothelial dysfunction is involved in the pathogenesis of migraine. Thus, the role of cerebral endothelial dysfunction in migraine pathogenesis should be investigated in future studies.

Additionally, as can be seen from the discussion above, there is still a variety of imaging techniques, acquisition methods and analysis strategies for CVR assessment. This certainly contributes to the heterogeneity and contrary findings of CVR studies in migraine performed so far. The lack of standardized methodologies makes it difficult to compare results across investigations, hinders the drawing of reproducible and robust conclusions regarding cerebrovascular physiology, and hampers the applicability of these methods in clinical applications. Thus, it would be a great step in the investigation of migraine to try to standardize the approaches used to assess CVR in these patients.

The results found in this study contribute with completely new evidence regarding CVR between ictal and interictal phases of migraine. These findings consist in a step closer to our knowledge and understanding of the pathophysiology of migraine.

Bibliography

[1] L. J. Stovner, E. Nichols, T. J. Steiner, F. Abd-Allah, A. Abdelalim, R. M. Al-Raddadi, M. G. Ansha, A. Barac, I. M. Bensenor, L. P. Doan, et al. Global, regional, and national burden of migraine and tension-type headache, 1990–2016: a systematic analysis for the global burden of disease study 2016. *The Lancet Neurology*, 17(11):954–976, 2018.

[2] P. J. Goadsby, P. R. Holland, M. Martins-Oliveira, J. Hoffmann, C. Schankin, and S. Akerman. Pathophysiology of migraine: a disorder of sensory processing. *Physiological reviews*, 2017.

[3] P. Stang, A. Carson, K. Rose, J. Mo, S. Ephross, E. Shahar, and M. Szklo. Headache, cerebrovascular symptoms, and stroke: the atherosclerosis risk in communities study. *Neurology*, 64 (9):1573–1577, 2005.

[4] M. Bigal, T. Kurth, N. Santanello, D. Buse, W. Golden, M. Robbins, and R. Lipton. Migraine and cardiovascular disease: a population-based study. *Neurology*, 74(8):628–635, 2010.

[5] D. Perko, J. Pretnar-Oblak, M. Šabovič, B. Žvan, and M. Zaletel. Cerebrovascular reactivity to l-arginine in the anterior and posterior cerebral circulation in migraine patients. *Acta Neurologica Scandinavica*, 124(4):269–274, 2011.

[6] J. P. P. V. I. M. R. G.-G. S. Cotrim, P. Figueiredo. Increased cerebrovascular reactivity during spontaneous migraine attacks compared to pain-free periods. *ESMRMB Congress*, 2020.

[7] D. Buse, A. Manack, D. Serrano, C. Turkel, and R. Lipton. Sociodemographic and comorbidity profiles of chronic migraine and episodic migraine sufferers. *Journal of Neurology, Neurosurgery & Psychiatry*, 81(4):428–432, 2010.

[8] M. Arnold. Headache classification committee of the international headache society (ihs) the international classification of headache disorders. *Cephalalgia*, 38(1):1–211, 2018.

[9] S. D. Silberstein. Migraine symptoms: Results of a survey of self-reported migraineurs. *Headache: The Journal of Head and Face Pain*, 35(7):387–396, 1995.

[10] R. B. Lipton, W. F. Stewart, S. Diamond, M. L. Diamond, and M. Reed. Prevalence and burden of migraine in the united states: data from the american migraine study ii. *Headache: The Journal of Head and Face Pain*, 41(7):646–657, 2001.

[11] L. Kelman and D. Tanis. The relationship between migraine pain and other associated symptoms. *Cephalalgia*, 26(5):548–553, 2006.

[12] D. C. Buse, E. W. Loder, J. A. Gorman, W. F. Stewart, M. L. Reed, K. M. Fanning, D. Serrano, and R. B. Lipton. Sex differences in the prevalence, symptoms, and associated features of migraine, probable migraine and other severe h eadache: Results of the a merican migraine prevalence and prevention (ampp) study. *Headache: The Journal of Head and Face Pain*, 53(8):1278–1299, 2013.

[13] F. M. Cutrer and J. Olesen. Migraines with aura and their subforms. *Olesen J, Goadsby PJ, Ramadan NM, Tfelt-Hansen P, Welch KMA (eds) The headaches, 3rd edn. Philadelphia, PA: Lippincott Williams & Wilkins*, pages 407–21, 2006.

[14] F. Puledda, R. Messina, and P. J. Goadsby. An update on migraine: current understanding and future directions. *Journal of Neurology*, 264(9):2031–2039, 2017.

[15] M. Ashina and P. Geppetti. *Pathophysiology of Headaches: From Molecule to Man*. Springer, 2015.

[16] H. G. Wolff. Headache and other head pain. In *Headache and other head pain*, pages 648–648. 1948.

[17] M. A. Moskowitz and F. M. Cutrer. Sumatriptan: a receptor-targeted treatment for migraine. *Annual review of medicine*, 44(1):145–154, 1993.

[18] S. Markowitz, K. Saito, and M. Moskowitz. Neurogenically mediated leakage of plasma protein occurs from blood vessels in dura mater but not brain. *Journal of Neuroscience*, 7(12):4129–4136, 1987.

[19] A. May and P. J. Goadsby. Substance p receptor antagonists in the therapy of migraine. *Expert Opinion on Investigational Drugs*, 10(4):673–678, 2001.

[20] S. J. Peroutka. Neurogenic inflammation and migraine: implications for the therapeutics. *Molecular interventions*, 5(5):304, 2005.

[21] A. Bahra, M. Matharu, C. Buchel, R. Frackowiak, and P. Goadsby. Brainstem activation specific to migraine headache. *The lancet*, 357(9261):1016–1017, 2001.

[22] A. Stankewitz, D. Aderjan, F. Eippert, and A. May. Trigeminal nociceptive transmission in migraineurs predicts migraine attacks. *Journal of Neuroscience*, 31(6):1937–1943, 2011.

[23] F. H. Maniyar, T. Sprenger, T. Monteith, C. Schankin, and P. J. Goadsby. Brain activations in the premonitory phase of nitroglycerin-triggered migraine attacks. *Brain*, 137(1):232–241, 2014.

[24] M. Denuelle, N. Fabre, P. Payoux, F. Chollet, and G. Geraud. Hypothalamic activation in spontaneous migraine attacks. *Headache: The Journal of Head and Face Pain*, 47(10):1418–1426, 2007.

[25] L. H. Schulte and A. May. The migraine generator revisited: continuous scanning of the migraine cycle over 30 days and three spontaneous attacks. *Brain*, 139(7):1987–1993, 2016.

[26] G. Coppola, E. Tinelli, C. Lepre, E. Iacovelli, C. Di Lorenzo, G. Di Lorenzo, M. Serrao, F. Pauri, G. Fiermonte, F. Bianco, et al. Dynamic changes in thalamic microstructure of migraine without aura patients: a diffusion tensor magnetic resonance imaging study. *European Journal of Neurology*, 21(2):287–e13, 2014.

[27] S. Magon, A. May, A. Stankewitz, P. J. Goadsby, A. R. Tso, M. Ashina, F. M. Amin, C. L. Seifert, M. M. Chakravarty, J. Müller, et al. Morphological abnormalities of thalamic subnuclei in migraine: a multicenter mri study at 3 tesla. *Journal of Neuroscience*, 35(40):13800–13806, 2015.

[28] D. J. Hodkinson, S. L. Wilcox, R. Veggeberg, R. Noseda, R. Burstein, D. Borsook, and L. Becerra. Increased amplitude of thalamocortical low-frequency oscillations in patients with migraine. *Journal of Neuroscience*, 36(30):8026–8036, 2016.

[29] R. Noseda, V. Kainz, M. Jakubowski, J. J. Gooley, C. B. Saper, K. Digre, and R. Burstein. A neural mechanism for exacerbation of headache by light. *Nature neuroscience*, 13(2):239, 2010.

[30] A. P. Andreou, K. G. Shields, and P. J. Goadsby. Gaba and valproate modulate trigeminovascular nociceptive transmission in the thalamus. *Neurobiology of disease*, 37(2):314–323, 2010.

[31] O. Summ, A. R. Charbit, A. P. Andreou, and P. J. Goadsby. Modulation of nocioceptive transmission with calcitonin gene-related peptide receptor antagonists in the thalamus. *Brain*, 133(9): 2540–2548, 2010.

[32] G. Tietjen. Migraine as a systemic vasculopathy. *Cephalalgia*, 29(9):989–996, 2009.

[33] J. Hoffmann, S. M. Baca, and S. Akerman. Neurovascular mechanisms of migraine and cluster headache. *Journal of Cerebral Blood Flow & Metabolism*, 39(4):573–594, 2019.

[34] C. Tzourio, S. Iglesias, J.-B. Hubert, J.-M. Visy, A. Alperovitch, A. Tehindrazanarivelo, V. Biousse, F. Woimant, and M.-G. Bousser. Migraine and risk of ischaemic stroke: a case-control study. *British Medical Journal*, 307(6899):289–292, 1993.

[35] J. E. Buring, P. Hebert, J. Romero, A. Kittross, J. Manson, R. Peto, C. Hennekens, et al. Migraine and subsequent risk of stroke in the physicians' health study. *Archives of neurology*, 52(2):129–134, 1995.

[36] C. Tzourio, A. Tehindrazanarivelo, S. Iglesias, A. Alperovitch, F. Chedru, J. d'Anglejan Chatillon, and M.-G. Bousser. Case-control study of migraine and risk of ischaemic stroke in young women. *Bmj*, 310(6983):830–833, 1995.

[37] T. Kurth, M. Schürks, G. Logroscino, J. M. Gaziano, and J. E. Buring. Migraine, vascular risk, and cardiovascular events in women: prospective cohort study. *Bmj*, 337, 2008.

[38] T. Kurth, J. M. Gaziano, N. R. Cook, V. Bubes, G. Logroscino, H.-C. Diener, and J. E. Buring. Migraine and risk of cardiovascular disease in men. *Archives of internal medicine*, 167(8):795–801, 2007.

[39] A. Arboix, J. Massons, L. Garcia-Eroles, M. Oliveres, M. Balcells, and C. Targa. Migrainous cerebral infarction in the sagrat cor hospital of barcelona stroke registry. *Cephalalgia*, 23(5):389–394, 2003.

[40] J. T. Spector, S. R. Kahn, M. R. Jones, M. Jayakumar, D. Dalal, and S. Nazarian. Migraine headache and ischemic stroke risk: an updated meta-analysis. *The American journal of medicine*, 123(7):612–624, 2010.

[41] S. Sacco, R. Ornello, P. Ripa, F. Pistoia, and A. Carolei. Migraine and hemorrhagic stroke: a meta-analysis. *Stroke*, 44(11):3032–3038, 2013.

[42] M. Schürks, P. M. Rist, M. E. Bigal, J. E. Buring, R. B. Lipton, and T. Kurth. Migraine and cardiovascular disease: systematic review and meta-analysis. *Bmj*, 339, 2009.

[43] T. Monteith, H. Gardener, T. Rundek, C. Dong, M. Yoshita, M. S. Elkind, C. DeCarli, R. L. Sacco, and C. B. Wright. Migraine, white matter hyperintensities, and subclinical brain infarction in a diverse community: the northern manhattan study. *Stroke*, 45(6):1830–1832, 2014.

[44] M. C. Kruit, L. J. Launer, M. D. Ferrari, and M. A. van Buchem. Infarcts in the posterior circulation territory in migraine. the population-based mri camera study. *Brain*, 128(9):2068–2077, 2005.

[45] M. C. Kruit, M. A. van Buchem, P. A. Hofman, J. T. Bakkers, G. M. Terwindt, M. D. Ferrari, and L. J. Launer. Migraine as a risk factor for subclinical brain lesions. *Jama*, 291(4):427–434, 2004.

[46] A. I. Scher, L. S. Gudmundsson, S. Sigurdsson, A. Ghambaryan, T. Aspelund, G. Eiriksdottir, M. A. van Buchem, V. Gudnason, and L. J. Launer. Migraine headache in middle age and late-life brain infarcts. *Jama*, 301(24):2563–2570, 2009.

[47] S.-P. Chen and K. Eikermann-Haerter. How imaging can help us better understand the migraine-stroke connection. *Headache: The Journal of Head and Face Pain*, 60(1):217–228, 2020.

[48] C. Bushnell, L. D. McCullough, I. A. Awad, M. V. Chireau, W. N. Fedder, K. L. Furie, V. J. Howard, J. H. Lichtman, L. D. Lisabeth, I. L. Piña, et al. Guidelines for the prevention of stroke in women: a statement for healthcare professionals from the american heart association/american stroke association. *Stroke*, 45(5):1545–1588, 2014.

[49] S. L. James, D. Abate, K. H. Abate, S. M. Abay, C. Abbafati, N. Abbasi, H. Abbastabar, F. Abd-Allah, J. Abdela, A. Abdelalim, et al. Global, regional, and national incidence, prevalence, and years lived with disability for 354 diseases and injuries for 195 countries and territories, 1990–2017: a systematic analysis for the global burden of disease study 2017. *The Lancet*, 392(10159): 1789–1858, 2018.

[50] J. E. Deanfield, J. P. Halcox, and T. J. Rabelink. Endothelial function and dysfunction: testing and clinical relevance. *Circulation*, 115(10):1285–1295, 2007.

[51] P. O. Bonetti, L. O. Lerman, and A. Lerman. Endothelial dysfunction: a marker of atherosclerotic risk. *Arteriosclerosis, thrombosis, and vascular biology*, 23(2):168–175, 2003.

[52] V. González-Quintanilla, M. Toriello, E. Palacio, M. A. González-Gay, J. Castillo, S. Montes, R. Martínez-Nieto, J. Fernandez, A. Rojo, S. Gutiérrez, et al. Systemic and cerebral endothelial dysfunction in chronic migraine. a case-control study with an active comparator. *Cephalalgia*, 36(6):552–560, 2016.

[53] S.-T. Lee, K. Chu, K.-H. Jung, D.-H. Kim, E.-H. Kim, V. Choe, J.-H. Kim, W.-S. Im, L. Kang, J.-E. Park, et al. Decreased number and function of endothelial progenitor cells in patients with migraine. *Neurology*, 70(17):1510–1517, 2008.

[54] X. Rodríguez-Osorio, T. Sobrino, D. Brea, F. Martínez, J. Castillo, and R. Leira. Endothelial progenitor cells: a new key for endothelial dysfunction in migraine. *Neurology*, 79(5):474–479, 2012.

[55] R. Rajan, D. Khurana, and V. Lal. Interictal cerebral and systemic endothelial dysfunction in patients with migraine: a case–control study. *Journal of Neurology, Neurosurgery & Psychiatry*, 86(11):1253–1257, 2015.

[56] J. B. De Vis, E. T. Petersen, A. Bhogal, N. S. Hartkamp, C. J. Klijn, L. Kappelle, and J. Hendrikse. Calibrated mri to evaluate cerebral hemodynamics in patients with an internal carotid artery occlusion. *Journal of Cerebral Blood Flow & Metabolism*, 35(6):1015–1023, 2015.

[57] F. Geranmayeh, R. J. Wise, R. Leech, and K. Murphy. Measuring vascular reactivity with breathholds after stroke: A method to aid interpretation of group-level bold signal changes in longitudinal f mri studies. *Human brain mapping*, 36(5):1755–1771, 2015.

[58] C. Molina, J. A. Sabin, J. Montaner, A. Rovira, S. Abilleira, and A. Codina. Impaired cerebrovascular reactivity as a risk marker for first-ever lacunar infarction: a case-control study. *Stroke*, 30 (11):2296–2301, 1999.

[59] J. Fierstra, B. van Niftrik, M. Piccirelli, J. K. Burkhardt, A. Pangalu, R. Kocian, A. Valavanis, M. Weller, L. Regli, and O. Bozinov. Altered intraoperative cerebrovascular reactivity in brain areas of high-grade glioma recurrence. *Magnetic Resonance Imaging*, 34(6):803–808, 2016.

[60] S.-t. Chan, K. C. Evans, B. R. Rosen, T.-y. Song, and K. K. Kwong. A case study of magnetic resonance imaging of cerebrovascular reactivity: a powerful imaging marker for mild traumatic brain injury. *Brain injury*, 29(3):403–407, 2015.

[61] M. J. Ellis, L. N. Ryner, O. Sobczyk, J. Fierstra, D. J. Mikulis, J. A. Fisher, J. Duffin, and W. A. C. Mutch. Neuroimaging assessment of cerebrovascular reactivity in concussion: current concepts, methodological considerations, and review of the literature. *Frontiers in neurology*, 7:61, 2016.

[62] S. Vorstrup, B. Brun, and N. A. Lassen. Evaluation of the cerebral vasodilatory capacity by the acetazolamide test before ec-ic bypass surgery in patients with occlusion of the internal carotid artery. *Stroke*, 17(6):1291–1298, 1986.

[63] H. Saito, K. Ogasawara, T. Suzuki, H. Kuroda, M. Kobayashi, K. Yoshida, Y. Kubo, and A. Ogawa. Adverse effects of intravenous acetazolamide administration for evaluation of cerebrovascular reactivity using brain perfusion single-photon emission computed tomography in patients with major cerebral artery steno-occlusive diseases. *Neurologia medico-chirurgica*, 51(7):479–483, 2011.

[64] W. M. Grossmann and B. Koeberle. The dose-response relationship of acetazolamide on the cerebral blood flow in normal subjects. *Cerebrovascular Diseases*, 10(1):65–69, 2000.

[65] S. Ito, A. Mardimae, J. Han, J. Duffin, G. Wells, L. Fedorko, L. Minkovich, R. Katznelson, M. Meineri, T. Arenovich, et al. Non-invasive prospective targeting of arterial p in subjects at rest. *The Journal of physiology*, 586(15):3675–3682, 2008.

[66] U. S. Yezhuvath, K. Lewis-Amezcua, R. Varghese, G. Xiao, and H. Lu. On the assessment of cerebrovascular reactivity using hypercapnia bold mri. *NMR in Biomedicine: An International Journal Devoted to the Development and Application of Magnetic Resonance In vivo*, 22(7):779–786, 2009.

[67] R. G. Wise, K. T. Pattinson, D. P. Bulte, P. A. Chiarelli, S. D. Mayhew, G. M. Balanos, D. F. O'Connor, T. R. Pragnell, P. A. Robbins, I. Tracey, et al. Dynamic forcing of end-tidal carbon dioxide and oxygen applied to functional magnetic resonance imaging. *Journal of Cerebral Blood Flow & Metabolism*, 27(8):1521–1532, 2007.

[68] A. Kassner, J. D. Winter, J. Poublanc, D. J. Mikulis, and A. P. Crawley. Blood-oxygen level dependent mri measures of cerebrovascular reactivity using a controlled respiratory challenge: reproducibility and gender differences. *Journal of Magnetic Resonance Imaging: An Official Journal of the International Society for Magnetic Resonance in Medicine*, 31(2):298–304, 2010.

[69] C. I. Mark, M. Slessarev, S. Ito, J. Han, J. A. Fisher, and G. B. Pike. Precise control of end-tidal carbon dioxide and oxygen improves bold and asl cerebrovascular reactivity measures. *Magnetic resonance in medicine*, 64(3):749–756, 2010.

[70] V. R. Spano, D. M. Mandell, J. Poublanc, K. Sam, A. Battisti-Charbonney, O. Pucci, J. S. Han, A. P. Crawley, J. A. Fisher, and D. J. Mikulis. Co2 blood oxygen level–dependent mr mapping of cerebrovascular reserve in a clinical population: safety, tolerability, and technical feasibility. *Radiology*, 266(2):592–598, 2013.

[71] M. A. Van den Hout and E. Griez. Panic symptoms after inhalation of carbondioxide. *The British Journal of Psychiatry*, 144(5):503–507, 1984.

[72] H. Markus and M. Harrison. Estimation of cerebrovascular reactivity using transcranial doppler, including the use of breath-holding as the vasodilatory stimulus. *Stroke*, 23(5):668–673, 1992.

[73] A. Kastrup, G. Krüger, T. Neumann-Haefelin, and M. E. Moseley. Assessment of cerebrovascular reactivity with functional magnetic resonance imaging: comparison of co2 and breath holding. *Magnetic resonance imaging*, 19(1):13–20, 2001.

[74] F. B. Tancredi and R. D. Hoge. Comparison of cerebral vascular reactivity measures obtained using breath-holding and co2 inhalation. *Journal of Cerebral Blood Flow & Metabolism*, 33(7): 1066–1074, 2013.

[75] M. G. Bright, M. J. Donahue, J. H. Duyn, P. Jezzard, and D. P. Bulte. The effect of basal vasodilation on hypercapnic and hypocapnic reactivity measured using magnetic resonance imaging. *Journal of Cerebral Blood Flow & Metabolism*, 31(2):426–438, 2011.

[76] S. S. Kannurpatti, M. A. Motes, B. Rypma, and B. B. Biswal. Neural and vascular variability and the fmri-bold response in normal aging. *Magnetic resonance imaging*, 28(4):466–476, 2010.

[77] R. V. Raut, V. A. Nair, J. A. Sattin, and V. Prabhakaran. Hypercapnic evaluation of vascular reactivity in healthy aging and acute stroke via functional mri. *NeuroImage: Clinical*, 12:173–179, 2016.

[78] B. Thomas, W. Logan, E. J. Donner, and M. Shroff. Assessment of cerebrovascular reactivity using real-time bold fmri in children with moyamoya disease: a pilot study. *Child's Nervous System*, 29 (3):457–463, 2013.

[79] A. M. Golestani, L. L. Wei, and J. J. Chen. Quantitative mapping of cerebrovascular reactivity using resting-state bold fmri: validation in healthy adults. *Neuroimage*, 138:147–163, 2016.

[80] H. Jahanian, W. W. Ni, T. Christen, M. E. Moseley, M. K. Tamura, and G. Zaharchuk. Spontaneous bold signal fluctuations in young healthy subjects and elderly patients with chronic kidney disease. *PLoS One*, 9(3):e92539, 2014.

[81] P. Liu, Y. Li, M. Pinho, D. C. Park, B. G. Welch, and H. Lu. Cerebrovascular reactivity mapping without gas challenges. *Neuroimage*, 146:320–326, 2017.

[82] S. S. Kannurpatti, M. A. Motes, B. B. Biswal, and B. Rypma. Assessment of unconstrained cerebrovascular reactivity marker for large age-range fmri studies. *PloS one*, 9(2):e88751, 2014.

[83] I. Lipp, K. Murphy, X. Caseras, and R. G. Wise. Agreement and repeatability of vascular reactivity estimates based on a breath-hold task and a resting state scan. *Neuroimage*, 113:387–396, 2015.

[84] R. Aaslid, T.-M. Markwalder, and H. Nornes. Noninvasive transcranial doppler ultrasound recording of flow velocity in basal cerebral arteries. *Journal of neurosurgery*, 57(6):769–774, 1982.

[85] N. B. Smith and A. Webb. *Introduction to medical imaging: physics, engineering and clinical applications*. Cambridge university press, 2010.

[86] R. B. Buxton. *Introduction to functional magnetic resonance imaging: principles and techniques*. Cambridge university press, 2009.

[87] D. F. Abbott, H. I. Opdam, R. S. Briellmann, and G. D. Jackson. Brief breath holding may confound functional magnetic resonance imaging studies. *Human brain mapping*, 24(4):284–290, 2005.

[88] H.-L. Liu, J.-C. Huang, C.-T. Wu, and Y.-Y. Hsu. Detectability of blood oxygenation level-dependent signal changes during short breath hold duration. *Magnetic resonance imaging*, 20(9):643–648, 2002.

[89] K. C. Andrade, O. M. Pontes-Neto, J. P. Leite, A. C. Santos, O. Baffa, and D. B. d. Araujo. Quantitative aspects of brain perfusion dynamic induced by bold fmri. *Arquivos de neuro-psiquiatria*, 64 (4):895–898, 2006.

[90] S. Magon, G. Basso, P. Farace, G. K. Ricciardi, A. Beltramello, and A. Sbarbati. Reproducibility of bold signal change induced by breath holding. *Neuroimage*, 45(3):702–712, 2009.

[91] A. L. Urback, B. J. MacIntosh, and B. I. Goldstein. Cerebrovascular reactivity measured by functional magnetic resonance imaging during breath-hold challenge: a systematic review. *Neuroscience & Biobehavioral Reviews*, 79:27–47, 2017.

[92] T.-Q. Li, A. Kastrup, A. M. Takahashi, and M. E. Moseley. Functional mri of human brain during breath holding by bold and fair techniques. *Neuroimage*, 9(2):243–249, 1999.

[93] A. Kastrup, G. Krüger, G. H. Glover, T. Neumann-Haefelin, and M. E. Moseley. Regional variability of cerebral blood oxygenation response to hypercapnia. *Neuroimage*, 10(6):675–681, 1999.

[94] M. E. Thomason and G. H. Glover. Controlled inspiration depth reduces variance in breath-holding-induced bold signal. *Neuroimage*, 39(1):206–214, 2008.

[95] A. Scouten and C. Schwarzbauer. Paced respiration with end-expiration technique offers superior bold signal repeatability for breath-hold studies. *NeuroImage*, 43(2):250–257, 2008.

[96] A. Kastrup, T.-Q. Li, G. H. Glover, and M. E. Moseley. Cerebral blood flow–related signalchanges during breath-holding. *American Journal of Neuroradiology*, 20(7):1233–1238, 1999.

[97] K. Murphy, R. M. Birn, and P. A. Bandettini. Resting-state fmri confounds and cleanup. *Neuroimage*, 80:349–359, 2013.

[98] M. Jenkinson and M. Chappell. *Introduction to neuroimaging analysis*. Oxford University Press, 2018.

[99] S. A. Huettel, A. W. Song, G. McCarthy, et al. *Functional magnetic resonance imaging*, volume 1. Sinauer Associates Sunderland, MA, 2004.

[100] M. M. Monti. Statistical analysis of fmri time-series: a critical review of the glm approach. *Frontiers in human neuroscience*, 5:28, 2011.

[101] K. J. Friston, P. Jezzard, and R. Turner. Analysis of functional mri time-series. *Human brain mapping*, 1(2):153–171, 1994.

[102] N. Lange and S. L. Zeger. Non-linear fourier time series analysis for human brain mapping by functional magnetic resonance imaging. *Journal of the Royal Statistical Society: Series C (Applied Statistics)*, 46(1):1–29, 1997.

[103] K. J. Friston, P. Fletcher, O. Josephs, A. Holmes, M. Rugg, and R. Turner. Event-related fmri: characterizing differential responses. *Neuroimage*, 7(1):30–40, 1998.

[104] F. Kruggel and D. Y. von Cramon. Temporal properties of the hemodynamic response in functional mri. *Human brain mapping*, 8(4):259–271, 1999.

[105] D. A. Handwerker, J. M. Ollinger, and M. D'Esposito. Variation of bold hemodynamic responses across subjects and brain regions and their effects on statistical analyses. *Neuroimage*, 21(4): 1639–1651, 2004.

[106] D. A. Handwerker, A. Gazzaley, B. A. Inglis, and M. D'Esposito. Reducing vascular variability of fmri data across aging populations using a breathholding task. *Human brain mapping*, 28(9): 846–859, 2007.

[107] M. E. Thomason, L. C. Foland, and G. H. Glover. Calibration of bold fmri using breath holding reduces group variance during a cognitive task. *Human brain mapping*, 28(1):59–68, 2007.

[108] M. G. Bright and K. Murphy. Reliable quantification of bold fmri cerebrovascular reactivity despite poor breath-hold performance. *Neuroimage*, 83:559–568, 2013.

[109] D. P. Bulte, K. Drescher, and P. Jezzard. Comparison of hypercapnia-based calibration techniques for measurement of cerebral oxygen metabolism with mri. *Magnetic Resonance in Medicine: An Official Journal of the International Society for Magnetic Resonance in Medicine*, 61(2):391–398, 2009.

[110] K. Murphy, A. D. Harris, and R. G. Wise. Robustly measuring vascular reactivity differences with breath-hold: normalising stimulus-evoked and resting state bold fmri data. *NeuroImage*, 54(1): 369–379, 2011.

[111] S. A. Sasse, R. B. Berry, T. K. Nguyen, R. W. Light, and C. K. Mahutte. Arterial blood gas changes during breath-holding from functional residual capacity. *Chest*, 110(4):958–964, 1996.

[112] X. Di, S. S. Kannurpatti, B. Rypma, and B. B. Biswal. Calibrating bold fmri activations with neurovascular and anatomical constraints. *Cerebral Cortex*, 23(2):255–263, 2013.

[113] S. S. Kannurpatti, M. A. Motes, B. Rypma, and B. B. Biswal. Increasing measurement accuracy of age-related bold signal change: Minimizing vascular contributions by resting-state-fluctuation-of-amplitude scaling. *Human brain mapping*, 32(7):1125–1140, 2011.

[114] R. M. Birn, M. A. Smith, T. B. Jones, and P. A. Bandettini. The respiration response function: the temporal dynamics of fmri signal fluctuations related to changes in respiration. *Neuroimage*, 40 (2):644–654, 2008.

[115] C. Chang, M. E. Thomason, and G. H. Glover. Mapping and correction of vascular hemodynamic latency in the bold signal. *Neuroimage*, 43(1):90–102, 2008.

[116] J. Pinto, J. Jorge, I. Sousa, P. Vilela, and P. Figueiredo. Fourier modeling of the bold response to a breath-hold task: optimization and reproducibility. *Neuroimage*, 135:223–231, 2016.

[117] S.-t. Chan, K. C. Evans, T.-y. Song, R. Gupta, B. R. Rosen, A. Singhal, and K. K. Kwong. Functional magnetic resonance imaging of regional impaired cerebrovascular reactivity for migraineurs in the interictal state. *bioRxiv*, page 859843, 2019.

[118] J. M. Soares, R. Magalhães, P. S. Moreira, A. Sousa, E. Ganz, A. Sampaio, V. Alves, P. Marques, and N. Sousa. A hitchhiker's guide to functional magnetic resonance imaging. *Frontiers in neuroscience*, 10:515, 2016.

[119] T. E. Nichols and A. P. Holmes. Nonparametric permutation tests for functional neuroimaging: a primer with examples. *Human brain mapping*, 15(1):1–25, 2002.

[120] R. A. Poldrack, J. A. Mumford, and T. E. Nichols. *Handbook of functional MRI data analysis*. Cambridge University Press, 2011.

[121] J. D. Fix. *Neuroanatomy*. Lippincott Williams & Wilkins, 2002.

[122] C. Weiller, A. May, V. a. Limmroth, M. Jüptner, H. Kaube, R. Schayck, H. Coenen, and H. Dlener. Brain stem activation in spontaneous human migraine attacks. *Nature medicine*, 1(7):658–660, 1995.

[123] E. Moulton, L. Becerra, N. Maleki, G. Pendse, S. Tully, R. Hargreaves, R. Burstein, and D. Borsook. Painful heat reveals hyperexcitability of the temporal pole in interictal and ictal migraine states. *Cerebral cortex*, 21(2):435–448, 2011.

[124] A. Stankewitz and A. May. Increased limbic and brainstem activity during migraine attacks following olfactory stimulation. *Neurology*, 77(5):476–482, 2011.

[125] The internet stroke center. `http://www.strokecenter.org/professionals/brain-anatomy/blood-vessels-of-the-brain/`.

[126] Science abc website. `https://www.scienceabc.com/humans/circle-of-willis-anatomy-diagram-and-functi html`.

[127] M. A. Piccinin and S. Munakomi. Neuroanatomy, vertebrobasilar system. In *StatPearls [Internet]*. StatPearls Publishing, 2020.

[128] F. Sakai and J. S. Meyer. Abnormal cerebrovascular reactivity in patients with migraine and cluster headache. *Headache: The Journal of Head and Face Pain*, 19(5):257–266, 1979.

[129] M. J. Lee, S. Cho, S.-Y. Woo, and C.-S. Chung. Paradoxical association between age and cerebrovascular reactivity in migraine: A cross-sectional study. *Journal of the neurological sciences*, 398:204–209, 2019.

[130] A. Arjona, L. A. P. de Torres, P. J. Serrano-Castro, P. L. Guardado-Santervas, J. Olivares, and J. Rubí-Callejon. A transcranial doppler study in interictal migraine and tension-type headache. *Journal of Clinical Ultrasound*, 35(7):372–375, 2007.

[131] M. Silvestrini, R. Baruffaldi, M. Bartolini, F. Vernieri, C. Lanciotti, M. Matteis, E. Troisi, and L. Provinciali. Basilar and middle cerebral artery reactivity in patients with migraine. *Headache: The Journal of Head and Face Pain*, 44(1):29–34, 2004.

[132] B. Dora and S. Balkan. Exaggerated interictal cerebrovascular reactivity but normal blood flow velocities in migraine without aura. *Cephalalgia*, 22(4):288–290, 2002.

[133] A. Kastrup, C. Thomas, C. Hartmann, and M. Schabet. Cerebral blood flow and co2 reactivity in interictal migraineurs: a transcranial doppler study. *Headache: The Journal of Head and Face Pain*, 38(8):608–613, 1998.

[134] R. Totaro, C. Marini, G. De Matteis, M. Di Napoil, and A. Carolei. Cerebrovascular reactivity in migraine during headache-free intervals. *Cephalalgia*, 17(3):191–194, 1997.

[135] M. Silvestrini, M. Matteis, E. Troisi, L. M. Cupini, and G. Bernardi. Cerebrovascular reactivity in migraine with and without aura. *Headache: The Journal of Head and Face Pain*, 36(1):37–40, 1996.

[136] A. Valikovics, L. Oláh, B. Fülesdi, Z. Káposzta, A. Ficzere, D. Bereczki, and L. Csiba. Cerebrovascular reactivity measured by transcranial doppler in migraine. *Headache: The Journal of Head and Face Pain*, 36(5):323–328, 1996.

[137] M. Silvestrini, L. M. Cupini, E. Troisi, M. Matteis, and G. Bernardi. Estimation of cerebrovascular reactivity in migraine without aura. *Stroke*, 26(1):81–83, 1995.

[138] C. Zwetsloot, J. Caekebeke, J. Jansen, J. Odink, and M. Ferrari. Blood flow velocities in the vertebrobasilar system during migraine attacks a transcranial doppler study. *Cephalalgia*, 12(1): 29–32, 1992.

[139] C. Zwetsloot, J. Caekebeke, J. Odink, and M. Ferrari. Vascular reactivity during migraine attacks: a transcranial doppler study. *Headache: The Journal of Head and Face Pain*, 31(9):593–595, 1991.

[140] C. Harer and R. Von Kummer. Cerebrovascular co 2 reactivity in migraine: assessment by transcranial doppler ultrasound. *Journal of neurology*, 238(1):23–26, 1991.

[141] T. D. Thomas, G. J. Harpold, and B. T. Troost. Cerebrovascular reactivity in migraineurs as measured by transcranial doppler. *Cephalalgia*, 10(2):95–99, 1990.

[142] M. Jenkinson, C. F. Beckmann, T. E. Behrens, M. W. Woolrich, and S. M. Smith. Fsl. *Neuroimage*, 62(2):782–790, 2012.

[143] S. M. Smith. Fast robust automated brain extraction. *Human brain mapping*, 17(3):143–155, 2002.

[144] M. Jenkinson, P. Bannister, M. Brady, and S. Smith. Improved optimization for the robust and accurate linear registration and motion correction of brain images. *Neuroimage*, 17(2):825–841, 2002.

[145] A. Jiang, D. N. Kennedy, J. R. Baker, R. M. Weisskoff, R. B. Tootell, R. P. Woods, R. R. Benson, K. K. Kwong, T. J. Brady, B. R. Rosen, et al. Motion detection and correction in functional mr imaging. *Human Brain Mapping*, 3(3):224–235, 1995.

[146] S. M. Smith and J. M. Brady. Susan—a new approach to low level image processing. *International journal of computer vision*, 23(1):45–78, 1997.

[147] J. Mazziotta, A. Toga, A. Evans, P. Fox, J. Lancaster, K. Zilles, R. Woods, T. Paus, G. Simpson, B. Pike, et al. A probabilistic atlas and reference system for the human brain: International consortium for brain mapping (icbm). *Philosophical Transactions of the Royal Society of London. Series B: Biological Sciences*, 356(1412):1293–1322, 2001.

[148] A. Kastrup, T.-Q. Li, A. Takahashi, G. H. Glover, and M. E. Moseley. Functional magnetic resonance imaging of regional cerebral blood oxygenation changes during breath holding. *Stroke*, 29 (12):2641–2645, 1998.

[149] F. Van Der Zande, P. Hofman, and W. Backes. Mapping hypercapnia-induced cerebrovascular reactivity using bold mri. *Neuroradiology*, 47(2):114–120, 2005.

[150] Templates and atlases included with fsl. `https://fsl.fmrib.ox.ac.uk/fsl/fslwiki/Atlases`.

[151] Donahue lab software. `https://www.vumc.org/donahue-lab/software`.

[152] J. D. Gibbons and S. Chakraborti. *Nonparametric Statistical Inference: Revised and Expanded*. CRC press, 2014.

[153] H. Ito, I. Kanno, C. Kato, T. Sasaki, K. Ishii, Y. Ouchi, A. Iida, H. Okazawa, K. Hayashida, N. Tsuyuguchi, et al. Database of normal human cerebral blood flow, cerebral blood volume, cerebral oxygen extraction fraction and cerebral metabolic rate of oxygen measured by positron emission tomography with 15 o-labelled carbon dioxide or water, carbon monoxide and oxygen: a multicentre study in japan. *European journal of nuclear medicine and molecular imaging*, 31(5): 635–643, 2004.

[154] L. C. Mckay, K. C. Evans, R. S. Frackowiak, and D. R. Corfield. Neural correlates of voluntary breathing in humans. *Journal of Applied Physiology*, 95(3):1170–1178, 2003.

[155] L. FRIBERG, T. S. OLSEN, P. E. ROLAND, and N. A. LASSEN. Focal ischaemia caused by instability of cerebrovascular tone during attacks of hemiplegic migraine: a regional cerebral blood flow study. *Brain*, 110(4):917–959, 1987.

[156] G. W. Petty, A. J. Orencia, B. K. Khandheria, and J. P. Whisnant. A population-based study of stroke in the setting of mitral valve prolapse: risk factors and infarct subtype classification. In *Mayo Clinic Proceedings*, volume 69, pages 632–634. Elsevier, 1994.

[157] M. J. Lee, C. Lee, and C.-S. Chung. The migraine–stroke connection. *Journal of stroke*, 18(2): 146, 2016.

[158] K. Eikermann-Haerter. Spreading depolarization may link migraine and stroke. *Headache: The Journal of Head and Face Pain*, 54(7):1146–1157, 2014.

[159] R. Hoekstra-van Dalen, J. Cillessen, L. Kappelle, and J. Van Gijn. Cerebral infarcts associated with migraine: clinical features, risk factors and follow-up. *Journal of neurology*, 243(7):511–515, 1996.

[160] T. Sacquegna, A. Andreoli, A. Baldrati, C. Lamieri, S. Guttmann, P. d. Carolis, G. D. Pasquale, G. Pinelli, C. Testa, and E. Lugaresi. Ischemic stroke in young adults: the relevance of migrainous infarction. *Cephalalgia*, 9(4):255–258, 1989.

[161] J. F. Rothrock, P. Walicke, M. R. Swenson, P. D. Lyden, and W. R. Logan. Migrainous stroke. *Archives of neurology*, 45(1):63–67, 1988.

[162] J. Bogousalavsky, F. Regli, G. Van Melle, M. Payot, and A. Uske. Migraine stroke. *Neurology*, 38 (2):223–223, 1988.

[163] H. J. Featherstone. Clinical features of stroke in migraine: a review. *Headache: The Journal of Head and Face Pain*, 26(3):128–133, 1986.

[164] M. C. Kruit, L. J. Launer, M. D. Ferrari, and M. A. Van Buchem. Brain stem and cerebellar hyperintense lesions in migraine. *Stroke*, 37(4):1109–1112, 2006.

[165] D. Milhaud, J. Bogousslavsky, G. van Melle, and P. Liot. Ischemic stroke and active migraine. *Neurology*, 57(10):1805–1811, 2001.

[166] J. P. Broderick and J. W. Swanson. Migraine-related strokes: clinical profile and prognosis in 20 patients. *Archives of neurology*, 44(8):868–871, 1987.

[167] S. Ibrahim, A. Nour, S. Magzoub, M. Ibrahim, and A. Jaber. Abnormal circle of willis among migraineurs in sudan. *Journal of the Neurological Sciences*, 333:e484–e485, 2013.

[168] A. Borogovac and I. Asllani. Arterial spin labeling (asl) fmri: advantages, theoretical constrains and experimental challenges in neurosciences. *International journal of biomedical imaging*, 2012, 2012.

[169] Y. Zhou, Z. B. Rodgers, and A. H. Kuo. Cerebrovascular reactivity measured with arterial spin labeling and blood oxygen level dependent techniques. *Magnetic resonance imaging*, 33(5):566–576, 2015.

[170] D. Bulte, P. Chiarelli, R. Wise, and P. Jezzard. Measurement of cerebral blood volume in humans using hyperoxic mri contrast. *Journal of Magnetic Resonance Imaging: An Official Journal of the International Society for Magnetic Resonance in Medicine*, 26(4):894–899, 2007.

[171] C. Willie, D. Macleod, A. Shaw, K. Smith, Y. Tzeng, N. Eves, K. Ikeda, J. Graham, N. Lewis, T. Day, et al. Regional brain blood flow in man during acute changes in arterial blood gases. *The Journal of physiology*, 590(14):3261–3275, 2012.

[172] E. Prisman, M. Slessarev, J. Han, J. Poublanc, A. Mardimae, A. Crawley, J. Fisher, and D. Mikulis. Comparison of the effects of independently-controlled end-tidal pco2 and po2 on blood oxygen level–dependent (bold) mri. *Journal of Magnetic Resonance Imaging: An Official Journal of the International Society for Magnetic Resonance in Medicine*, 27(1):185–191, 2008.

[173] J. Pillai and D. Mikulis. Cerebrovascular reactivity mapping: an evolving standard for clinical functional imaging. *American Journal of Neuroradiology*, 36(1):7–13, 2015.

[174] S. Goode, S. Krishan, C. Alexakis, R. Mahajan, and D. Auer. Precision of cerebrovascular reactivity assessment with use of different quantification methods for hypercapnia functional mr imaging. *American Journal of Neuroradiology*, 30(5):972–977, 2009.